MEASUREMENTS OF ENERGY EXCHANGE BETWEEN ACOUSTIC FIELDS AND NON-UNIFORM STEADY FLOW FIELDS

Thesis by

Kiran Ramanlal Magiawala

In Partial Fulfillment of the Requirements

For the Degree of

Doctor of Philosophy

California Institute of Technology

Pasadena, California

1978

(Submitted May, 1978)

To All My Relatives

Friends and Well-wishers

ACKNOWLEDGEMENTS

I take this opportunity to sincerely thank all those who helped me to make this research work a success. In particular, many thanks to Professor Fred Culick for suggesting this problem and for his constant interest and encouragement throughout the course of this project. Also I wish to express my appreciation to personnel at the Jet Propulsion Laboratory; without their help work reported here would have been inestimably more difficult. Particularly, the generous help of the following persons is gratefully acknowledged:

Section 345 Solid Propulsion and Environmental Systems:
R. Kumar, L. Strand, T. Shively and R. Opp

Section 346 Energy and Materials Research:
S. Parthasarathy

Section 351 Instrumentation:
M. Miller, R. Lindsey, F. Reinhart,
R. Camara, R. Tayler, R. Hansen, J. Wise
and R. Slusser

Section 352 Project Development:
H. Roe

Section 662 Plant Facilities:
R. King

The staff members of the aeronautics workshop, mechanical engineering workshop, aero-electronics shop and various other laboratories and physical plant facilities on the campus, also deserve

a special word of thanks for their expert assistance in the construction and development of the experimental set-up and instrumentation. Also my sincere thanks to Mr. Yuk Lun Chan for his generous help in performing some of the experiments and reduction of data. Indeed, I am indebted to Mrs. Karen Valente and Ms. Marcia Clark for their splendid job of typing the manuscript patiently and to Mr. Frank Linton and Graphic Arts for their excellent job of preparing the many figures.

I am sincerely grateful for the personal financial support provided to me by the California Institute of Technology, National Aeronautics and Space Administration, Jet Propulsion Laboratory and Air Force Rocket Propulsion Laboratory.

Finally, I am gratefully indebted to all of my relatives, friends and well-wishers who helped both to spring and nourish the process of revitalization within me which has been the major emotional support throughout.

ABSTRACT

Study of the unsteady burning of solid propellants can be best carried out under widely varying conditions and at relatively inexpensive cost in a simple test device known as the T-burner. This simple configuration is used to observe the spontaneous growth and decay of oscillations. Knowing the losses involved in the system, one can infer the frequency response of the burning surface within the approximations of linearity.

A significant undertainty in the interpretation of data taken with T-burners arises because very little has been known about some of the acoustics, in particular the influence of the exhaust vent. The present investigation is a study of the influence of a subsonic exhaust vent. The primary apparatus is a resonance tube operated at room temperature with different resonance frequencies of the first longitudinal mode of oscillation. Experiments have been done over ranges of the average Mach number of the flow in the resonance tube, and with vent having different sizes and shapes.

According to the one-dimensional linear stability analysis, the attenuation constant associated with the influence of the exhaust vent is given by the product of four times the resonance frequency of oscillation times the average Mach number of the flow in the resonance tube. The following major conclusions were predicted and verified:

(i) the vent produces a gain of acoustic energy proportional to the average Mach number of the flow in main resonance tube

(ii) the gain is proportional to the frequency of the fundamental longitudinal mode

(iii) the gain is independent of the shape and size of the vent.

The influence of the exhaust vent, hence, cannot be neglected in the interpretation of T-burner data.

TABLE OF CONTENTS

TABLE OF CONTENTS (Continued)

TABLE OF CONTENTS (Continued)

I. INTRODUCTION

Oscillating motions must be anticipated in every solid propellant rocket motor. These unsteady motions are sustained by conversion of some of the energy released in the combustion process, to mechanical energy of the waves. The amount of energy required to drive the waves is a very small fraction of the total available energy and final characteristics of resultant combustion driven instability depend on the internal geometry of the rocket motor and the composition of the propellant used. The oscillations of chamber pressure produce a large oscillatory force acting on the ends of the chamber and this then is transmitted to the structures. If the driving by the propellant is sufficiently strong, it will spontaneously excite the acoustic modes of the chamber. Loss mechanisms in a rocket motor are generally rather weak and the cavity itself serves as a narrow band resonator. This may lead to structural vibration problems if proper attention is not paid to studying the unsteady burning of the propellant. Combustion driven acoustic instabilities have been recognized as one of the serious problems encountered in the development of solid propellant rocket motors. The fluid mechanics of unsteady flow in the chamber (i.e., acoustics), coupling between the wave motions and the combustion and other energy losses involved in the system must be understood separately for a better grasp of the problem. References 1 and 2, for example, address the problems of research on combustion instability and its application to solid propellant rocket motors.

To facilitate the study of unsteady burning of propellants under widely varying situations and at relatively low cost, a simple device, the T-burner, has been widely used. Figures 1.1 and 1.2 describe the details of the typical T-burner. This test apparatus is used to observe the spontaneous growth and decay of the oscillations. There are two broad applications:

(i) to determine the qualitative behavior of different propellants; and

(ii) to measure quantitatively the response of the burning surface to unsteady motions.

A T-burner consists of a straight tube with a central exhaust vent. The length of the tube determines the lowest longitudinal acoustic mode of oscillation. Propellant grains may be placed either at the ends (end burning grains) or on the lateral boundary (cylindrical grains). The lower end of the exhaust vent is connected to a surge tank. This tank and hence the T-burner are pressurized using nitrogen gas. The propellant grain can be ignited using a pallet ignitor paste mounted on the heated nichrome wire. References 3, 4 and 5 describe in detail other related hardware used for the evaluation of combustion instability of solid propellants.

If the driving by the propellant is sufficiently strong, then an acoustic instability occurs and it will spontaneously excite the longitudinal mode of the tube. Observing the growth and decay rate of these oscillations in this simple rocket motor (i.e., T-burner) and knowing the other losses involved in the system, one can infer the frequency response of the burning surface. Ideally, one would prefer

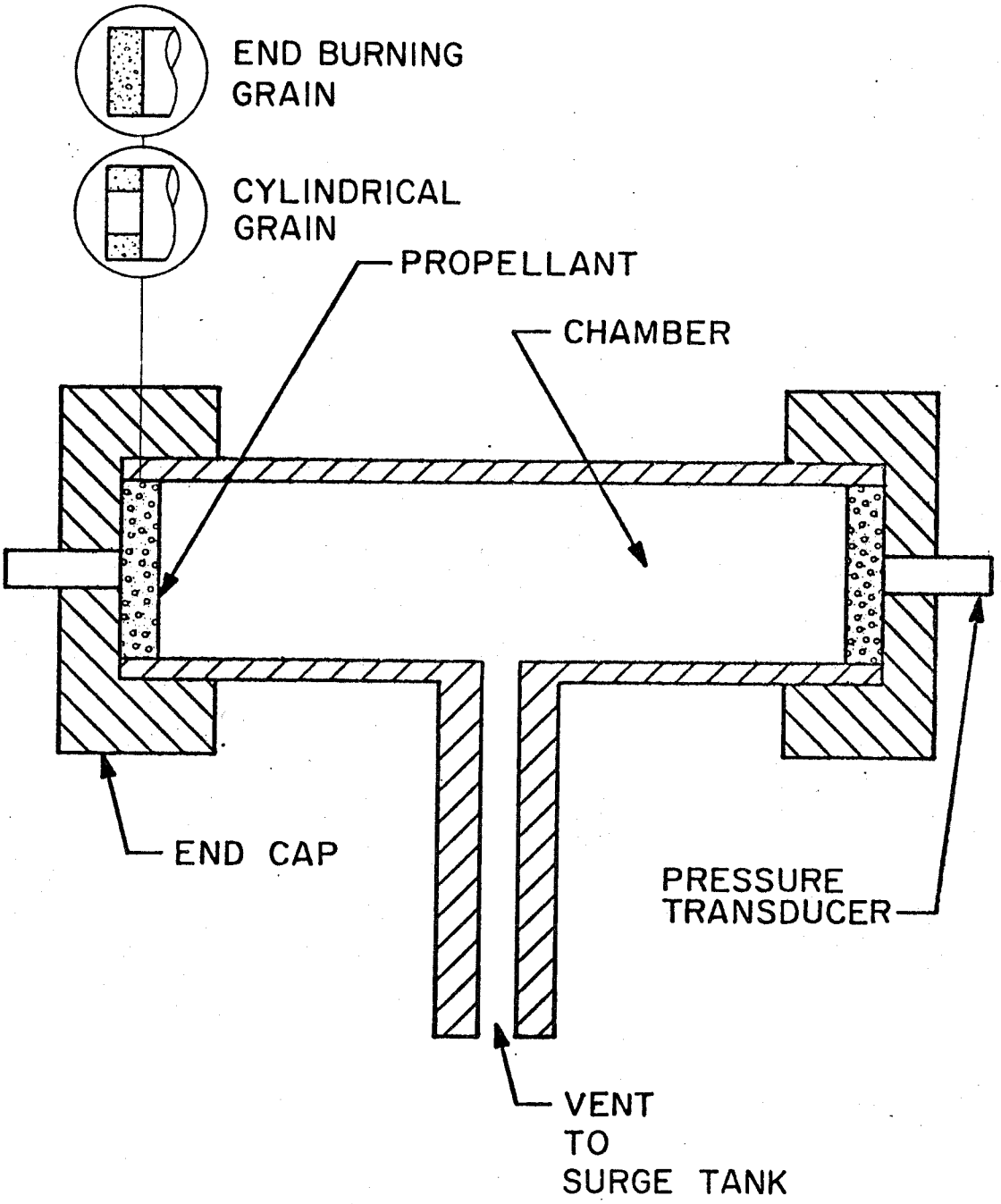

Figure 1.1 Typical T-burner Configuration

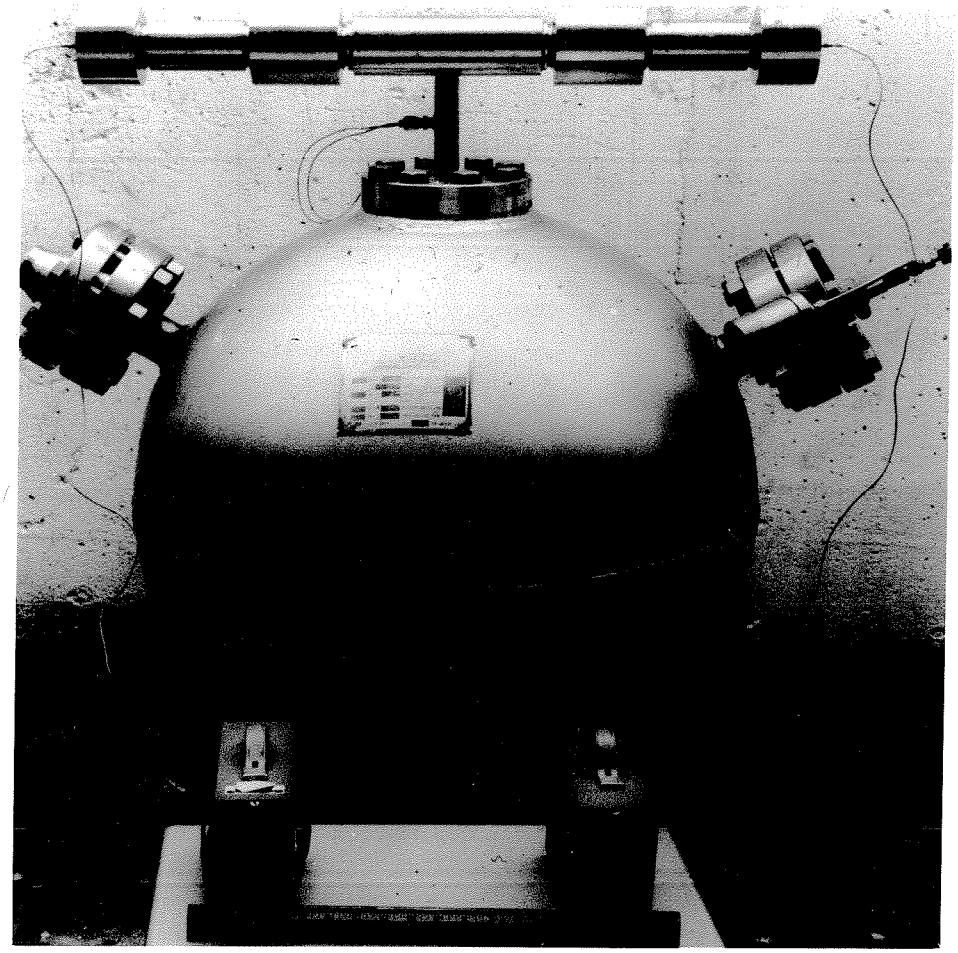

Figure 1.2 Assembled T-burner Mounted on the Surge Tank

to have the response of a burning surface to steady oscillations having fixed amplitude and frequency. As the T-burner is presently used and described above, these ideal situations are not realized. The response is obtained always under the conditions when the amplitudes of oscillations are growing or decaying. The further assumption of linearity is applied that the response is independent of the rate of change of amplitude.

The major losses involved in the system are the viscous and heat transfer losses at the wall of the tube; the influence of the exhaust vent (including radiation losses through it), the flow turning losses, and the particle damping losses. There are no suitable theoretical calculations for acoustic energy loss associated with radiation through the vent. The viscous and heat transfer losses at the wall of the tube can be predicted fairly well using theoretical calculations described in Appendix A. The stability of one-dimensional motions in a rocket motor described in Appendix A also predicts the other two losses. The result explicitly shows that the flow-turning in unsteady flow is indeed a dissipative inelastic process. Chapter 3 and Appendix A further describe the interactions between acoustics and turning flow. In practice, the fluid motions near the exhaust vent for end burning grains and near the inflow for cylindrical grains being three-dimensional, they raise a question about the validity of one-dimensional calculations. To reduce the dependence of this uncertainty on the final calculations of frequency response of a propellant some special devices were developed. Reference 4 describes them in detail. Also presence of metal

powder in propellants introduces the losses associated with the particulate damping forces. This asks for more elaborate test procedures as summarized in references 4 and 5.

The purpose of this work is to measure the influence of the exhaust vent and to check the validity of one-dimensional calculations which are intended as approximations to these influences. Reference 6 describes the one-dimensional calculations. Chapter 2 and Appendix A discuss this problem in further detail. The losses associated with interactions between the waves in the chamber and the average flow entering from the burning surface (the case is reversed for the exhaust vent) are solely described by fluid-mechanics. In the real flow, the losses ultimately arise due to the viscous effects and are the unsteady counterpart of the pressure losses found for steady flow in a duct with mass addition at the boundary. These influences, both flow turning and vent effects, appear to be impossible to determine with hot firings in a T-burner. Because the effects in question are independent of combustion, it is adequate to carry out the experimental evaluation of them at room temperature. Chapters 3, 4, 5 and Appendix A describe further rationale and experiments involved in coldflow (room temperature) testing. The influence of the exhaust vent must be determined first and results obtained must then be used in determining the flow turning losses. This work reports only the experiments carried out to determine the influence of the vent. Our experiments cover a wide range of the important parameters: resonance frequency, flow Mach number, vent size and shape. Because the indirect method was used to

determine the influence of the exhaust vent (described in chapter 4), extreme accuracies are required to measure the other losses present, such as net losses, wall losses, and the influence of the driving pistons. Knowing these very accurately we may then determine the influence of the exhaust vent. A statistical approach adopted to minimize the experimental errors, is described in chapter 7.

It has been found that one-dimensional approximation predicts the influence of the exhaust vent within reasonable accuracy. Though the actual processes are three-dimensional, these results are encouraging. The major conclusions are described in chapter 9.

Two important general conclusions follow from the present work:

(i) Cold flow testing can be used successfully to determine the influence of the exhaust vent. The technique can be made much more sophisticated to reduce the sources of errors and hence to eventually determine the flow turning effects more precisely.

(ii) The influence of the exhaust vent cannot be neglected and hence proper correction must be applied in determining the response function (frequency response) of a burning surface from data obtained with T-burner experiments.

II. SUMMARY DESCRIPTION OF LINEAR ANALYTICAL TECHNIQUES IN COMBUSTION INSTABILITY

Analytical work on combustion instability in solid propellant rocket motors provides the basic framework for treating all the experimental measurements. A complete discussion of all present techniques is summarized in reference 5. Because the physical situations are so complicated (e.g., general three-dimensionality of the processes involved, presence of combustion and various losses difficult to predict from first principles) that successful treatment of these problems requires a combination of both experimental and analytical techniques.

This chapter comprises a description of the analytical approach for a full scale rocket motor in general and the T-burner in particular, which is just a special kind of rocket motor. In chapter 1, the relative merits of using the T-burner were discussed. The simplicity involved with geometry makes it very convenient to check certain major features of the analysis. As described earlier, use of the T-burner is restricted to observing the spontaneous growth and the decay of oscillations within its cylindrical cavity. The analysis described here produces a formula for the growth or decay constant α, which appears in linear analysis as a constant in the exponential growth of the pressure amplitude: a small initial disturbance of pressure increases in time as $\exp(\alpha t)$. The quantity α contains contributions from the burning propellant; viscous and heat transfer losses; flow turning losses; and the influence of exhaust vent or

nozzle. Knowing this α from experiments with the T-burner and knowing other influences, the contribution from burning propellants and hence the frequency response function, can be calculated using this analysis. Providing the acoustic Mach number M' is much smaller than the flow Mach number $\overline{M}_b$, the governing equations remain linear. With this and the linear combustion process, all the disturbances due to combustion and flow addition can be treated as perturbation to the classical acoustic modes of the tube. The central idea is that an arbitrary disturbance within the chamber can be represented as a superposition of its Fourier components; i.e., as a superposition of the normal modes of the chamber. In order that the disturbance should be stable, all of its components hence must be stable. This is hence sufficient to study linear stability of the normal modes of the chamber.

2.1 One-Dimensional Linear Analysis

The most important reason for carrying out analysis of the T-burner is to provide a formula for the growth constant α. It is a very nice feature of this linear analysis that the formula for the growth constant has the form of a sum of contributions from both the losses and gains of acoustic energy. Basic assumptions involved for linearization of equation of motions are discussed in detail in Appendix A and reference 6.

After the conservation equations are linearized, a linear wave equation for pressure fluctuations is constructed. The right hand side contains perturbations representing influences of the mean flow,

particulate matter and residual combustion. The boundary conditions are also inhomogeneous and contain the direct effect of surface combustion, the exhaust nozzle, mean flow and particulate matter. The homogeneous equations define the classical problem for determining the acoustical modes of the chamber. For analyzing the stability of motions, it is sufficient to consider harmonic motions as described earlier. Finally, the problem comes down to determining the complex wave number k defined by the exponential time dependence

$$p' = \hat{p}\, e^{i a_o k t} \tag{2.1}$$

where

$$k = (\omega - i\alpha)/a_o \tag{2.2}$$

It is the imaginary part α which is most useful for interpreting experimental data. A convenient interpretation of α is a fundamental result of linear theory

$$\alpha = \frac{1}{2}\frac{\dot{\bar{\mathcal{E}}}}{\bar{\mathcal{E}}} \tag{2.3}$$

where $\bar{\mathcal{E}}$ is the time averaged acoustic energy and $\dot{\bar{\mathcal{E}}}$ is the time average of the rate of change of acoustic energy in the chamber. The details are summarized in Appendix A. The one-dimensional result for α is:

$$\alpha = -\frac{\gamma p_o}{2E_\ell^2}\left\{\left[\hat{p}_\ell\left(\hat{u}_b^{(r)} + \frac{\bar{u}_b \hat{p}_\ell}{\rho_o a_o^2}\right) S_c\right]_0^L - \bar{u}_b \int_0^L \hat{p}_\ell \iint \left[\frac{\hat{m}_b}{\bar{m}_b} + \frac{\hat{\Delta T}}{T_o}\right]^{(r)} dq\, dz\right\}$$

Combustion and exhaust nozzle

$$-\frac{\bar{u}_b}{2E_\ell^2}\int_0^L \frac{1}{k_\ell^2}\left(\frac{d\hat{p}_\ell}{dz}\right)^2 dq\,dz$$

mean flow/acoustic interactions (both flow turning losses and influence of vent)

+ contribution from particulate matter

+ contribution from residual combustion (2.4)

Contributions from viscous stresses and heat transfer can be incorporated directly by adding:

$$\alpha_d = -\oint\!\!\!\oint\left[\left(\mu\frac{\partial\hat{u}^{(i)}}{\partial y}\right)_{y=0}\frac{d\hat{p}_\ell}{dz} + \frac{\omega}{a_o^2}\frac{R_o}{C_v}\left(\lambda_c\frac{\partial\hat{T}^{(r)}}{\partial y}\right)_{y=0}\hat{p}_\ell\right]\frac{a_o^2\,dS}{2\omega E_\ell^2} \tag{2.5}$$

to equation (2.4). For the propellant with no particulate matter, the last two terms in equation (2.4) are dropped and α can be given by a sum of its contributions as :

$$\alpha = \alpha_{be} + \alpha_{bs} + \alpha_{ft} + \alpha_v + \alpha_d \tag{2.6}$$

This form is valid for the T-burner with propellant grains placed at the ends and on the lateral boundary. The various contributions are discussed in Appendix A. For the typical T-burner with end burning grains only, equation (2.6) simplifies to:

$$\alpha = \alpha_{be} + \alpha_v + \alpha_d \tag{2.7}$$

This shows that the total attenuation constant α comprises contributions from end burning propellant grains; influence of the exhaust

vent (including radiation losses through it); and losses associated with viscosity and heat transfer at the walls of the T-burner. Further the admittance function of the burning surface is given by:

$$A_b = \frac{\hat{u}_b/a_o}{\hat{p}/\gamma p_o} \tag{2.8}$$

It can be related to α_{be} by:

$$\alpha_{be} = 4f\ (A_b^{(r)} + \overline{M}_b) \tag{2.9}$$

Details of the derivations of these formulas are given in Appendix A.

In T-burner tests, α is measured from pressure record; and α_d is found from the theoretical calculations. In the absence of suitable theoretical calculations and experimental measurements for the centrally located exhaust vent, radiation losses are assumed to be zero for the fundamental longitudinal mode of oscillation within the T-burner main tube. Until fairly recently, it had been assumed that the vent has no effect on the fundamental mode i.e., $\alpha_v \approx 0$. This is because three-dimensional analysis discussed later (see Appendix A) leads to the general expression for the decay constant due to the vent:

$$\alpha_v = \frac{-a_o}{2 E_N^2} \oiint \left[A_v^{(r)} + \overline{M}_v\right] \hat{p}_N^2\, dS \tag{2.10}$$

where A_v is the admittance function for the exhaust vent given by

$$A_v = \frac{\hat{u}_v/a_o}{\hat{p}/\gamma p_o}$$

and $\overline{M}_v$ is the Mach number of the flow through the exhaust vent.

For the fundamental mode of a T-burner, $\hat{p}_N$ vanishes at the center of the burner where the vent is located. So, α_v given by equation (2.10) is negligibly small for either sonic or subsonic vents. Thus using equations (2.7) and (2.9) together with known values of α and α_d, the combination $(A_b^{(r)} + \overline{M}_b)$ can easily be calculated.

But a formal deduction from the one-dimensional analysis, that the vent produces a gain of acoustic energy for the fundamental mode given by:

$$\alpha_v = 4f\,\overline{M}_b \neq 0 \qquad (2.11)$$

conflicts with the simpler result described above which suggests that $\alpha_v \approx 0$. It is important to resolve this controversy, because the value of $(A_b^{(r)} + \overline{M}_b)$ deduced from the data taken with the T-burner depends directly on what contributions are assigned to the vent. Neither the use of formal analysis nor the use of T-burner data has satisfactorily resolved this difficulty. Therefore, special tests have been performed to obtain results that would assist in the selection of correct representation. Reference 5 contains a summary of useful equations, a description of the tests, a summary of results and the conclusions reached. It is the purpose of this work to measure the influence of the exhaust vent and hence to check the validity of one-dimensional calculations.

2.2 Three-Dimensional Linear Analysis

The purpose of this analysis is to account the actual process in the combustion chamber which is three-dimensional in nature and to treat general acoustic modes. The expression procedures and

techniques used to find the complex wave number are identical with those discussed for the one-dimensional approach. The formula obtained for the growth constant α is similar in form except for the contributions to the stability of waves arising from the flow turning at the boundary, which does not appear explicitly here. The reason for this is that the viscous forces acting in the boundary regions are the ultimate cause of the process called 'flow turning'; the three-dimensional analysis therefore does not process that contribution. In principle, all of the processes could be analyzed exactly if the complete equations for three-dimensional viscous flow are used. This is indeed a complicated problem. Another approach is the following. All of the viscous effects may be added in the formula for the complex wave number computed with a classical inviscid analysis. Thus, one should include not only viscous and heat transfer effects at the boundary, but also the flow turning effect which is known as a result of the one-dimensional analysis. Reference 7 discusses this problem while Appendix A briefly describes it for our purpose.

For most of the work with T-burners commonly used, the one-dimensional analysis has been used and seems to work well. But it is important to have an independent and accurate check of its validity to predict certain losses in simple systems. Three-dimensional analysis should yield more precise results, but at the expense of greater effort and cost. For practical purposes, there are great advantages gained from applying the simple one-dimensional results.

III. DESCRIPTION OF INTERACTIONS BETWEEN ACOUSTICS AND FLOW FIELDS

As described in the previous chapter, one of the sources of energy loss is associated with interactions between the acoustic waves in the chamber and the average flow entering from the burning surface. As a result of the approximate one-dimensional analysis this loss is expressed as a part of the decay constant by:

$$\alpha_{ft} = -\frac{1}{2E_\ell^2 \rho_o} \int_0^L \frac{1}{k_\ell^2} \left(\frac{d\hat{p}_\ell}{dz}\right)^2 \int \overline{m}_b \, dq \, dz \qquad (3.1)$$

See Appendix A for details. This is, however, described solely by fluid mechanics and no combustion is required. This may be elaborated upon as follows.

Consider the case of longitudinal waves in a uniform port. The fluctuating acoustic velocity is parallel to the burning surface and the direction of flow entering the port is normal to the burning surface. Initially the gasses departing the surface in normal direction have no unsteady motion because they come from the solid surface. Eventually they must participate in the unsteady motion, acquiring some acoustic energy. For doing so, the flow must turn from the direction normal to the surface, to the direction parallel to the surface. It is this process which is accompanied by a loss of acoustic energy from the waves in the main port. The loss is, in the real flow, ultimately due to viscous effects. One-dimensional analysis provides a simple estimate of this loss. This loss essentially is the counterpart in unsteady flow, of the process which has

long been recognized in steady flow as described by reference 8, p. 225. For one-dimensional flow with mass addition at the boundary, the pressure drop can be written as:

$$\frac{dp}{p} = - \gamma M^2 (1 - y_g) \frac{dw_g}{w} - \frac{\gamma M^2}{2} \frac{4f}{D} dz - \frac{\gamma M^2}{2} \frac{dV^2}{V^2} \qquad (3.2)$$

The first term is associated with the pressure drop which is a result of the gain of momentum by the injected flow at the boundary of the main tube, given by $dw_g (V - V'_g)$. While the second term is related to the wall shearing stress, given by $f \rho V^2/2$. The third and the last term can be related to the loss of momentum of the mass flow of the main gas stream, given by wdV. Further details of the physical equations and definitions can be obtained from reference 8. Figure 3.1 describes the geometry of the problem involved in greater detail. It is the first term on the right hand side of equation (3.2) which can be looked upon as a counterpart of the flow turning losses in our unsteady flow problem. References 9, 10 and Appendix A discuss in detail the calculations involved from the standpoint of boundary viscous losses and entropy production associated with these interactions.

Though the previous formulation of energy loss was carried out for flow entering the chamber, the same analysis may be formally applied to the problem of the exhaust vent, i.e., for flow leaving the chamber. This situation arises in the T-burner having a subsonic exhaust vent on the lateral boundary. Figure 3.2 shows a typical T-burner configuration for end burning propellants. The sign of the flow through the vent is negative because the flow leaves the chamber,

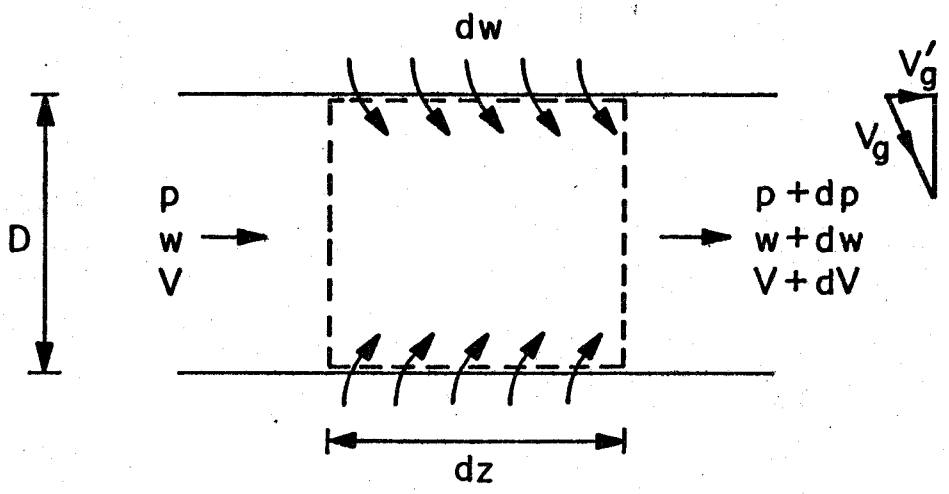

Figure 3.1 Schematic of Flow in a Constant Area Duct with Mass Addition at Boundary

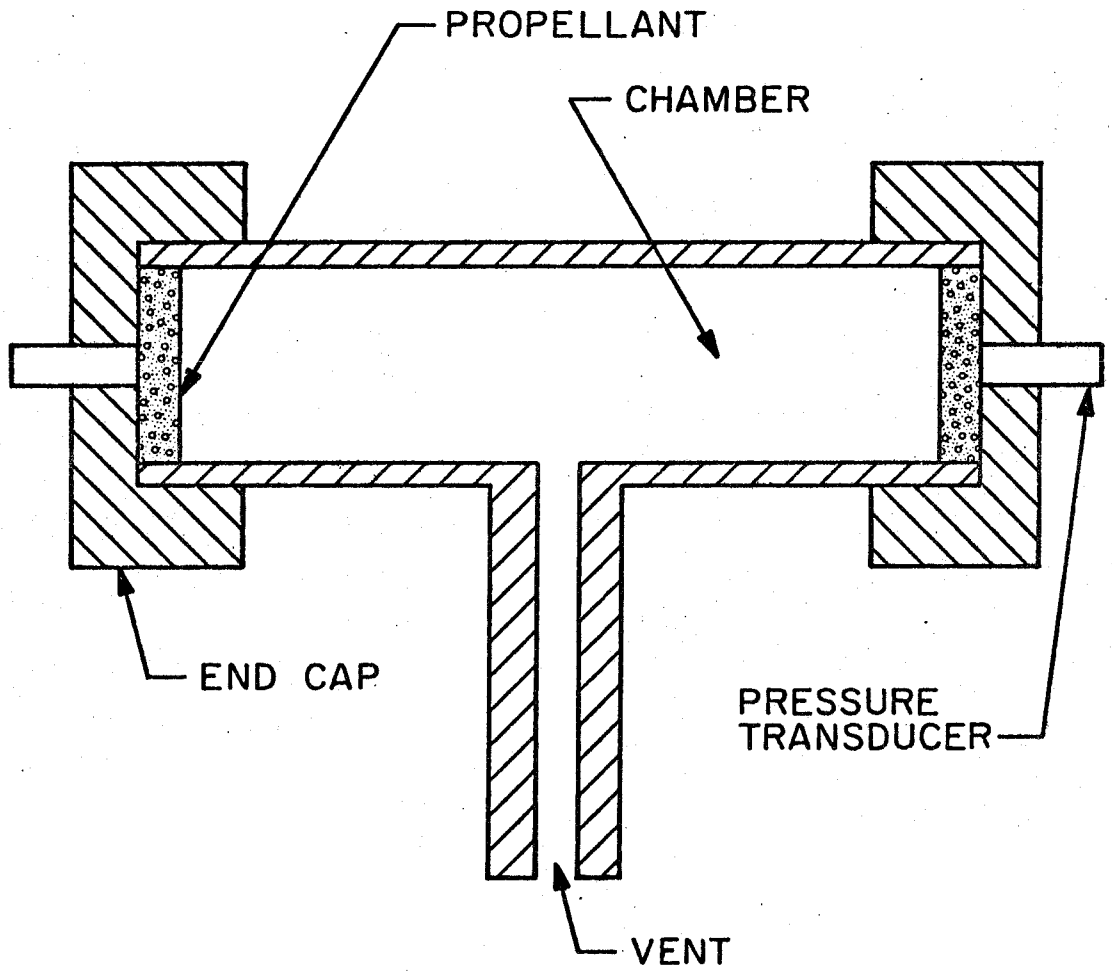

Figure 3.2 Typical T-burner Configuration

and the analysis predicts a gain of acoustic energy for the waves in the chamber; see equation (3.7). The approximation will be assumed true here that α_v may be written as:

$$\alpha_v = \left(\alpha_{ft}\right)_{\overline{m}_b \to -\overline{m}_v} + \alpha_{rad} \tag{3.3}$$

where α_{rad} is the attenuation constant associated with radiation through the exhaust vent with $\overline{m}_v = 0$. For the geometry of interest here, equation (3.1) can be written as:

$$\alpha_{ft} = -\frac{1}{2 E_\ell^2 \rho_o k_\ell^2} \oiint (\nabla \hat{p}_\ell)^2 \, \overline{m}_b \, dS \tag{3.4}$$

where $dS = dq\,dz$. For the longitudinal mode of waves within the T-burner main tube;

$$\hat{p}_\ell \sim \cos k_\ell z \ , \quad \text{where} \quad k_\ell = \pi/L \quad \text{and} \quad f = a_o/2L \ .$$

Also, $(\nabla \hat{p}_\ell)^2 = k_\ell^2$ at $z = L/2$ and $E_\ell^2 = S_c L/2$.

With $\overline{m}_b$ now replaced by $-\overline{m}_v$, equation (3.4) becomes

$$\left(\alpha_{ft}\right)_{\overline{m}_b \to -\overline{m}_v} = \frac{\left[\oiint \overline{m}_v \, dS \right]_{vent}}{\rho_o L S_c} \tag{3.5}$$

The term in brackets is the total mass flow through the vent, which must equal $2 \overline{m}_b S_b = 2 \rho_o \overline{u}_b S_b$, the total average mass flow in from the burning surfaces at the propellants. Hence, equation (3.5) becomes:

$$\left(\alpha_{ft}\right)_{\overline{m}_b \to -\overline{m}_v} = 2 \frac{\overline{u}_b}{L} \frac{S_b}{S_c} \tag{3.6}$$

Also here $S_b = S_c$ and $f = a_o/2L$. Thus for the case of the centrally located vent,

$$\left(\alpha_{ft}\right)_{\overline{m}_b \to -\overline{m}_v} = 4 f \overline{M}_b \qquad (3.7)$$

where $\overline{M}_b = u_b/a_o$. Equation (3.3) can now be written as:

$$\alpha_v = 4 f \overline{M}_b + \alpha_{rad} \qquad (3.8)$$

It must be noted here that these results are clearly a formal consequence of the one-dimensional analysis. The fact that the flow near the exhaust vent is strongly three-dimensional raises questions about the direct application of these results. Because of the associated viscous effects (including possible separation of the flow) one must be aware that the results may, in fact, be severely limited if not invalid. The major purpose of this work is to determine the validity of these one-dimensional calculations. This point will be further elaborated in chapter 4. Reference 5 describes the problem of the vent in historical perspective and emphasizes the need to investigate it in detail.

Moreover, as mentioned before, there are no calculations available for α_{rad} and hence it is measured experimentally as discussed in § 7.1.

IV. DESCRIPTION OF EXPERIMENTS INVOLVED IN COLD FLOW TESTING

As described in chapter 1, it is important to know the flow turning losses and the influence of the exhaust vent, in order to extract meaningful results from the measurements taken with hot firing in T-burners. Knowing these, the data obtained from the firings can be used to calculate the interaction between wave motions and the burning surface. This interaction is conveniently expressed as a sum of the real part of the admittance function and Mach number of the gases at the edge of the combustion zone. This can then be related to the response function of the burning propellant as described later. Because the influence of the vent in particular is not known precisely, there is a large uncertainty attached to values of the response function of a burning propellant. It is the purpose of this study to investigate this problem of the vent experimentally. Because the effects in question are independent of combustion as described in chapter 3, it is adequate to carry out the experiments at room temperature using air as the working fluid. Such a technique is called cold flow testing. See, for an example, reference 11 for an application of this technique to rocket chambers. Cold flow simulation converts the actual problem of combustion driven acoustics in rocket chambers to externally driven acoustics at room temperature converting the self-excited system of oscillation into a forced system of oscillation. This is further discussed in detail in Appendix B. Two measurement techniques well known in acoustics will be used: determination of the

resonance curve of the system and measurement of the acoustic admittance of a surface using an impedance tube. The reasons for using these methods will become more clear below.

The central item of figure 4.1 is a cold flow resonance tube which is essentially an analogue of a T-burner, as shown in figure 4.2. End burning propellants driving the fundamental acoustic mode of oscillation of a T-burner are replaced by pistons fitted with porous plates permitting flow of air. They are driven by electromagnetic shakers exciting the standing waves in the resonance tube at room temperature and pressure. The flow exhausts through the center vent. The configuration shown in figure 4.2 is used to measure the influence of the vent. The influence of the pistons (porous plates with and without flow through them) on the waves, which can be best expressed in terms of admittance function,is measured using an impedance tube. The arrangement is shown in figure 4.3.

Separate flow calibration is required for both the porous plates. The amplitude of oscillation of the pistons driving standing waves in the resonance tube is determined using the output of the accelerometer housed within the piston. The signals from the accelerometers are used to measure the relative phase difference between them. Both electromagnetic shakers driving the pistons are operated at the same frequency from a single audio oscillator. The amplitudes of the drivers are independently variable; the correct relative phase for a standing wave pattern is maintained with a phase shifter.

The primary measurement in both the resonance tube and the impedance tube is the oscillating pressure. For acoustical pressure

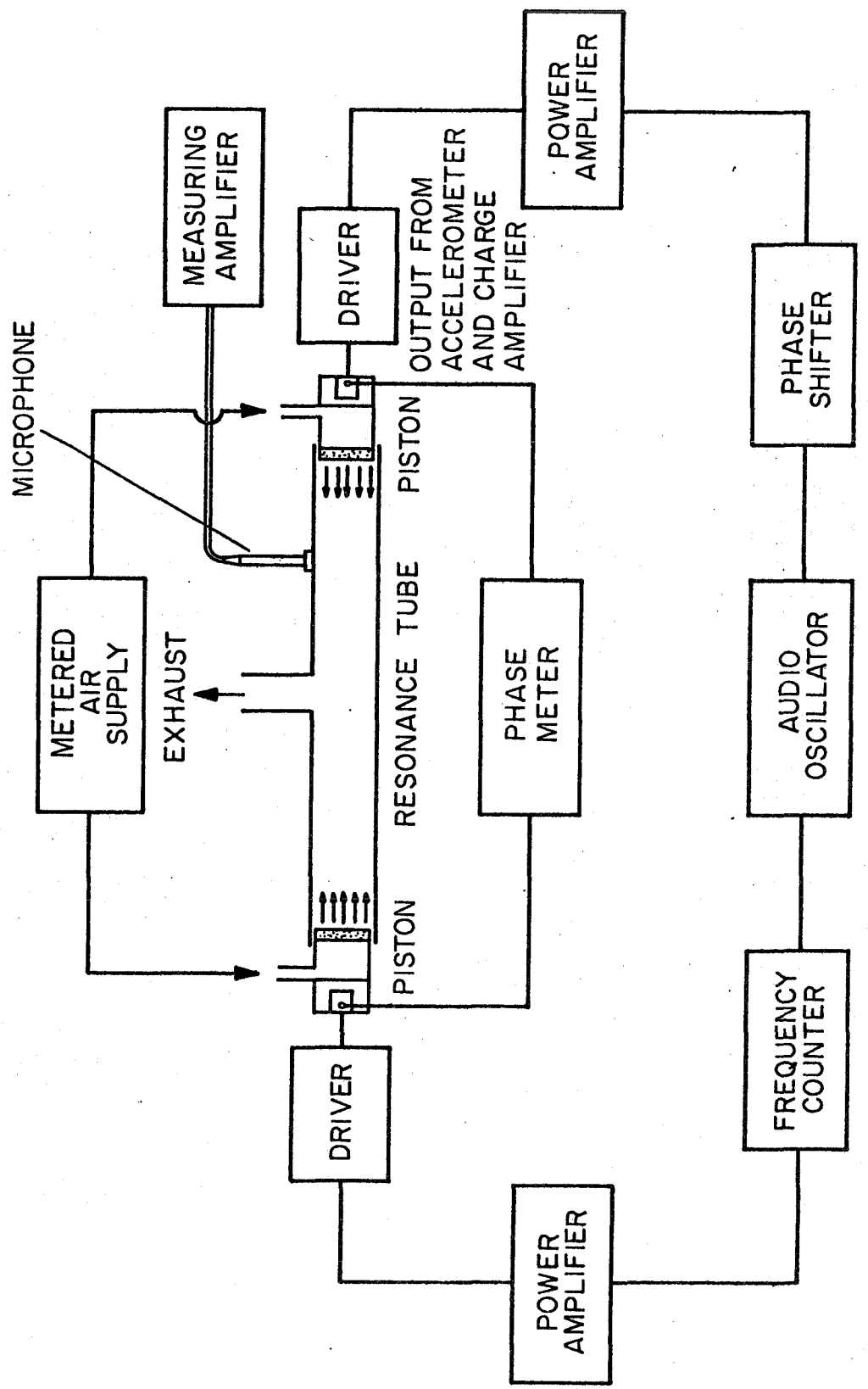

Figure 4.1 Schematic Diagram of the Apparatus

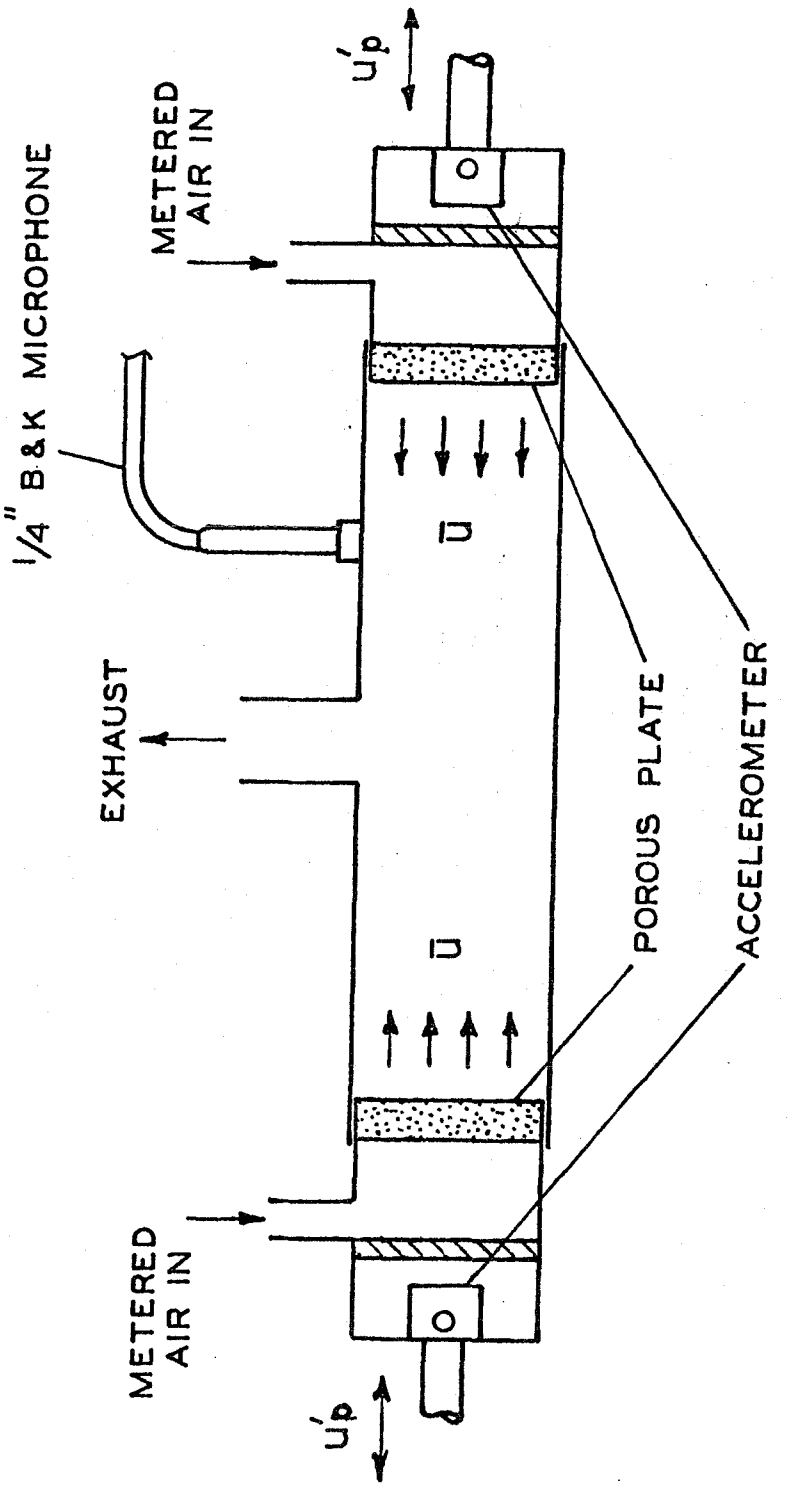

Figure 4.2 Schematic for Measurement of the Influence of the Vent

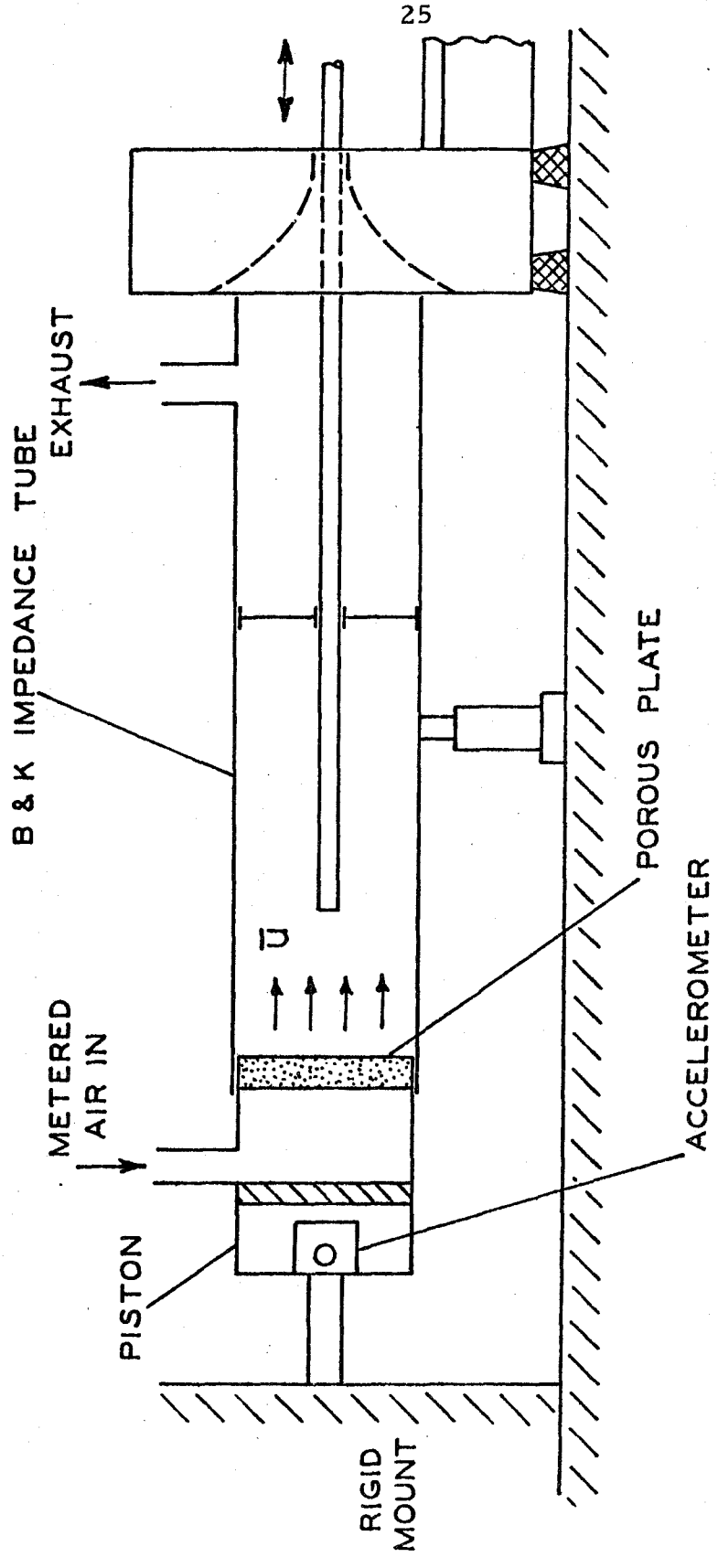

Figure 4.3 Sketch of the Impedance Tube

measurements taken with the resonance tube, the resonance curve is obtained by varying the input frequency to the driver; the relative phase is maintained to be 180° while the amplitude of driver is held constant. The width of the curve at the half power points is proportional to the rate at which acoustic energy is dissipated within the system. The impedance tube experiment requires measurement of the maxima and minima of acoustic pressure and their location along the tube. These measurements are then related to the admittance function of the piston having flow through it.

In all the experiments with resonance tubes, the exhaust vent is located at the center of the tube. Flow Mach numbers, fundamental longitudinal mode frequencies, vent sizes and shapes are the major parameters of interest. For the case of axial flow only, and with $\alpha = \alpha_{net}$ and $\alpha_{be} = \alpha_b$, equation (2.7) simplifies to

$$\alpha_{net} = \alpha_b + \alpha_v + \alpha_d \tag{4.1}$$

For this case, following is a summary of procedures:

(1) Characterize the drivers by tests in the impedance tube without average flow to measure the admittance function for the pistons.

(2) Measure the total losses by tests in resonance tube without average flow and vent closed.

(3) Results of (1) and (2) give a measure of the viscous, heat transfer and radiation losses at the wall of the resonance tube.

(4) Measure the total loss by test in the resonance tube

without average flow and vent open.

(5) The results of (2) and (4) give the radiation loss through the exhaust vent given by α_{rad}.

(6) Characterize the drivers by tests in the impedance tube with average flow.

(7) Measure the total losses by tests in the resonance tube with average flow and vent open.

(8) The results of (3), (6) and (7) give the influence of the vent for outflow given by α_v.

(9) Repeat (1) to (8) for different sizes and shapes of vents and for different fundamental frequencies.

As described above, the influence of the exhaust vent is obtained as a result of subtraction of large numbers. Thus great care must be exercised to measure these numbers with precision. This calls for the highest possible accuracies of the various operating parameters. To help reduce the uncertainties, a statistical approach was adopted as described in chapter 7. Appendix D deals with the calibration procedures and error estimates necessary to obtain the accuracies of the various operating parameters.

V. DESCRIPTION OF EXPERIMENTAL EQUIPMENT

As described earlier, cold flow testing involves acoustic pressure measurements in a resonance tube resembling a T-burner and in an impedance tube used to characterize the driving surfaces of the resonance tube.

5.1 Resonance Tubes

The central feature of figure 5.1 is the resonance tube. The tube itself is made of brass with internal diameter of $1\frac{1}{2}$" and wall thickness of 1/8". Table 5.1 lists the resonance tubes used in this work. All of the circular vents are of length 1.4" and are centrally located. Each has a plug, machined so that when inserted the vent is closed by a surface smoothly fitting the inside surface of the main resonance tube. Resonance tubes with slots were constructed so that the annular slots have areas, distributed on the internal periphery of the main tube, equal to the areas of circular vents having internal diameter of 1" and $1\frac{1}{2}$". Plugs to close the slot vents were constructed, so that, as described later, the absolute values of the attenuation constant associated with these two vents could not be determined. Photographs of two of the resonance tubes are shown in figures 5.2 and 5.3. Figure 5.2 shows the resonance tube with a 1" circular vent while figure 5.3 shows the resonance tube with equivalent area slot vent and having the same resonance frequency.

The resonance tubes are fitted at the ends with caps and teflon inserts to provide a close fit with the pistons. The most successful

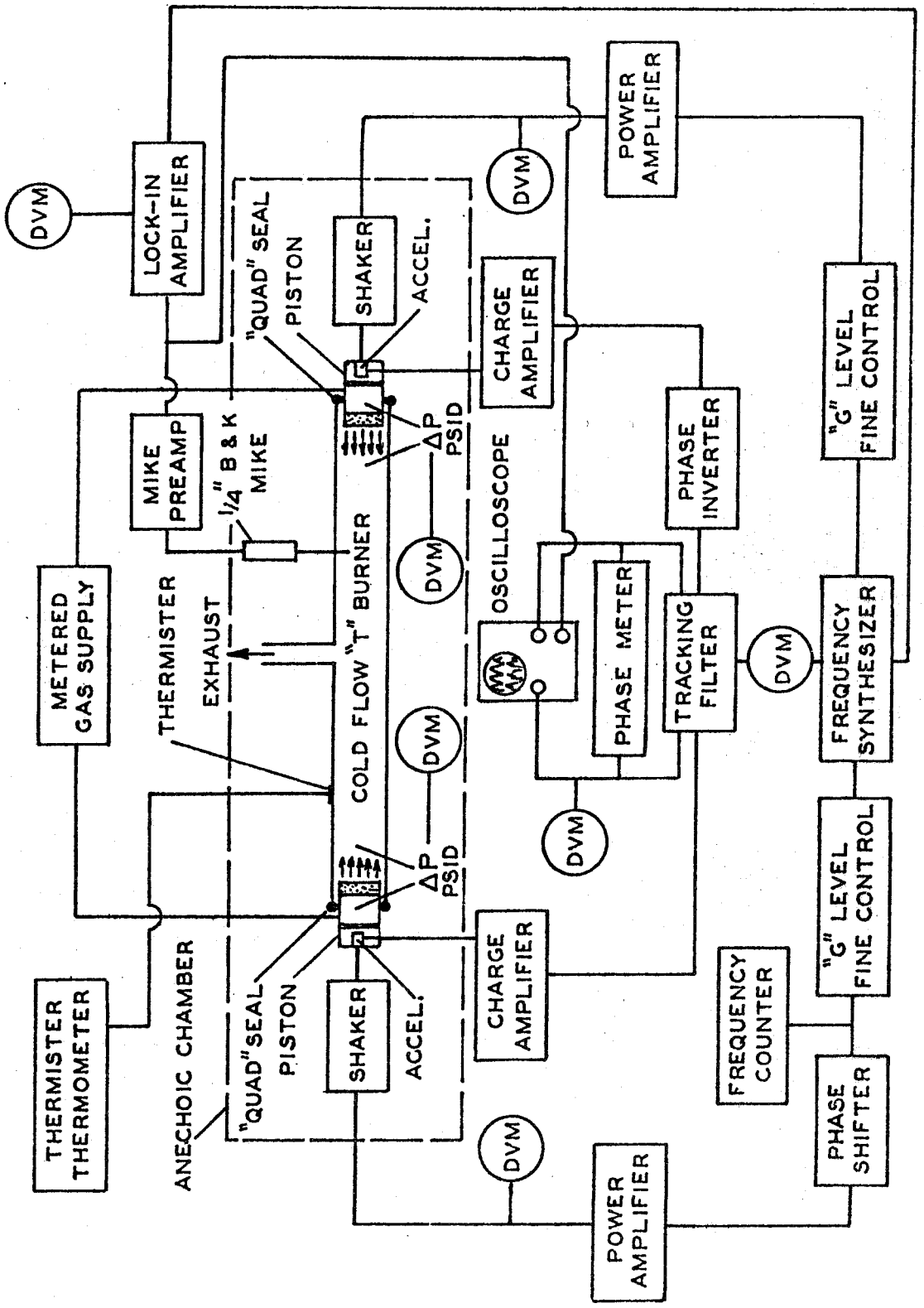

Figure 5.1 Schematic Diagram of Resonance Tube and Apparatus

TABLE 5.1

TYPES OF THE RESONANCE TUBE CONSTRUCTED TO DETERMINE THE INFLUENCE OF THE VENT

Resonance Frequency in Hz	Diameter of Central Circular Vent in Inches	Width of Central Slot in Inches
445	$\frac{1}{2}$	---
	1	0.167
	$1\frac{1}{2}$	0.375
1345	$\frac{1}{2}$	---
2645	$\frac{1}{2}$	---

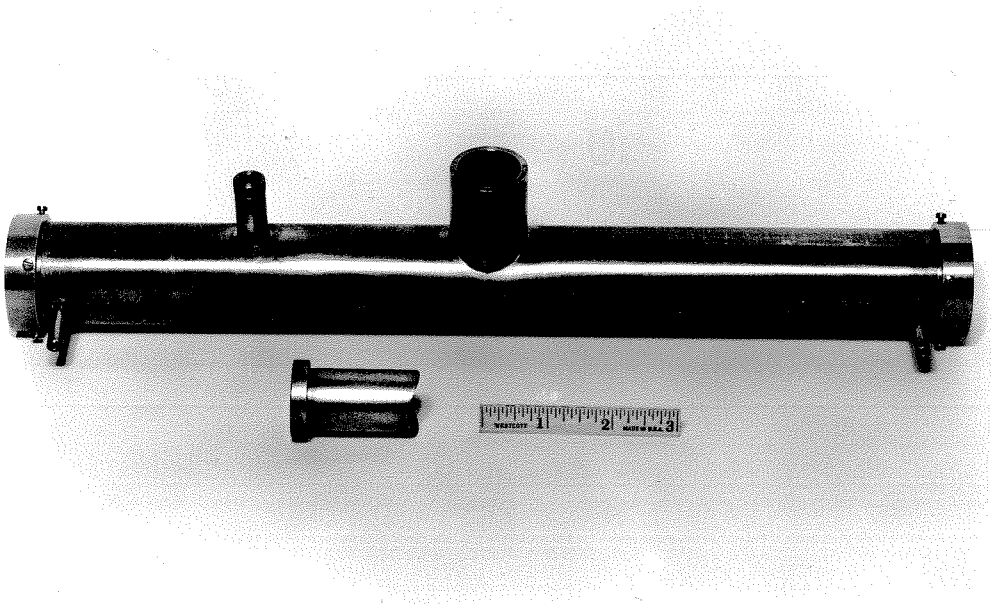

Figure 5.2 The Resonance Tube Used to Determine the Influence of the Circular Vent

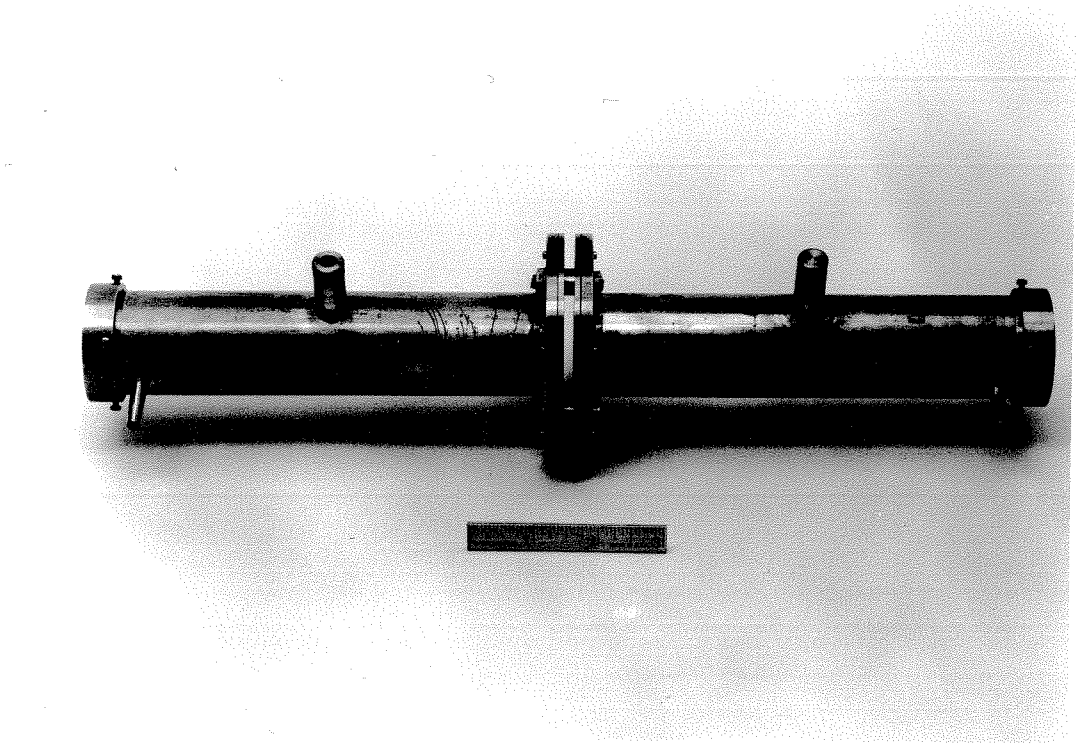

Figure 5.3 The Resonance Tube Used to Determine the Influence of the Slot Vent

of the various designs tried is shown in figure 5.4. Figure 5.5 shows the details of the mountings. The radial clearance is about 0.002" and is filled with silicon oil to prevent the leakage of flow and acoustic energy. An external quad seal also helps to prevent leakage. The pistons are machined of aluminum with a grade "G" porous sintered steel plate (Pall Western Co.) 1/8" thick glued to the front through which the axial flow enters. The porous material has an absolute removal rating for gas of 1.8 microns. Both the amplitude and phase of the pistons are measured with accelerometers mounted close to the axis of the piston in the rear chambers. A sealing and smooth operation of the pistons are essential for reliable data. Failure to meet either of these two requirements will be reflected in poor reproducibility of data. The reason associated with the soft electromechanical shaker mounts is due to a shift of the average position of the pistons, resulting in a measurable change in resonance frequency and asymmetry of the acoustic pressure field with respect to the center of the vent. As an additional help to solve this problem, the pressure was equalized between the main resonance tube and the inside mount of the shaker. This reduces the unbalance of forces on the mount itself.

Both coarse and fine regulators (Moore products; nullmatic, model 40 - 100) are used in series to provide the average axial flow at a fairly constant supply of pressure from a reservoir tank which is filled from the air supply in the building. Failure to regulate the supply pressure seems to change the average position of the piston at the end of the resonance tube, causing the difficulties described in the

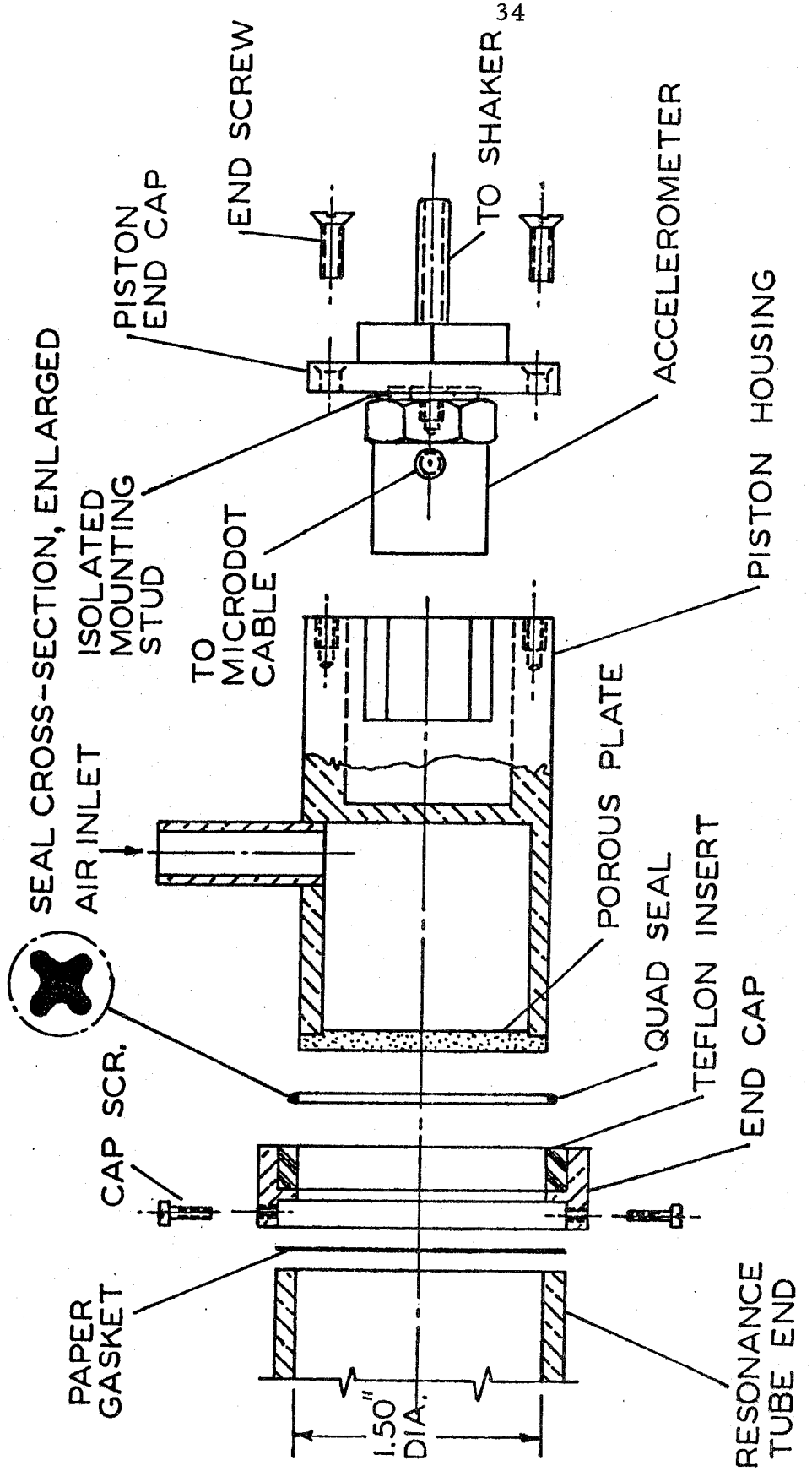

Figure 5.4 Details of the Piston Mounting

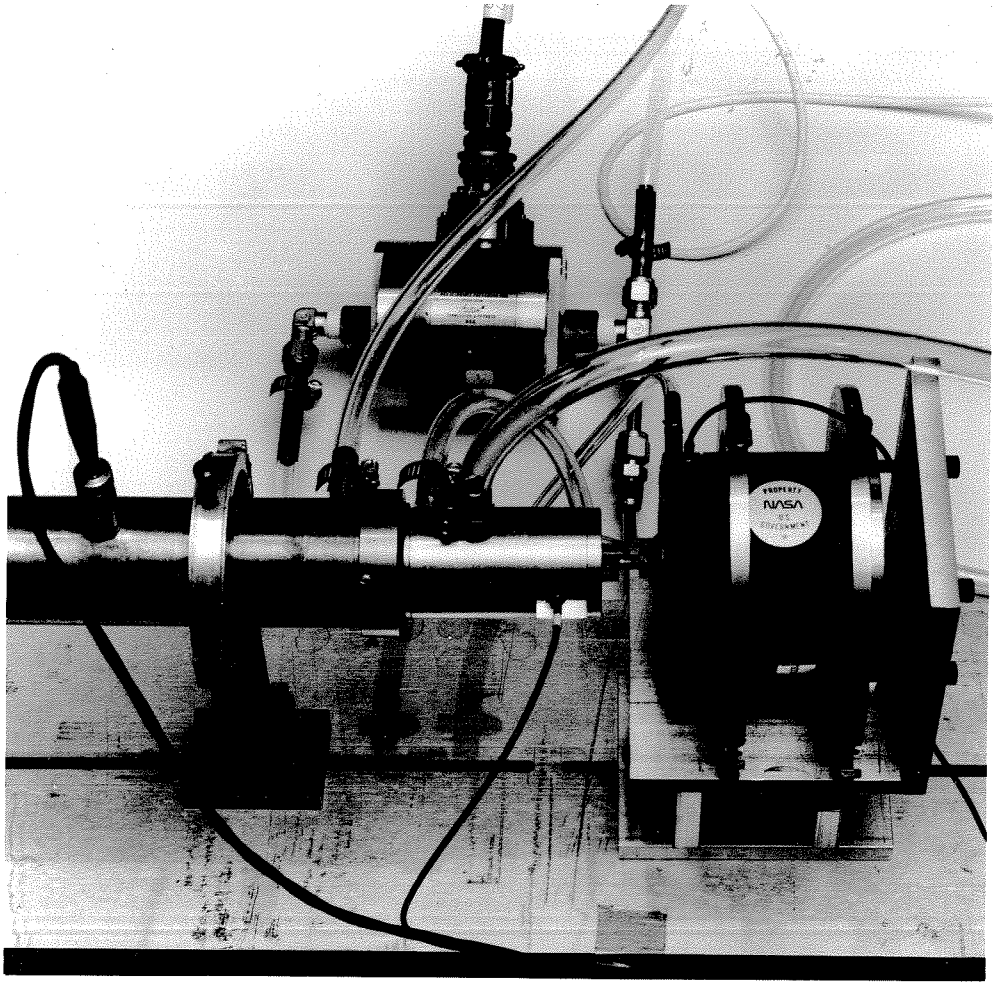

Figure 5.5 Piston Mounting in the Resonance Tube with Electro-Mechanical Shaker

preceding paragraph. The supply pressure is monitored with a Statham differential pressure gauge (range ± 50 psid). Two similar gauges (range ± 10 psid) are used to measure the pressure drop across the porous plates and therefore to maintain the desired flow rates into the tube.

It is important to note that failure to maintain the above mentioned parameters within reasonable accuracies is reflected directly in the measurements of total losses in the resonance tube. The error bars on the final values of α_v are crude cumulative estimates of all these errors.

The apparatus shown in figure 5.1 can be best understood by considering the following four subsystems:

(i) air supply

(ii) the equipment required to drive the waves

(iii) the instrumentation used to measure the amplitudes and relative phase of the piston motions

(iv) the instrumentation used to measure the waves in the resonance tube.

The air supply is described in appendix D. A Wavetek frequency synthesizer, Model 171, provides the signal to drive B & K electromagnetic shakers, Model 4810. An amplifier, Realistic Model SA10, is used with each of the shakers and in series is a phase shafter.

Each piston is fitted with an accelerometer, Endevco, Model 2275, isobase type; the signal is amplified by a charge ampflifier, Unholtz-Dickie Model D-11. Both amplified signals are filtered through a two channel unity gain tracking filter, Spectral Dynamics

Model SD-122 (with 10 Hz bandpass filter) driven by carrier generator, Spectral-Dynamics Model SD-120. The relative phase of the signal is detected with a Wavetek phase meter, Model 740 and the accuracy of the phase measurement is improved by including a phase inversion technique.

All data for acoustic pressure are taken with a B & K, $\frac{1}{4}$" microphone, Model 4136. The desired signal is extracted from the noise, generated by the mean flow, using a Princeton Applied Research Lock-in Amplifier, Model 124 A. This technique is in fact effective up to the largest possible flow speed of 4 ft/sec*. The output of the lock-in amplifier and all other d. c. outputs used for monitoring various parameters are measured with a $5\frac{1}{2}$ digit Data Precision Voltmeter, Model 3500.

To minimize the interference from airborne noise and local reflections within the room, the resonance tube with necessary equipment were placed in an anechoic chamber; see figures 5.6 and 5.7. Reference 12 gives the constructional details and data for qualitative performance of this anechoic chamber. The air supply and instrumentation were located outside the chamber. Though the chamber was mounted on vibration isolating pads, it was found that the setup was not completely isolated from the building vibrations. Typical building vibrations were found sufficient to alter the relative phase and amplitudes of oscillation of pistons. To minimize the influence of this on

---

* The highest speed for data included here is 2.5 ft/sec. The sole reason to restrict ourselves to this speed is the fact that at higher speeds, in flow jet impingement on the side walls of the pistons causes abrupt imbalance of forces on the pistons causing sudden fluctuations in both phase and amplitude of oscillation of pistons.

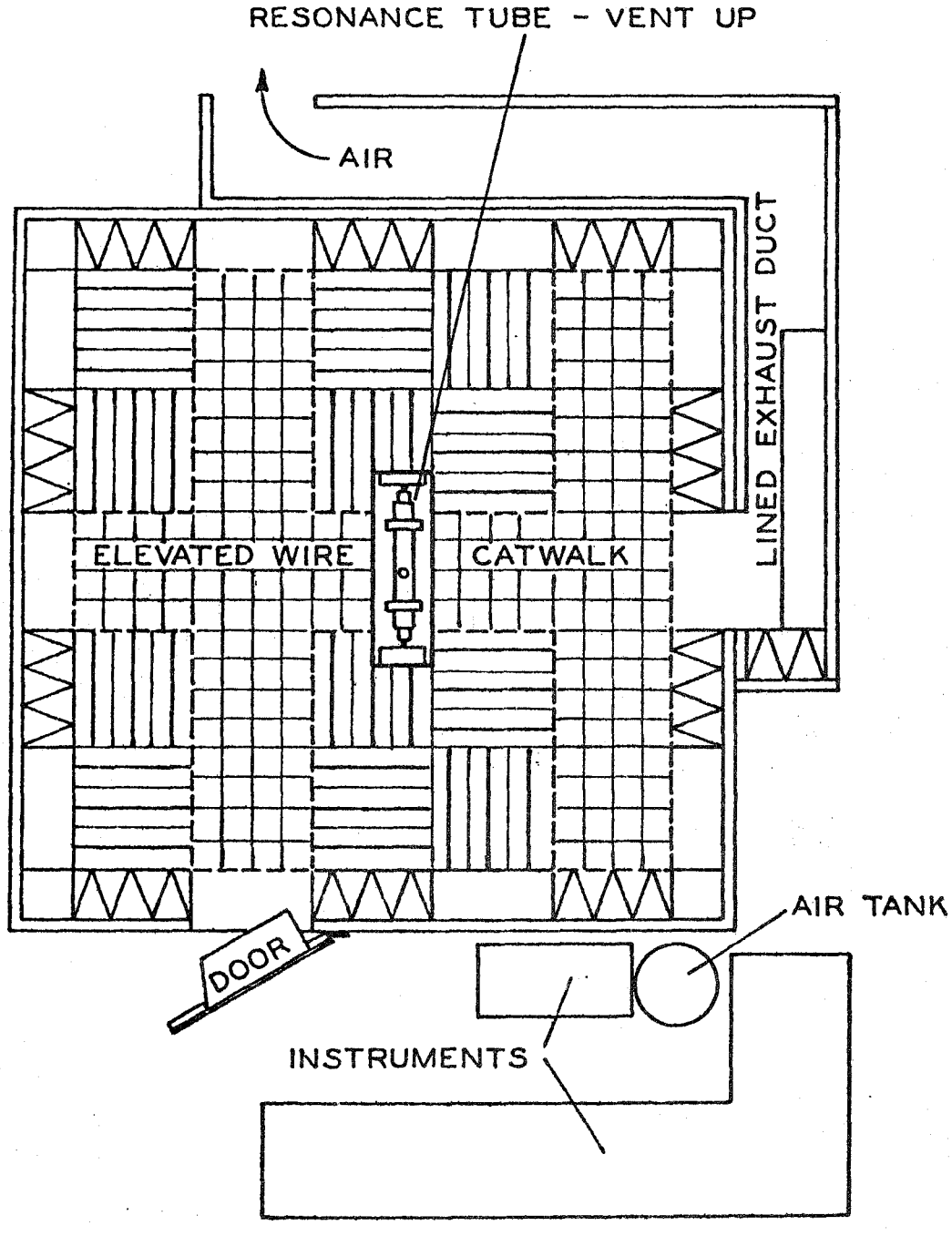

Figure 5.6 Anechoic Chamber Floor Plan
Showing Location of Apparatus

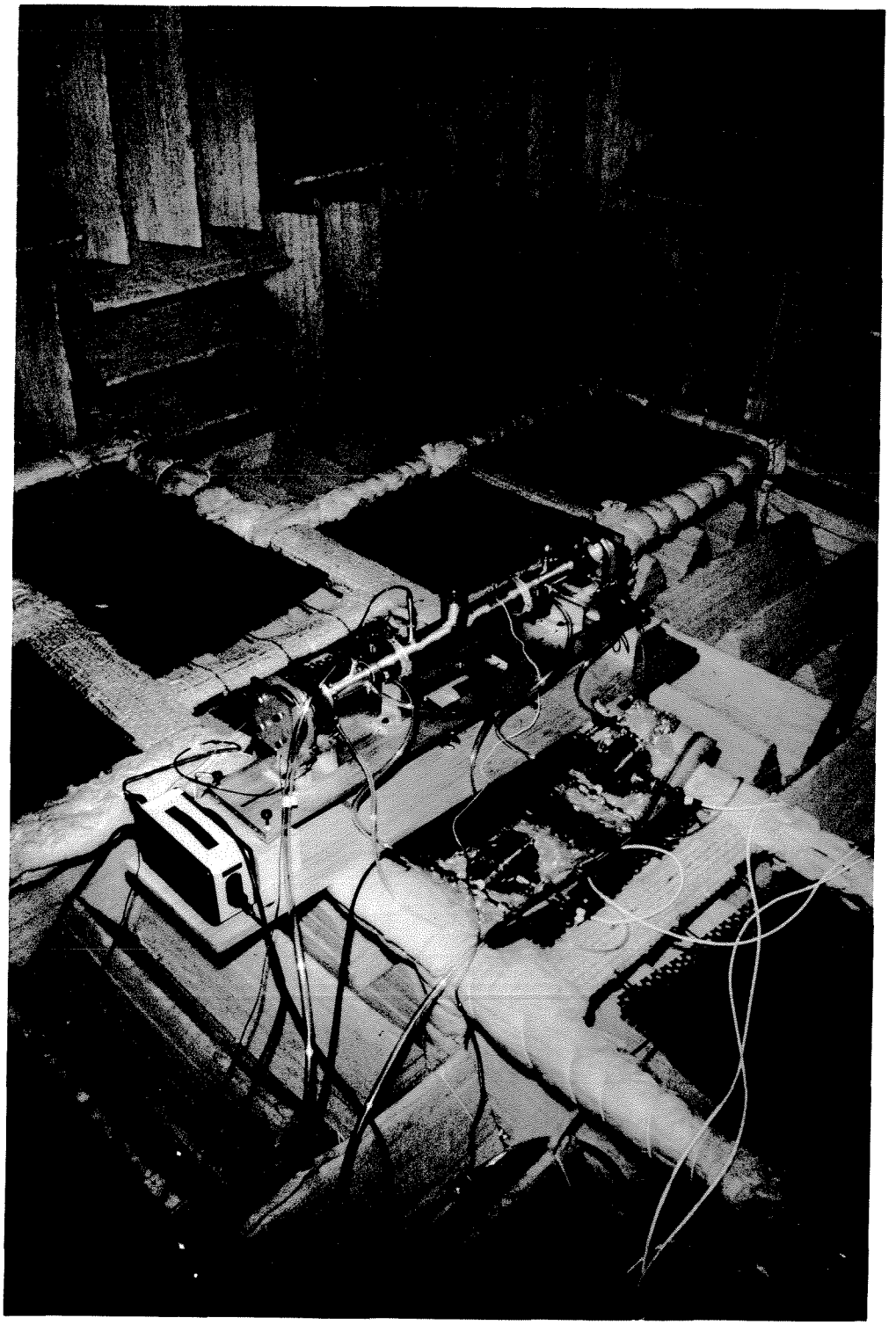

Figure 5.7 Experimental Set-up for Determining the Influence of the Vent in Anechoic Chamber

final results, most of the data were taken on relatively quiet days.

5.2 Impedance Tube

The impedance tube used to measure the influence of the pistons on the waves is a modified B & K standing wave apparatus, Model 4002. The test section is a brass tube about 40" long having an internal diameter of $1\frac{1}{2}$" and wall thickness of 1/8". At one end, the piston is rigidly mounted using a clamp type of holder, while at the other end an exhaust vent is mounted close to the speaker. The tube and ancillary apparatus are shown in figures 5.8 and 5.9. A major advantage of this arrangement with the microphone probe passed through the speaker is the accuracy with which the acoustic pressure minima can be located. A $\frac{1}{2}$" B & K microphone, Model 4133, is mounted on elastic supports within the microphone trolley. The trolley is filled with cotton balls to aid insulation against both external airborne noise and structural vibrations.

In addition to the air supply, the apparatus shown in figure 5.8 can be divided into two subsystems:

(i) the equipment required to drive the waves in the tube

(ii) instrumentation for measuring the waves in the tube .

The same Wavetek frequency synthesizer, Model 171, together with a Raymer amplifier, Model 790-6 are used to excite the speaker. Pressure signals from the tube are picked up by a $\frac{1}{2}$" B & K microphone, Model 4133, supported at the end of a 40" long probe. A track scale is used to measure the distance of pressure maxima and minima from the piston face. The pressure signal is first fed to a

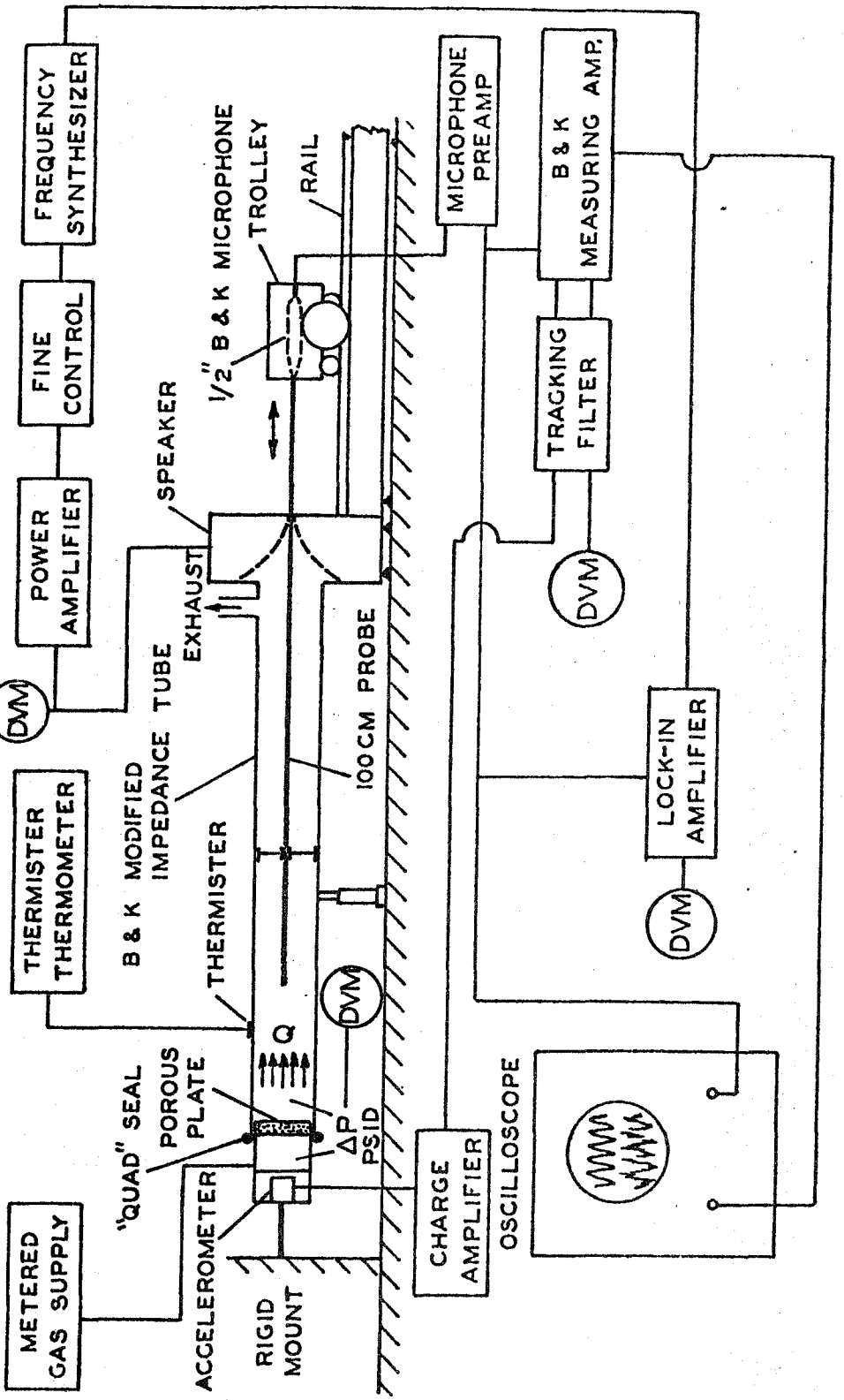

Figure 5.8 Schematic Diagram of Impedance Tube and Apparatus

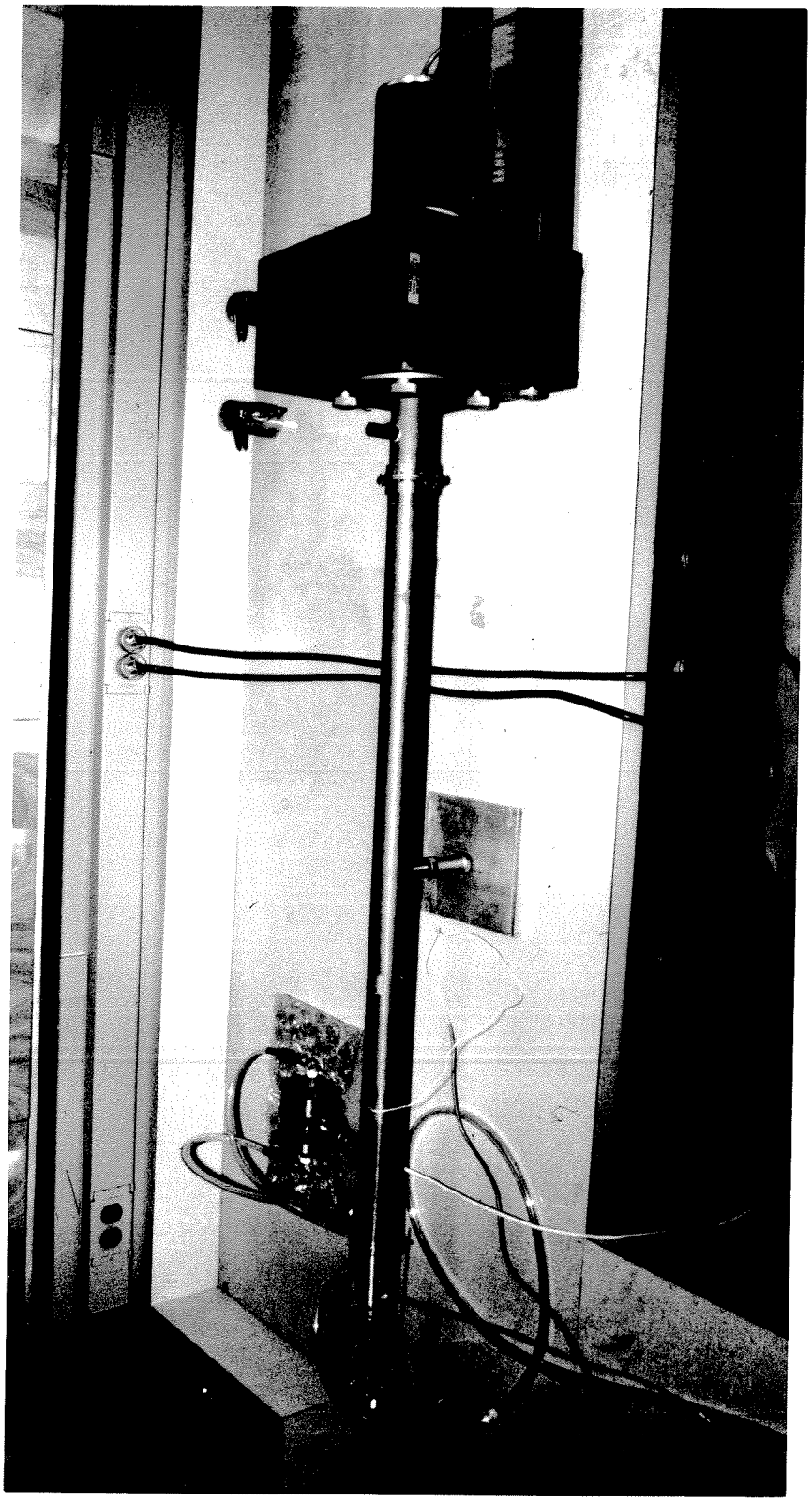

Figure 5.9 Experimental Set-up for Tests with Impedance Tube

B & K measuring amplifier, Model 2607. The amplified signal is filtered through a single channel of tracking filter as described earlier. The output of the tracking filter is fed back to the B & K measuring amplifier and is attenuated and then measured on percent absorption coefficient scale to locate approximate pressure maxima and minima. The final output is also displayed on the dual beam oscilloscope; Tektronix, Model 551. At maxima and minima, rms pressure signals are then measured directly using the Princeton Applied Research lock-in amplifier as described earlier. The rigidity of the clamp holding device is monitored by measuring its response with an accelerometer, charge amplifier and tracking filter as described earlier. It is desirable to keep the excitation of the speaker as low as possible to reduce motions of the pistons but this is ultimately limited by signal/noise problem. Details are described in appendix D.

VI. TEST DATA

As described by equation (4.1), α_{net}, α_b and α_d are the losses of acoustic energy and are therefore negative numbers. While α_v, as given by equation (3.8), is a gain of acoustic energy and hence is a positive number. From this point onward, for convenience in typing and plotting, it was decided not to carry these negative signs for α_{net}, α_b and α_d. The sign conventions were hence reversed, i.e., positive values of α_{net}, α_b and α_d correspond to energy losses and negative values of α_v correspond to energy gains. These sign conventions, however, are not consistant with the current literature, e.g., reference 6.

6.1 Measurements of the Admittance Function for the Porous Plates

To achieve effective acoustic isolation of the air supply system from the flow in the resonance tube, it is necessary to use porous plates having very high acoustic impedance. This means that the acoustic admittance, in particular the real part, is very small. As mentioned before, see equation (2.9), this number is to be multiplied by a factor of four times frequency, leading to a substantial contribution. Thus, if this small number is not measured very accurately, the indirect method of measurement described in chapter 4 leads to quite a large uncertainty, which should be avoided. This is why it has been necessary to achieve high accuracies (described in Appendix D) and to treat the data statistically (described in chapter 7).

Tables 6.1 and 6.2 contain the values of the real part of the admittance function, found for two porous plates in the three series

of tests, average values, and the standard deviation, all at 442.70 Hz. Tables 6.3 and 6.4, and 6.5 and 6.6 contain corresponding results at 1345 Hz and 2645 Hz, respectively.

Computer programs were developed to determine and statistically treat the data obtained for the real part of the admittance function of both porous plates. These programs (discussed in detail in Appendix E) are based on the theories discussed in Appendix C and chapter 7.

Figures 6.1, 6.2 and 6.3 show the variations of average values of the real part of the admittance function of porous plates as functions of flow Mach numbers in the $1\frac{1}{2}$" diameter tube at the frequency of 442.70 Hz, 1345 Hz and 2645 Hz. The solid lines represent least squares fit to the data, assuming a linear variation of $-\overline{A}_b^{(r)}$ with $\overline{M}$.

6.2 Measurements of the Net Acoustic Losses in the Resonance Tubes

α_{net} is a measure of total losses within the resonance tube. As discussed in Appendix B, 2 α_{net} equals the width of the resonance curve at the half power points (-3db down bandwidth $\Delta\omega$). According to convention, α_{net} (losses) is a positive number and is the sum of contributions from various sources of loss: porous piston surface; viscous and heat transfer losses; radiation losses through the wall of the resonance tube; and the influence of the exhaust vent.

Tables 6.7 - 6.11 contain data taken for three series of tests performed at each Mach number for the five vents at 442.70 Hz. Tables 6.12 and 6.13 contain data for only the $\frac{1}{8}$" diameter circular vent tested at 1345 Hz and 2645 Hz, respectively. The average

values and standard deviations of both net attenuation constant and resonance frequency are also given. Note that for all the circular vents, two series of tests have been carried out with no flow: one series with the vent open and the other series with the vent closed. The difference between these two cases should represent the losses due to radiation through the vent.

Figures 6.4 - 6.8 show variations of the average values of the net attenuation coefficient with respect to Mach number of average flow at resonance frequency near 445 Hz, for experiments with different vent sizes and shapes. Figures 6.9 and 6.10 show similar variation for the tests with circular vent with $\frac{1}{2}$" diameter, near the resonance frequency of 1345 Hz and 2645 Hz. Again solid lines in the figures represent least squares fits, assuming that $\overline{\alpha}_{net}$ varies linearly with the average Mach number. Details of the computer program developed for this purpose are given in Appendix E.

TABLE 6.1

DATA TAKEN WITH IMPEDANCE TUBE,
POROUS PLATE (1), FREQUENCY 442.70 Hz

$\overline{M} \times 10^4$	$-A_b^{(r)} \times 10^2$	$-\overline{A}_b^{(r)} \times 10^2$	$\sigma \times 10^6$
0	1.3752 1.3948 1.3947	1.3882	92
4.43	1.3570 1.3948 1.4010	1.3843	194
8.86	1.3826 1.3890 1.3960	1.3892	55
13.29	1.3837 1.3800 1.3965	1.3867	71
17.72	1.3470 1.3435 1.3868	1.3591	196
22.15	1.3494 1.3400 1.3722	1.3539	135

TABLE 6.2

DATA TAKEN WITH IMPEDANCE TUBE,
POROUS PLATE (2), FREQUENCY 442.70 Hz

$\overline{M} \times 10^4$	$-A_b^{(r)} \times 10^2$	$-\overline{A}_b^{(r)} \times 10^2$	$\sigma \times 10^6$
0	1.6879 1.6999 1.7084	1.6987	84
4.43	1.6914 1.7344 1.7210	1.7156	180
8.86	1.7050 1.6814 1.7116	1.6993	130
13.29	1.6227 1.6528 1.6608	1.6454	164
17.72	1.5961 1.6270 1.6505	1.6245	223
22.15	1.5893 1.6025 1.6147	1.6022	104

TABLE 6.3

DATA TAKEN WITH IMPEDANCE TUBE,
POROUS PLATE (1), FREQUENCY 1345 Hz

$\overline{M} \times 10^4$	$-A_b^{(r)} \times 10^2$	$-\overline{A}_b^{(r)} \times 10^2$	$\sigma \times 10^6$
0	1.4949 1.4744 1.4623	1.4772	135
4.43	1.5005 1.4989 1.4648	1.4881	165
8.86	1.5742 1.5584 1.5614	1.5647	69
13.29	1.5133 1.5133 1.4723	1.4996	194
17.72	1.5080 1.5311 1.5027	1.5139	123
22.15	1.4974 1.4922 1.4817	1.4904	65

TABLE 6.4

DATA TAKEN WITH IMPEDANCE TUBE,
POROUS PLATE (2), FREQUENCY 1345 Hz

$\overline{M} \times 10^4$	$-A_b^{(r)} \times 10^2$	$-\overline{A}_b^{(r)} \times 10^2$	$\sigma \times 10^6$
0	1.6454 1.6719 1.6346	1.6506	157
4.43	1.7000 1.6948 1.6986	1.6978	22
8.86	1.7011 1.7255 1.6826	1.7031	176
13.29	1.7135 1.6997 1.6870	1.7001	108
17.72	1.6478 1.6401 1.6737	1.6539	144
22.15	1.6012 1.6331 1.6296	1.6213	143

TABLE 6.5

DATA TAKEN WITH IMPEDANCE TUBE,
POROUS PLATE (1), FREQUENCY 2645 Hz

$\overline{M} \times 10^4$	$-A_b^{(r)} \times 10^2$	$-\overline{A}_b^{(r)} \times 10^2$	$\sigma \times 10^6$
0	2.4508 2.4326 2.4204	2.4346	125
4.43	2.4584 2.5066 2.4928	2.4859	203
8.86	2.5097 2.5461 2.4859	2.5139	248
13.29	2.4301 2.4388 2.4486	2.4392	76
17.72	2.4041 2.3933 2.4289	2.4088	149
22.15	2.4062 2.4105 2.4083	2.4083	18

TABLE 6.6

DATA TAKEN WITH IMPEDANCE TUBE,
POROUS PLATE (2), FREQUENCY 2645 Hz

$\overline{M} \times 10^4$	$-A_b^{(r)} \times 10^2$	$-\overline{A}_b^{(r)} \times 10^2$	$\sigma \times 10^6$
0	2.9892 2.9575 2.9512	2.9660	166
4.43	2.9705 2.9467 2.9333	2.9502	154
8.86	2.9183 2.9019 2.9009	2.9070	80
13.29	2.8892 2.8938 2.8810	2.8880	53
17.72	2.8564 2.8245 2.8255	2.8355	148
22.15	2.8316 2.8007 2.7994	2.8106	149

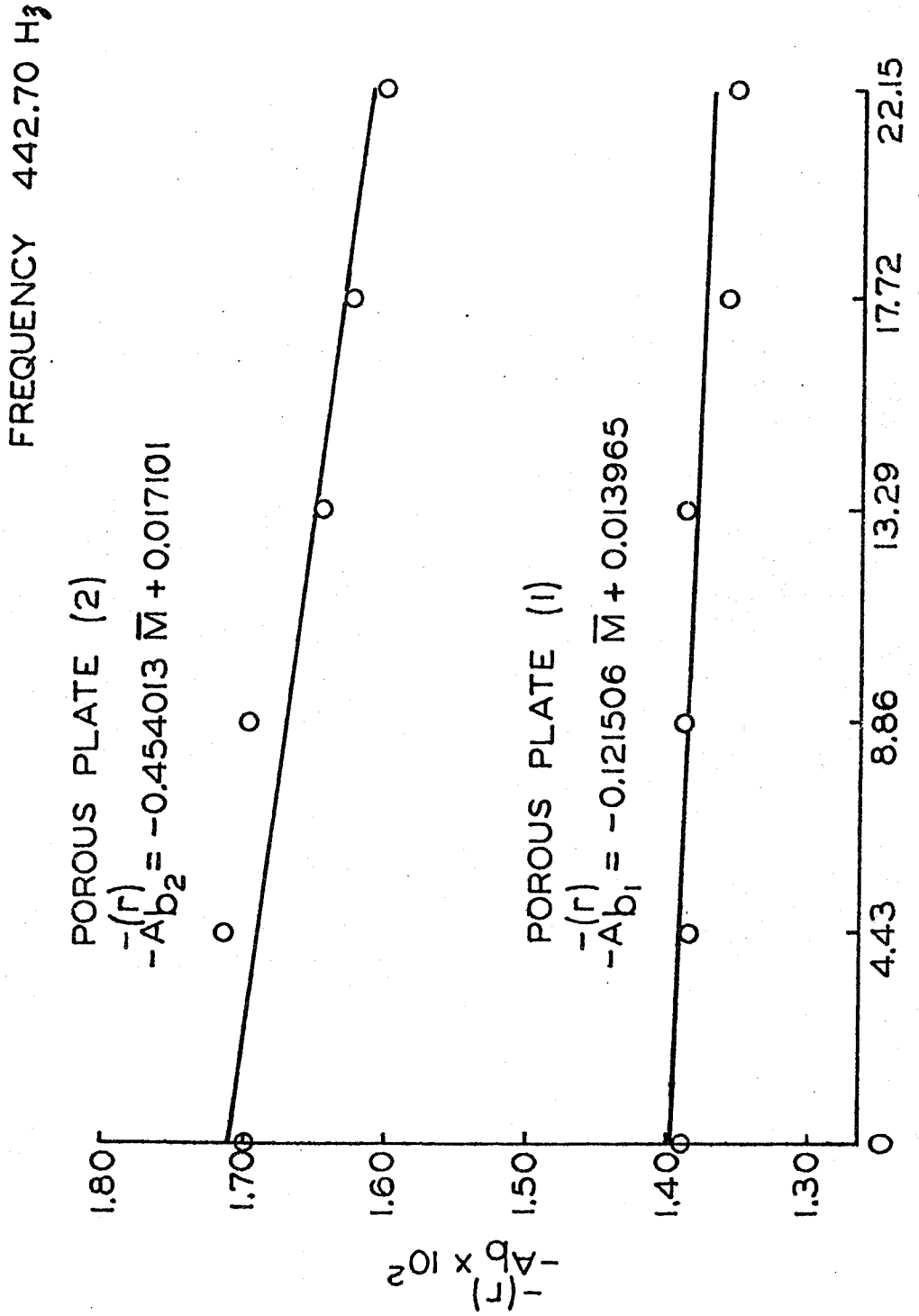

Figure 6.1 Measured Admittance Functions at Frequency 442.70 Hz

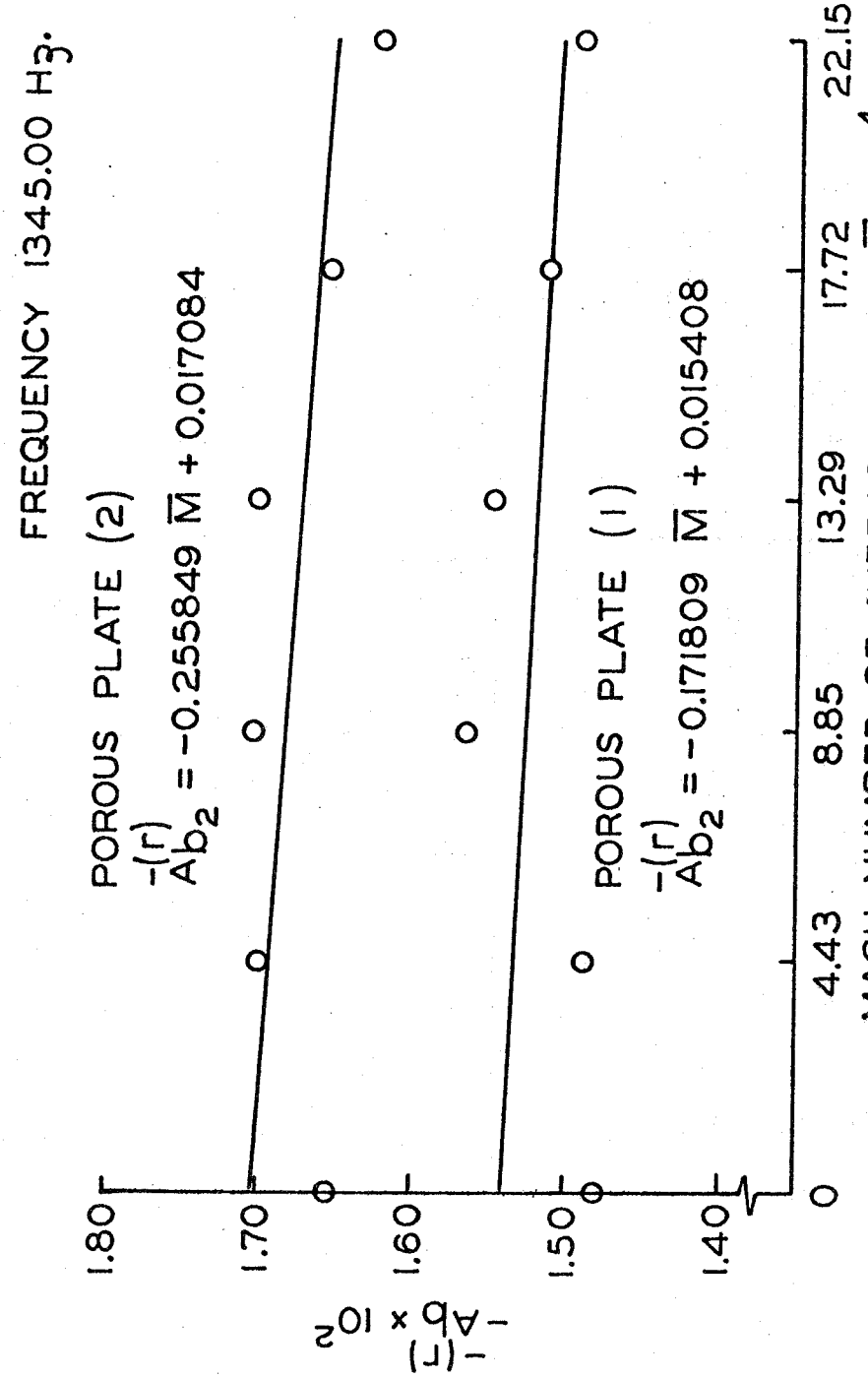

Figure 6.2 Measured Admittance Functions at Frequency 1345 Hz

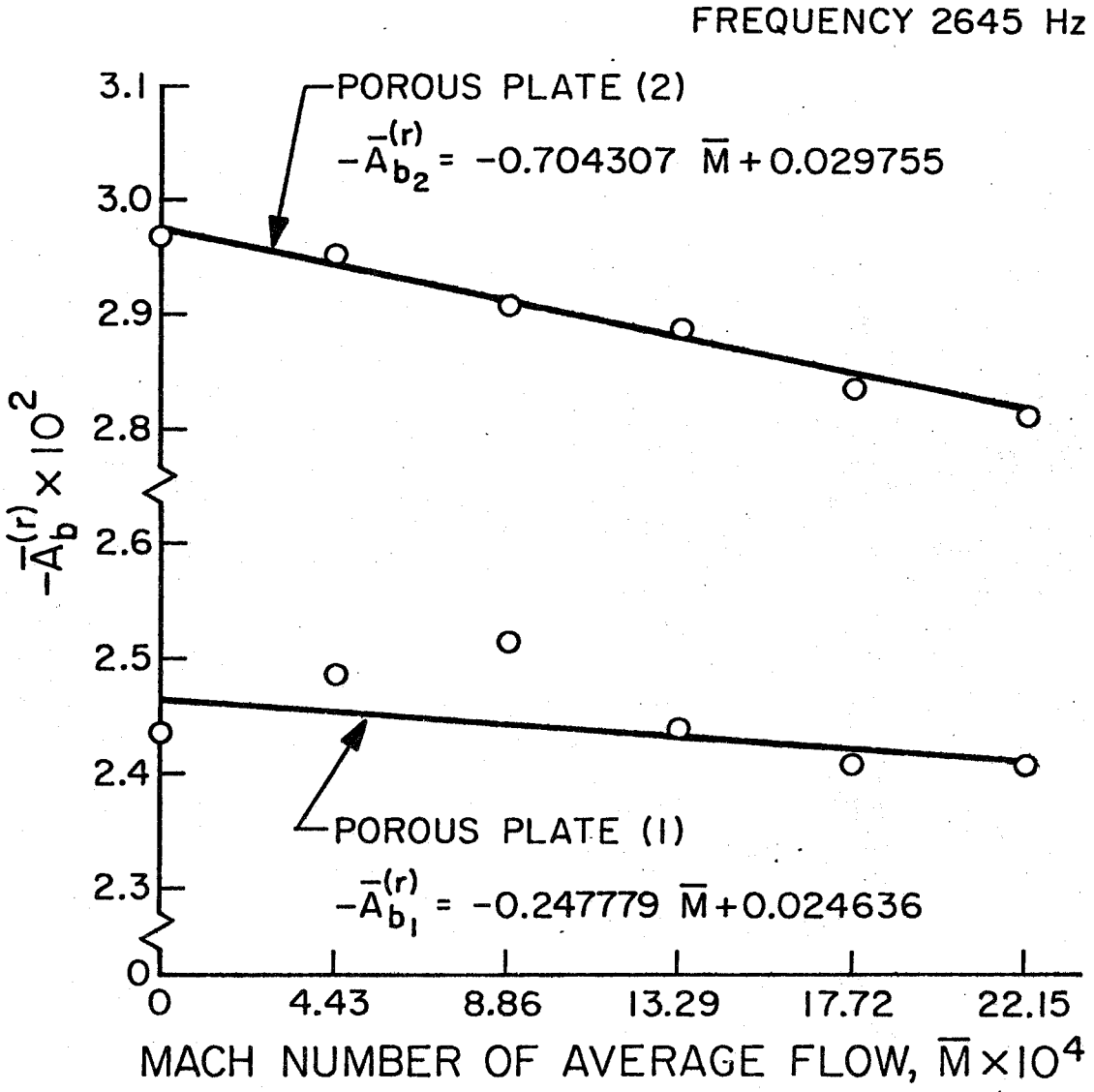

Figure 6.3 Measured Admittance Function at Frequency 2645 Hz

TABLE 6.7

DATA TAKEN WITH RESONANCE TUBE, $\frac{1}{2}$" CIRCULAR VENT, FREQUENCY 442.70 Hz

$\overline{M} \times 10^4$	α_{net} (sec^{-1})	f (Hz)	$\overline{\alpha}_{net}$ (sec^{-1})	σ_α (sec^{-1})	$\overline{f}$ (Hz)	σ_f (Hz)
0	41.94 41.55 41.82	444.10 443.50 443.90	41.77	0.16	443.83	0.25
4.43	41.88 42.21 41.98	442.00 441.90 443.40	42.02	0.14	442.43	0.68
8.86	42.06 42.55 42.57	442.50 442.30 442.90	42.39	0.24	442.57	0.25
13.29	42.26 41.48 42.56	442.50 442.40 442.30	42.43	0.13	442.40	0.08
17.72	41.87 41.46 41.28	442.60 442.10 442.40	41.54	0.25	442.37	0.21
22.15	41.20 41.52 41.27	442.50 443.10 441.50	41.33	0.14	442.70	0.28
0 (vent closed)	41.43 41.97 41.73	443.20 443.00 443.00	41.71	0.22	443.07	0.09

TABLE 6.8

DATA TAKEN WITH RESONANCE TUBE,
1" CIRCULAR VENT, FREQUENCY 444.79 Hz

$\overline{M} \times 10^4$	α_{net} (sec^{-1})	f (Hz)	$\overline{\alpha}_{net}$ (sec^{-1})	σ_{α} (sec^{-1})	$\overline{f}$ (Hz)	σ_f (Hz)
0	40.85	446.50	40.45	0.43	444.83	1.43
	39.86	443.00				
	40.64	445.00				
4.43	40.86	445.10	40.77	0.15	444.30	1.34
	40.56	443.90				
	40.88	442.90				
8.86	40.71	446.20	40.54	0.12	444.73	1.11
	40.49	444.50				
	40.42	443.50				
13.29	40.75	446.30	40.64	0.10	445.10	0.85
	40.50	444.50				
	40.66	444.50				
17.72	40.39	445.50	40.13	0.21	444.43	1.11
	40.13	442.90				
	39.87	444.90				
22.15	40.61	446.00	40.70	0.23	445.33	1.01
	41.02	443.90				
	40.48	446.10				
0 (vent closed)	40.03	444.50	39.88	0.14	442.70	1.61
	39.69	444.60				
	39.91	443.00				

TABLE 6.9

DATA TAKEN WITH RESONANCE TUBE,
$1\frac{1}{2}$" CIRCULAR VENT, FREQUENCY 451.61 Hz

$\overline{M} \times 10^4$	α_{net} (sec^{-1})	f (Hz)	$\overline{\alpha}_{net}$ (sec^{-1})	σ_α (sec^{-1})	$\overline{f}$ (Hz)	σ_f (Hz)
0	43.02 42.36 41.78	452.30 450.10 455.10	42.39	0.51	452.50	2.05
4.43	42.74 42.34 41.52	450.80 449.50 454.60	42.20	0.51	451.63	2.16
8.86	42.31 42.07 41.19	451.20 450.00 452.00	41.86	0.48	451.07	0.82
13.29	41.86 42.00 41.50	451.60 450.00 452.00	41.79	0.21	451.20	0.86
17.72	41.72 42.27 41.27	450.90 450.20 452.90	41.75	0.41	451.33	1.14
22.15	41.47 41.26 40.84	451.40 451.00 453.40	41.19	0.26	451.93	1.05
0 (vent closed)	41.24 41.37 41.42	444.00 444.00 444.00	41.34	0.08	444.00	0.00

TABLE 6.10

DATA TAKEN WITH RESONANCE TUBE,
SLOT VENT WIDTH 0.167", FREQUENCY 446.72 Hz

$\overline{M} \times 10^4$	α_{net} (sec^{-1})	f (Hz)	$\overline{\alpha}_{net}$ (sec^{-1})	σ_α (sec^{-1})	$\overline{f}$ (Hz)	σ_f (Hz)
	41.44	444.80				
0	41.05	447.90	41.24	0.16	447.07	1.62
	41.24	448.50				
	41.37	445.30				
4.43	41.33	446.50	41.34	0.02	446.33	0.78
	41.31	447.20				
	41.45	445.50				
8.86	40.90	446.50	41.23	0.24	446.40	0.70
	41.34	447.20				
	40.95	446.90				
13.29	41.15	447.60	41.17	0.19	447.20	0.29
	41.42	447.10				
	41.50	445.50				
17.72	41.56	448.00	41.43	0.14	446.60	1.04
	41.23	446.30				
	41.06	446.70				
22.15	41.45	447.00	41.25	0.16	446.70	0.24
	41.23	446.40				

TABLE 6.11

DATA TAKEN WITH RESONANCE TUBE,
SLOT VENT WIDTH 0.375", FREQUENCY 446.00 Hz

$\overline{M} \times 10^4$	α_{net} (sec^{-1})	f (Hz)	$\overline{\alpha}_{net}$ (sec^{-1})	σ_α (sec^{-1})	$\overline{f}$ (Hz)	σ_f (Hz)
	39.46	447.80				
0	39.54	447.80	39.70	0.28	447.20	0.85
	40.09	446.00				
	39.69	447.30				
4.43	39.40	444.50	39.63	0.17	445.77	1.16
	39.80	445.50				
	39.63	447.70				
8.86	39.38	445.00	39.52	0.10	446.00	1.08
	39.54	445.50				
	39.47	447.70				
13.29	39.26	445.50	39.43	0.13	446.27	1.01
	39.57	445.60				
	39.26	446.20				
17.72	30.18	446.30	39.13	0.14	445.83	0.59
	38.94	445.00				
	38.99	444.90				
22.15	39.24	446.50	39.95	0.25	445.47	0.73
	38.63	445.00				

TABLE 6.12

DATA TAKEN WITH RESONANCE TUBE,
$\frac{1}{2}$" CIRCULAR VENT, FREQUENCY 1340.88 Hz

$\overline{M} \times 10^4$	α_{net} (sec^{-1})	f (Hz)	$\overline{\alpha}_{net}$ (sec^{-1})	σ_α (sec^{-1})	$\overline{f}$ (Hz)	σ_f (Hz)
0	124.13 124.16 124.41	1341.00 1341.10 1341.10	124.23	0.13	1341.07	0.05
4.43	123.79 124.31 124.10	1343.50 1343.60 1343.70	124.07	0.21	1343.60	0.08
8.86	124.22 123.81 123.89	1341.60 1341.60 1341.70	123.97	0.18	1341.63	0.05
13.29	124.05 123.88 123.98	1342.10 1342.10 1342.00	123.97	0.07	1342.07	0.05
17.72	123.98 124.41 124.49	1337.40 1337.40 1337.40	124.29	0.22	1337.40	0.00
22.15	125.84 126.00 126.29	1339.50 1339.50 1339.50	126.04	0.19	1339.50	0.00
0 (vent closed)	123.60 124.29 124.00	1340.10 1340.50 1340.90	123.96	0.28	1340.50	0.33

TABLE 6.13

DATA TAKEN WITH RESONANCE TUBE,
$\frac{1}{2}$" CIRCULAR VENT, FREQUENCY 2651.78 Hz

$\overline{M} \times 10^4$	α_{net} (sec^{-1})	f (Hz)	$\overline{\alpha}_{net}$ (sec^{-1})	σ_α (sec^{-1})	$\overline{f}$ (Hz)	σ_f (Hz)
0	343.69 343.69 342.98	2659 2653 2657	343.45	0.33	2656.33	2.49
4.43	344.67 344.33 344.73	2651 2653 2652	344.58	0.18	2652.00	0.82
8.86	345.72 343.44 343.55	2658 2652 2655	344.24	1.05	2655.00	2.45
13.29	340.02 339.03 338.60	2645 2649 2648	339.22	0.59	2647.33	1.70
17.72	339.87 339.32 340.60	2550 2651 2652	339.93	0.52	2651.00	0.82
22.15	335.59 336.30 340.48	2649 2648 2650	337.46	2.16	2649.00	0.82
0 (vent closed)	345.19 344.81 345.45	2637 2641 2638	345.15	0.26	2638.67	1.70

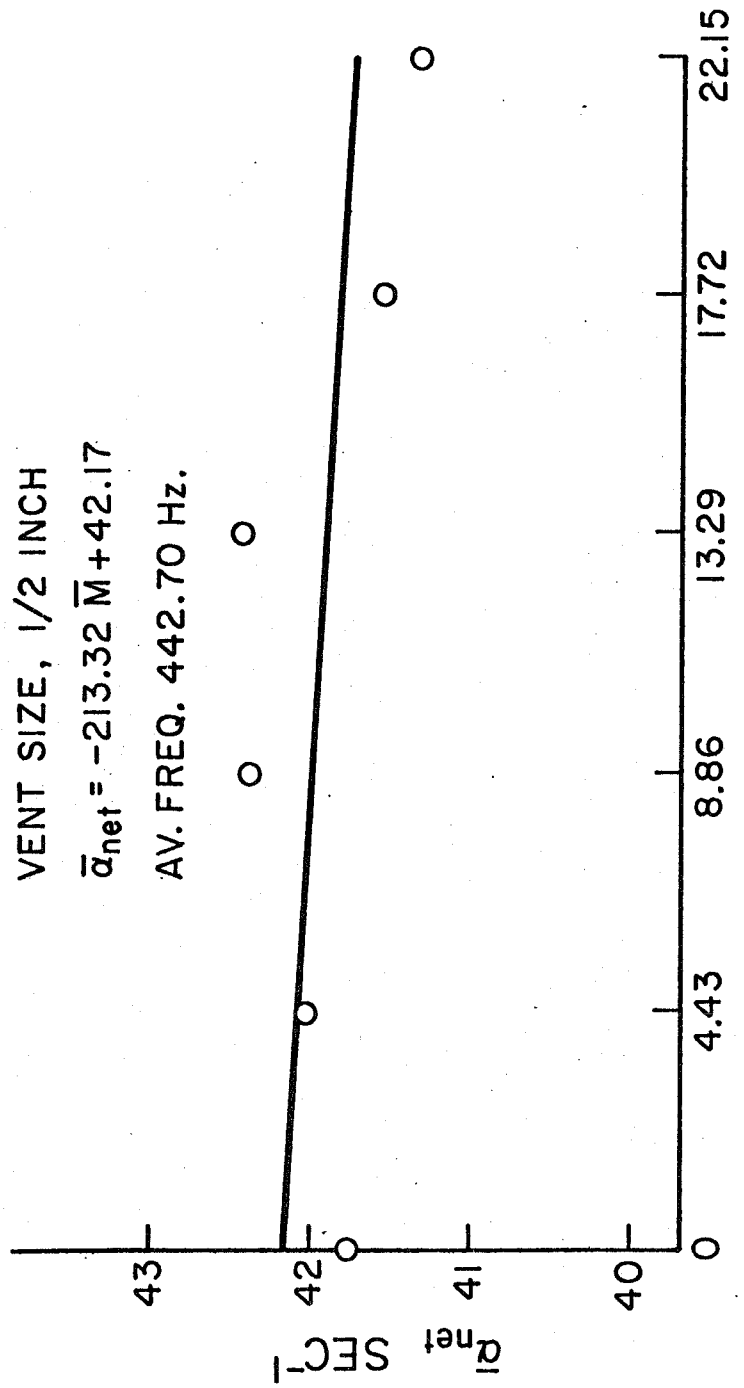

Figure 6.4 Net Values of Attenuation Constant, 1/2" Circular Vent, Frequency 442.70 Hz

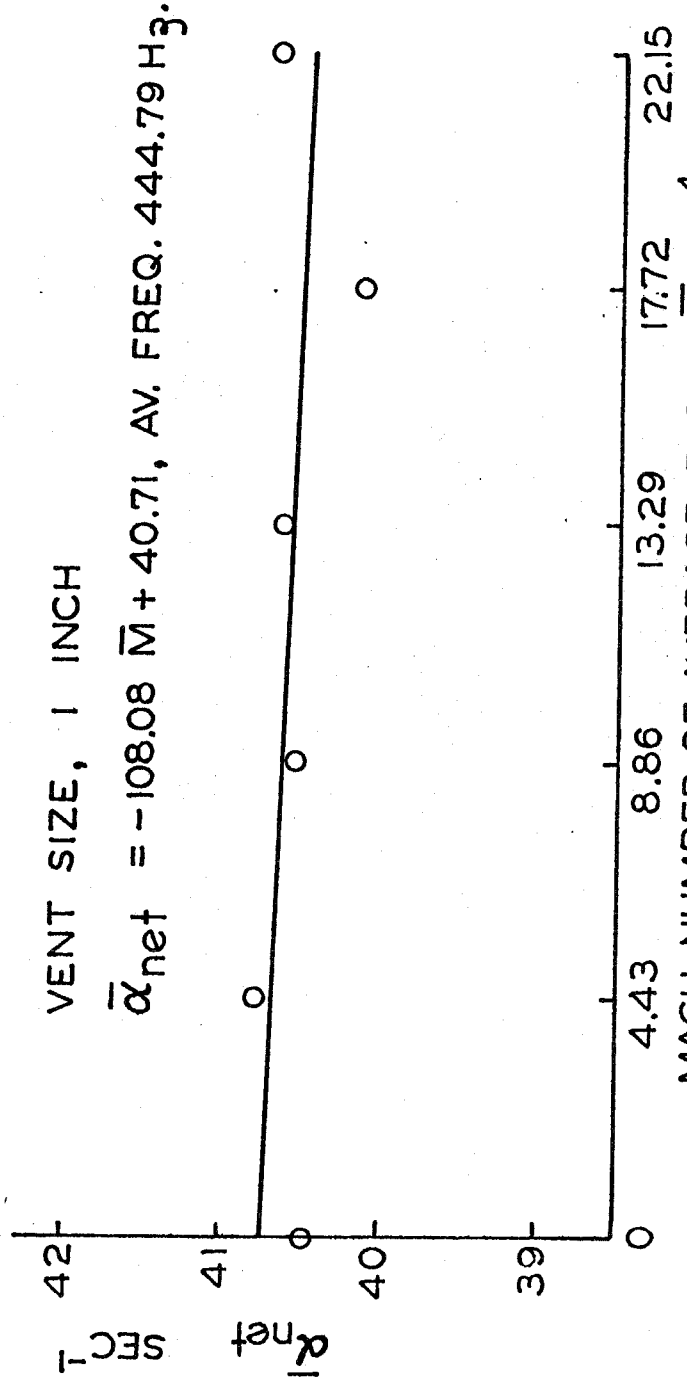

Figure 6.5 Net Values of Attenuation Constant, 1"
Circular Vent, Frequency 444.79 Hz

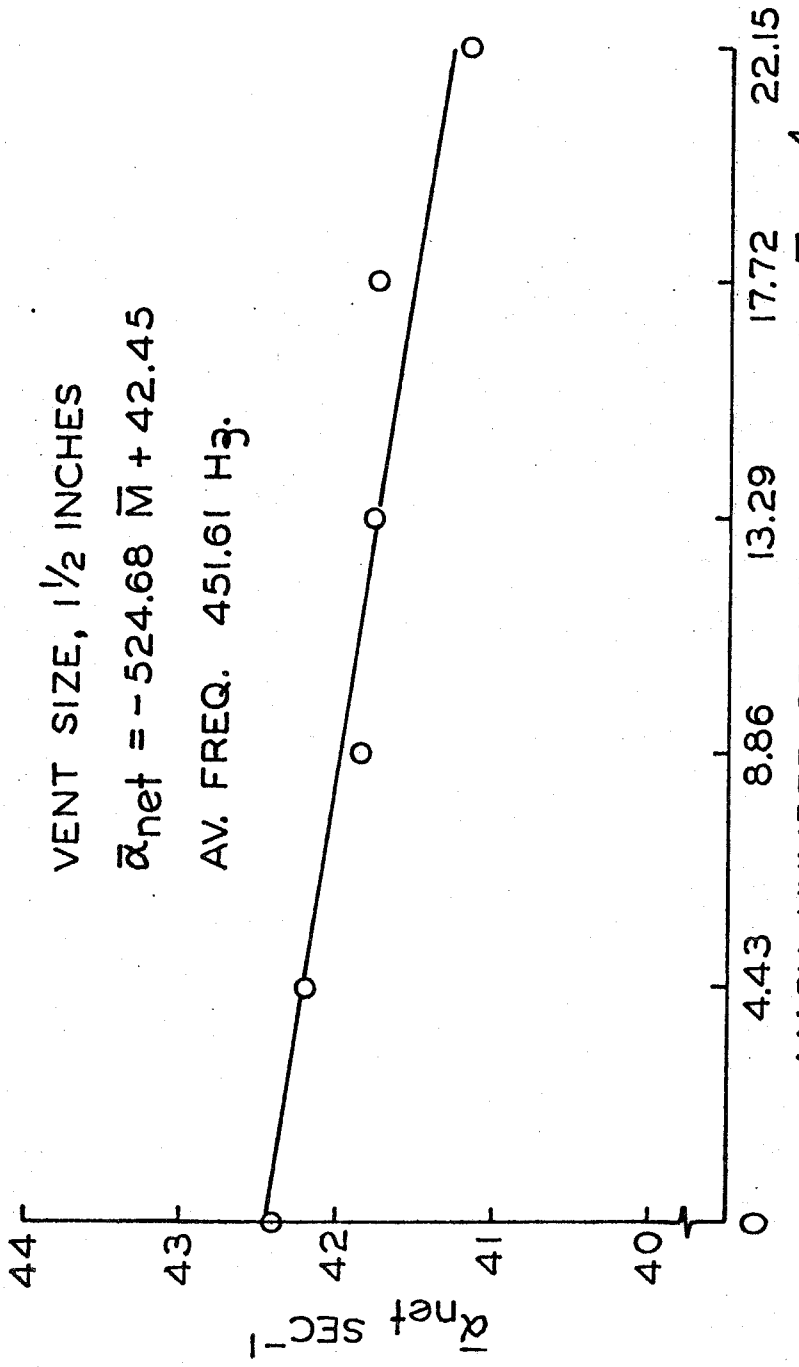

Figure 6.6 Net Values of Attenuation Constant, 1-1/2" Circular Vent, Frequency 451.61 Hz

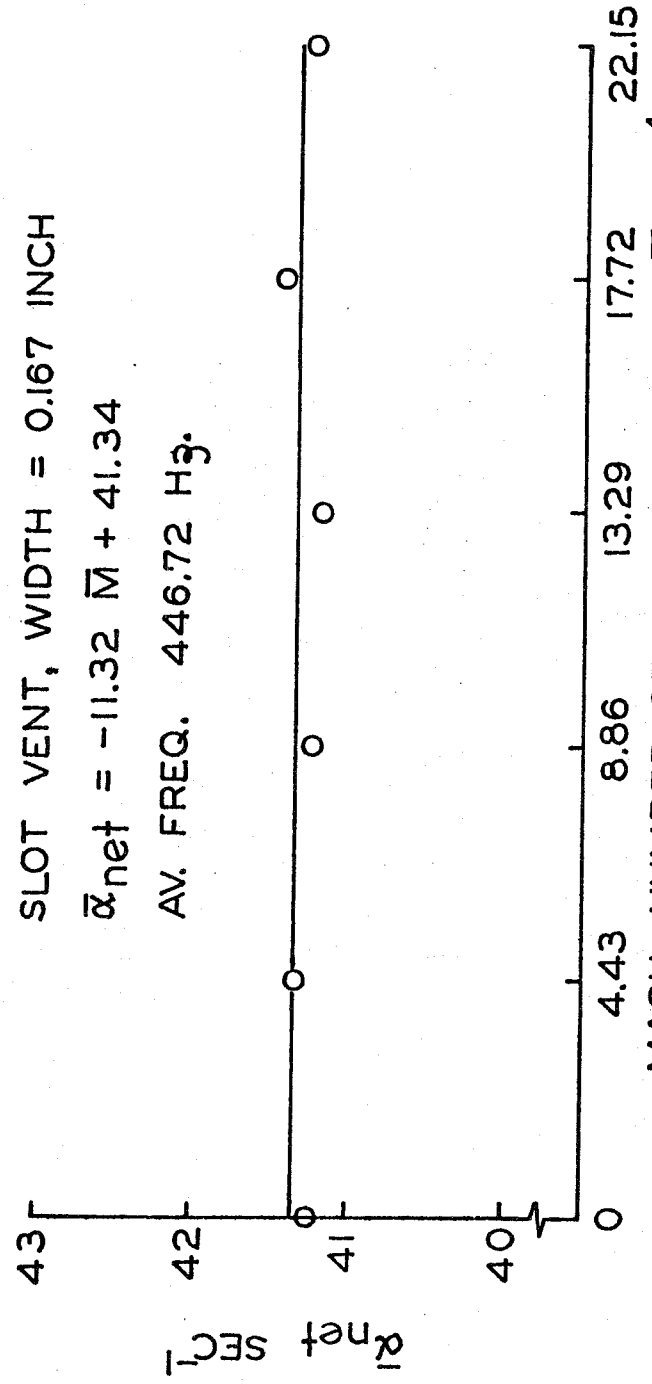

Figure 6.7 Net Values of Attenuation Constant, 0.167" Slot Vent, Frequency 446.72 Hz

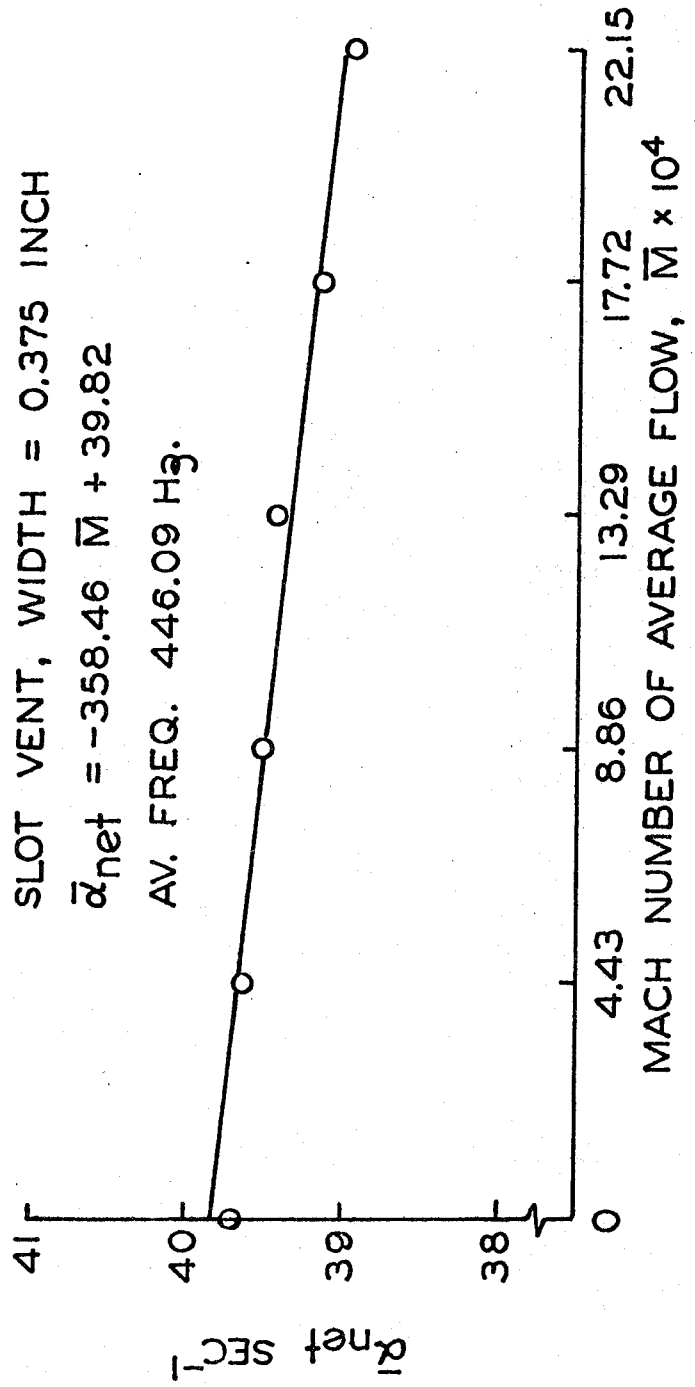

Figure 6.8 Net Values of Attenuation Constant, 0.375" Slot Vent, Frequency 446.09 Hz

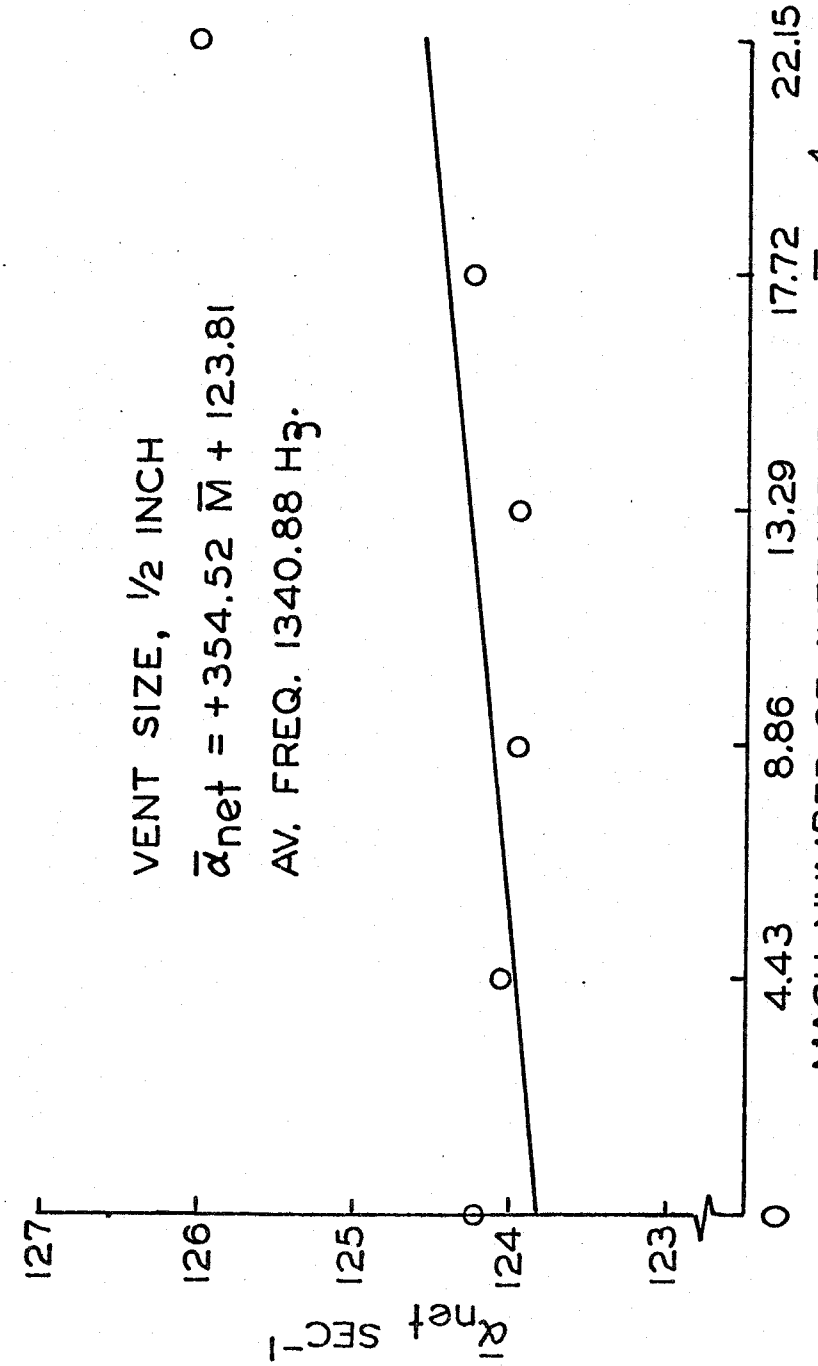

Figure 6.9 Net Values of Attenuation Constant, 1/2" Circular Vent, Frequency 1340.88 Hz

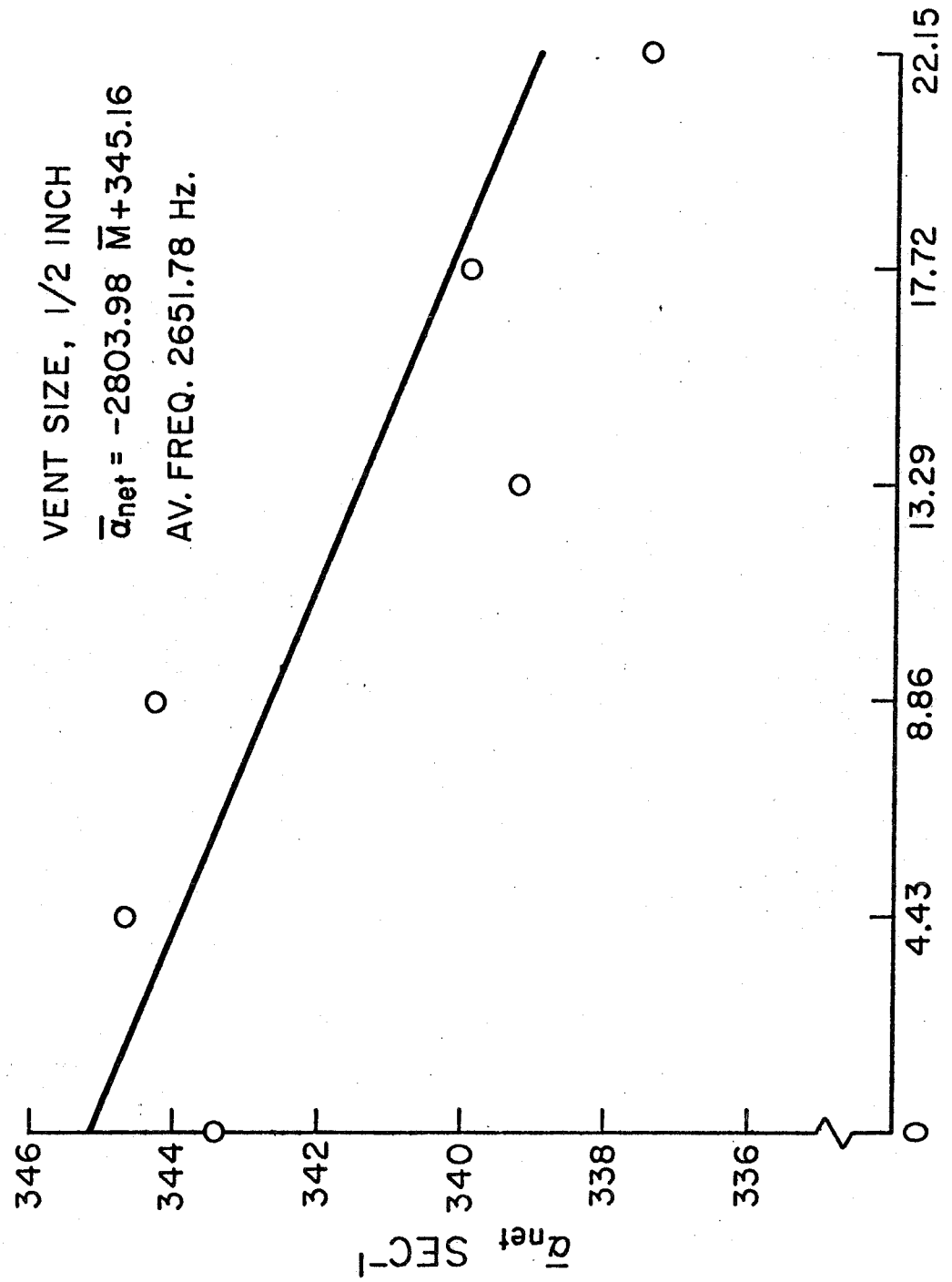

Figure 6.10 Net Values of Attenuation Constant, 1/2" Circular Vent, Frequency 2651.78 Hz

VII. STATISTICAL TREATMENT OF DATA AND ANALYSIS OF RESULTS

Because of the indirect method of determining the influence of the exhaust vent described earlier, and practical difficulties involved in measuring small quantities, a statistical approach was adopted to reduce some of the random errors. This chapter covers calculations of radiation losses through the vent; viscous and heat transfer losses at the tube wall together with internal consistency of data; and finally, the influence of the exhaust vent. Once again, rewriting the basic equation (4.1) for our cold flow resonance tube with axial flow only (see figure 4.2), we have:

$$\alpha_{net} = \alpha_b + \alpha_v + \alpha_d \qquad (7.1)$$

where

α_{net} net measured attenuation constant

α_b attenuation constant associated with admittance function A_b for porous plates on the face of pistons

α_v attenuation constant associated with the influence of the vent, to be determined

α_d attenuation constant associated with acoustic radiation losses and viscous and heat transfer losses along the lateral boundary.

According to sign convention used here, a negative value of the attenuation coefficient corresponds to a gain of acoustic energy and vice-versa. The average Mach number of the flow in each of the

branches of the cold flow resonance tube is denoted by $\overline{M}$ here.

7.1 Determination of Radiation Losses Through the Vent

For this case, and when there is no flow, flow Mach number $\overline{M} = 0$. There are two cases for which data have been taken: one for the vent closed and the second for the vent open. It should be recalled that the vent is closed with a plug machined to match smoothly with the internal boundary of the resonance tube. The value of α_b remains the same for the two cases, but the values of α_d differ by an amount due to radiation loss through the open vent given by α_{rad} (a positive number now). Hence,

$$(\alpha_{net})_{open} - (\alpha_{net})_{closed} = (\alpha_d)_{open} - (\alpha_d)_{closed} = \alpha_{rad} \tag{7.2}$$

The average values and standard deviations for three series of tests can be calculated for any measured number x using the formulas:

$$\overline{x} = \frac{1}{3}(x_1 + x_2 + x_3) \tag{7.3}$$

and

$$\sigma_x = \left\{ \frac{1}{3} \sum_{i=1}^{i=3} (x_i - \overline{x})^2 \right\}^{1/2} \equiv \Delta x \tag{7.4}$$

For this case:

$$\sigma^2_{rad} = (\alpha_{rad} - \overline{\alpha}_{rad})^2 = \sigma^2_{open} + \sigma^2_{closed} - \frac{2}{3} \sum_{i=1}^{i=3} (\alpha_{open} - \overline{\alpha}_{open})(\alpha_{closed} - \overline{\alpha}_{closed}) \tag{7.5}$$

Note that ($\bar{}$) here indicates the average of measured numbers. These results are given in table 7.1. As mentioned earlier, it was not possible to plug the slot vents easily and hence corresponding data cannot be deduced. At higher resonance frequencies of 1345 Hz and 2645 Hz, plugging of the vent seems to change the average resonating length between the pistons a great deal because the lengths of the resonance tubes are fairly small; this change seems to alter the subsequent resonance frequency. It was found that α_{net} is also affected by a small amount by this change. Hence it is very difficult to extract any meaningful data for these radiation losses. However, the experiments were conducted with great care. For the sake of comparison, the influences described above were neglected and data obtained were reduced and included in table 7.1.

7.2 Internal Consistency of the Data and Losses Through the Lateral Boundary

Consider the case of no average flow with the vent closed. Equation (7.1) becomes:

$$\alpha_{net} = \alpha_b + \alpha_d \tag{7.6}$$

Internal consistancy can be obtained by checking whether or not equation (7.6) can be satisfied experimentally. From the data taken with the impedance tube and no flow, α_b can be calculated using the equation (2.9):

$$\alpha_b = 4 \; f \; A_b^{(r)} \tag{7.7}$$

Equation (7.6) can be written with average values and standard deviation as:

TABLE 7.1

ATTENUATION CONSTANTS DUE TO RADIATION OF ACOUSTIC ENERGY FROM CIRCULAR EXHAUST VENTS

$\overline{f}$ (Hz)	$-\Delta\overline{f}/\Delta L$ (Hz/Inch)	Diameter (Inches)	$\overline{\alpha}_{rad}$ (sec^{-1})	σ_{rad} (sec^{-1})
445	29.25	1/2	0.06	0.38
		1	0.57	0.29
		1 1/2	1.05	0.58
1345	267.17	1/2	0.27	0.29
2645	1033.21	1/2	-1.70	0.57

$$\bar{a}_d \pm \Delta a_d = (\bar{a}_{net} \pm \Delta a_{net}) - 4\,\bar{f}(\bar{A}_b^{(r)} \pm \Delta A_b^{(r)}) \qquad (7.8)$$

Here $\bar{f}$ is the frequency at which the data were taken with the impedance tube experiments. As discussed in Appendix D, both Δf and contributions arising from it are relatively small and hence are neglected. In practice, the resonance frequency for each of the experiments performed with the resonance tube was found little different from the corresponding frequency at which the data were taken with the impedance tube. This is mainly due to building vibrations (and flow through the pistons, as discussed later). Moreover, electro-mechanical shakers have weak flexure (flexure stiffness 12 lb/inch) which seems to facilitate these changes. These errors and the associated changes in the end conditions at the pistons are unavoidable and great care was taken to reduce them. See Appendix D for further details. For the purpose of data reduction here, the following assumptions were made:

(i) The real part of the admittance function of the porous plates measured with experiments in the impedance tube is not affected by these small changes in the frequency.

(ii) The resonance curve wanders around the center resonance frequency (as determined by the average resonating length between the two pistons) without letting the total losses in the system be affected by it.

No special efforts were carried out to justify the first assumption,

but small values of $\Delta\alpha_{net}$ found for all the experiments seem to justify the second assumption. For $\overline{A}_b^{(r)}$ and $\Delta A_b^{(r)}$, averages of the values for the two porous plates are used.

The equation (7.8) can now be used to determine the losses represented by α_d, mainly viscous and heat transfer losses at the boundary and other losses at joints in the hardware and radiation through the tube wall. There have been doubts concerning the accuracy of the classical results discussed in Appendix C, equation (C-5). Experimental results given by reference 13 have usually been larger by roughly 10% than those predicted by the formula given by equation (C.5). However, recently very careful work reported in reference 14 has produced measured results within less than 1% of the theoretical values. Thus, we are justified in ignoring any errors associated with calculating the losses in the acoustic boundary layer. Assuming linearity, equation (7.8) becomes:

$$(\overline{\alpha}_d \pm \Delta\alpha_d)_{\substack{other \\ losses}} = (\overline{\alpha}_{net} \pm \Delta\alpha_{net}) - 4\,\overline{f}\,(\overline{A}_b^{(r)} \pm \Delta A_b^{(r)}) - \kappa\, a_o \qquad (7.9)$$

Table 7.2 summarizes the numerical values for all the resonance tubes with circular vents. As mentioned earlier, because of no provision for closing the slot vents, data for the slot cannot be treated similarly.

It is obvious from table 7.2 that "other losses" constitute approximately 4% to 17% of the total losses in the system. Larger values of "other losses" at higher frequencies tends to support the conjecture that the losses associated with the pistons fitting in the

TABLE 7.2

VERIFICATION OF THE DATA FOR CIRCULAR VENTS WITH NO FLOW, VENT CLOSED CASE

Description	$\overline{f}$ = 442.70 (Hz)			$\overline{f}$ = 1345 (Hz)	$\overline{f}$ = 2645 (Hz)
Diameter (inches)	1/2	1	1 1/2	1/2	1/2
$\overline{\alpha}_{net}(sec^{-1})$	41.71	39.88	41.34	123.96	345.15
$\Delta\alpha_{net}(sec^{-1})$	0.22	0.14	0.08	0.28	0.26
$\overline{A}_b^{(r)} \times 10^2$	1.5435	1.5435	1.54345	1.5639	2.7003
$\Delta A_b^{(r)} \times 10^6$	88	88	88	146	145.50
$Ka_o (sec^{-1})$	11.17	11.17	11.17	19.47	27.30
$(\overline{\alpha}_d)_{other\ losses}\ (sec^{-1})$	3.21	1.38	2.84	20.35	32.16
$(\Delta\alpha_d)_{other\ losses}\ (sec^{-1})$	0.38	0.30	0.24	1.07	1.80

teflon inserts at the ends of the resonance tube increases approximately linearly. The data taken were with the best efforts to minimize these numbers, using larger amounts of silicon oil to fill the cracks, and tightening the end quad seal to the face of the end cap as much as the smooth functioning of the pistons allows. See figure 5.4 for details. The influence of the "other losses" does not seem to affect the overall conclusion for α_v, as discussed later.

7.3 Determination of the Influence of the Exhaust Vents

The results for the influence of the exhaust vents will be discussed in two ways:

(i) data for $\bar{\alpha}_v$ as a function of Mach number $\bar{M}$

(ii) calculation of the slope $\frac{d\bar{\alpha}_v}{d\bar{M}}$ from data.

As discussed in Appendix D, $\bar{M}$ is treated as an independent parameter precisely known (i.e., $\Delta\bar{M} = 0$), and equation (7.1) can be written as:

$$(\bar{\alpha}_v \pm \Delta\alpha_v) = (\bar{\alpha}_{net} \pm \Delta\alpha_{net}) - 4\,\bar{f}\left\{(\bar{A}_b^{(r)} \pm \Delta A_b^{(r)}) + \bar{M}\right\} - (\bar{\alpha}_d \pm \Delta\alpha_d) \qquad (7.10)$$

As discussed earlier, $\bar{f}$ is the frequency at which the data were taken with the impedance tube and $\Delta f = 0$. For $\bar{A}_b^{(r)}$ and $\Delta A_b^{(r)}$, averages of the values for the two porous plates are used.

All the necessary data on the right hand side of equation (7.10) are known now from the experimental results and $\bar{\alpha}_v \pm \Delta\alpha_v$ can be calculated. Table 7.3 gives the values of the attenuation coefficient

TABLE 7.3

VALUES OF THE AVERAGE ATTENUATION COEFFICIENT AND STANDARD DEVIATION FOR CIRCULAR VENTS, FREQUENCY 442.70 Hz

Diameter (inches)	1/2		1		1 1/2	
$\overline{M} \times 10^4$	$\overline{\alpha}_v$ (sec^{-1})	$\Delta\alpha_v$ (sec^{-1})	$\overline{\alpha}_v$ (sec^{-1})	$\Delta\alpha_v$ (sec^{-1})	$\overline{\alpha}_v$ (sec^{-1})	$\Delta\alpha_v$ (sec^{-1})
0	+0.06	0.70	+0.57	0.89	+1.05	0.91
4.43	-0.59	0.85	-0.01	0.78	-0.04	1.08
8.86	-0.90	0.78	-0.92	0.58	-1.06	0.88
13.29	-1.15	0.72	-1.11	0.61	-1.35	0.93
17.72	-2.39	1.00	-1.97	0.88	-1.77	0.82
22.15	-3.15	0.73	-1.95	0.74	-2.36	0.86

and standard deviation for circular vents, sizes 1/2", 1" and 1-1/2" at the frequency of 442.70 Hz. Table 7.4 gives similar data for the circular vent, size 1/2" and at the frequencies of 1345 Hz and 2645 Hz. The results are plotted in figures 7.1 - 7.5

The dotted straight lines in figures 7.1 - 7.5 represent the theoretical variation of α_v given by:

$$\alpha_v = -4 f \overline{M} \tag{7.11}$$

Equation (7.11) was obtained by rewriting equation (3.8) for our case with the sign convention adoped in chapter 6. Here, in the absence of suitable theoretical calculations for acoustic energy losses associated with radiation through the centrally located vent, α_{rad} was assumed to be zero for the fundamental longitudinal mode of oscillation of the tube because of the presence of the node at the vent. The solid straight lines in figures 7.1-7.5 represent the equation:

$$\overline{\alpha}_v = \overline{\alpha}_{rad} + \overline{M} \frac{d\overline{\alpha}_v}{d\overline{M}} \tag{7.12}$$

The slope $\frac{d\overline{\alpha}_v}{d\overline{M}}$ can be computed by taking the derivative of equation (7.10) and it can be written as:

$$\frac{d\overline{\alpha}_v}{d\overline{M}} \pm \Delta\left(\frac{d\alpha_v}{d\overline{M}}\right) = \frac{d\overline{\alpha}_{net}}{d\overline{M}} \pm \Delta\left(\frac{d\alpha_{net}}{d\overline{M}}\right) - 4\overline{f}\left\{\left[\frac{d\overline{A}_b^{(r)}}{d\overline{M}} \pm \Delta\left(\frac{dA_b^{(r)}}{d\overline{M}}\right)\right] + 1.0\right\} \tag{7.13}$$

TABLE 7.4

VALUES OF THE AVERAGE ATTENUATION COEFFICIENT AND STANDARD DEVIATION FOR CIRCULAR VENT SIZE 1/2"

$\overline{f}$ (Hz)	1345		2645	
$\overline{M} \times 10^4$	$\overline{\alpha}_v$ (sec^{-1})	$\Delta\alpha_v$ (sec^{-1})	$\overline{\alpha}_v$ (sec^{-1})	$\Delta\alpha_v$ (sec^{-1})
0	+0.27	1.99	-1.70	3.67
4.43	-3.83	1.78	-7.14	3.87
8.86	-8.52	1.91	-11.36	4.59
13.29	-9.07	1.95	-16.04	3.07
17.72	-10.28	2.01	-15.71	3.89
22.15	-9.40	1.82	-21.52	4.84

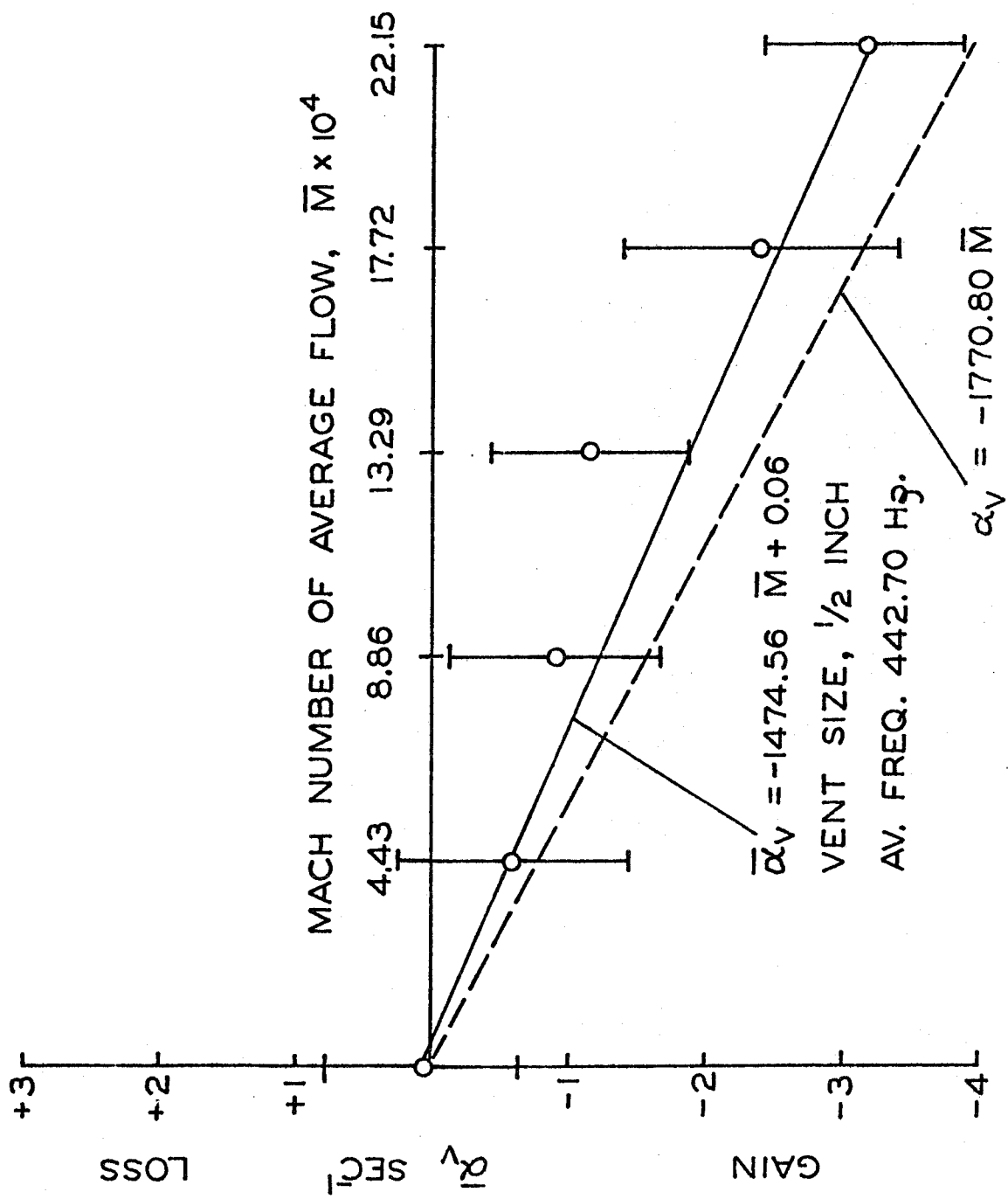

Figure 7.1 Attenuation Constant for 1/2" Circular Vent, Frequency 442.70 Hz

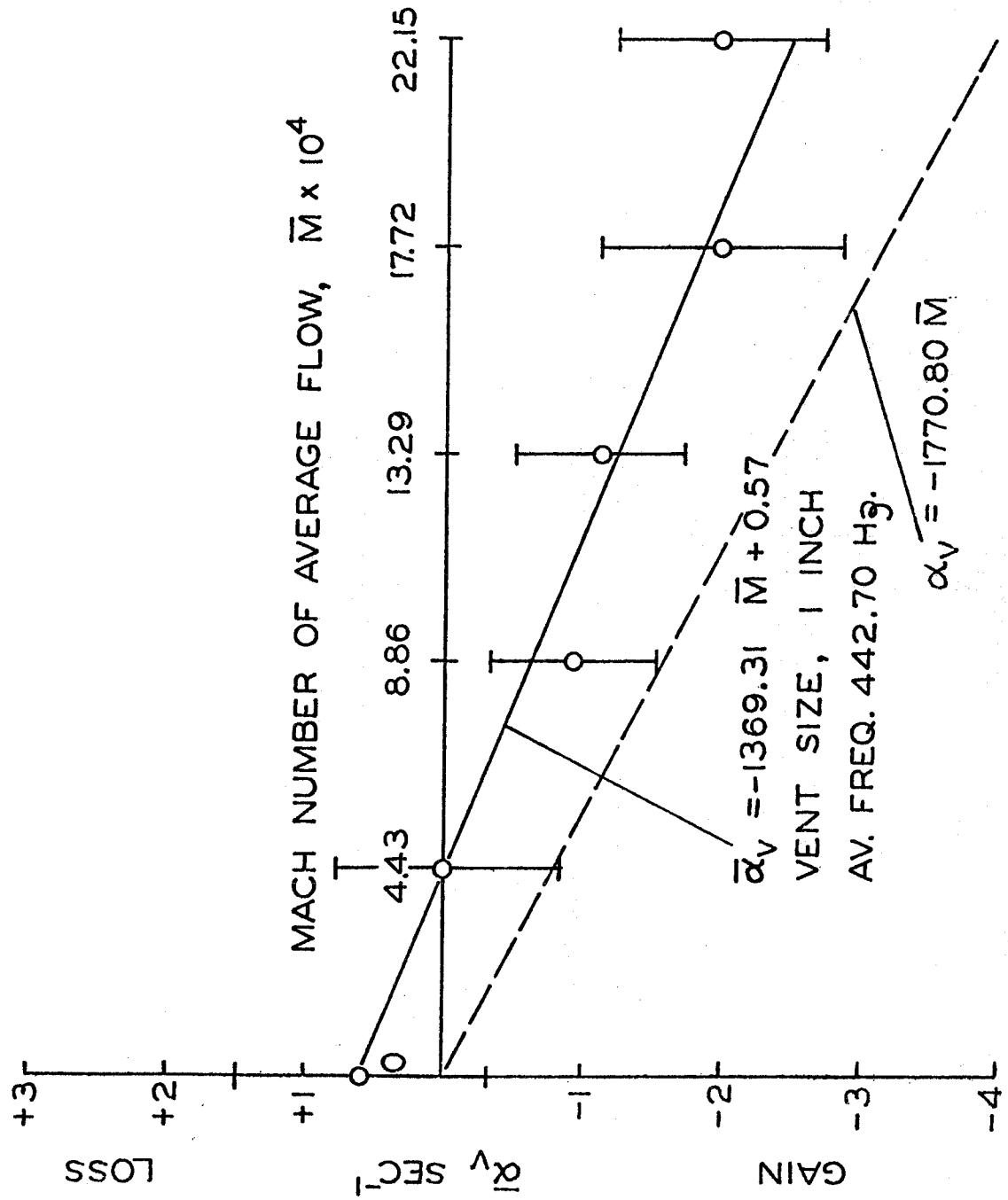

Figure 7.2 Attenuation Constant for 1"
Circular Vent, Frequency 442.70 Hz

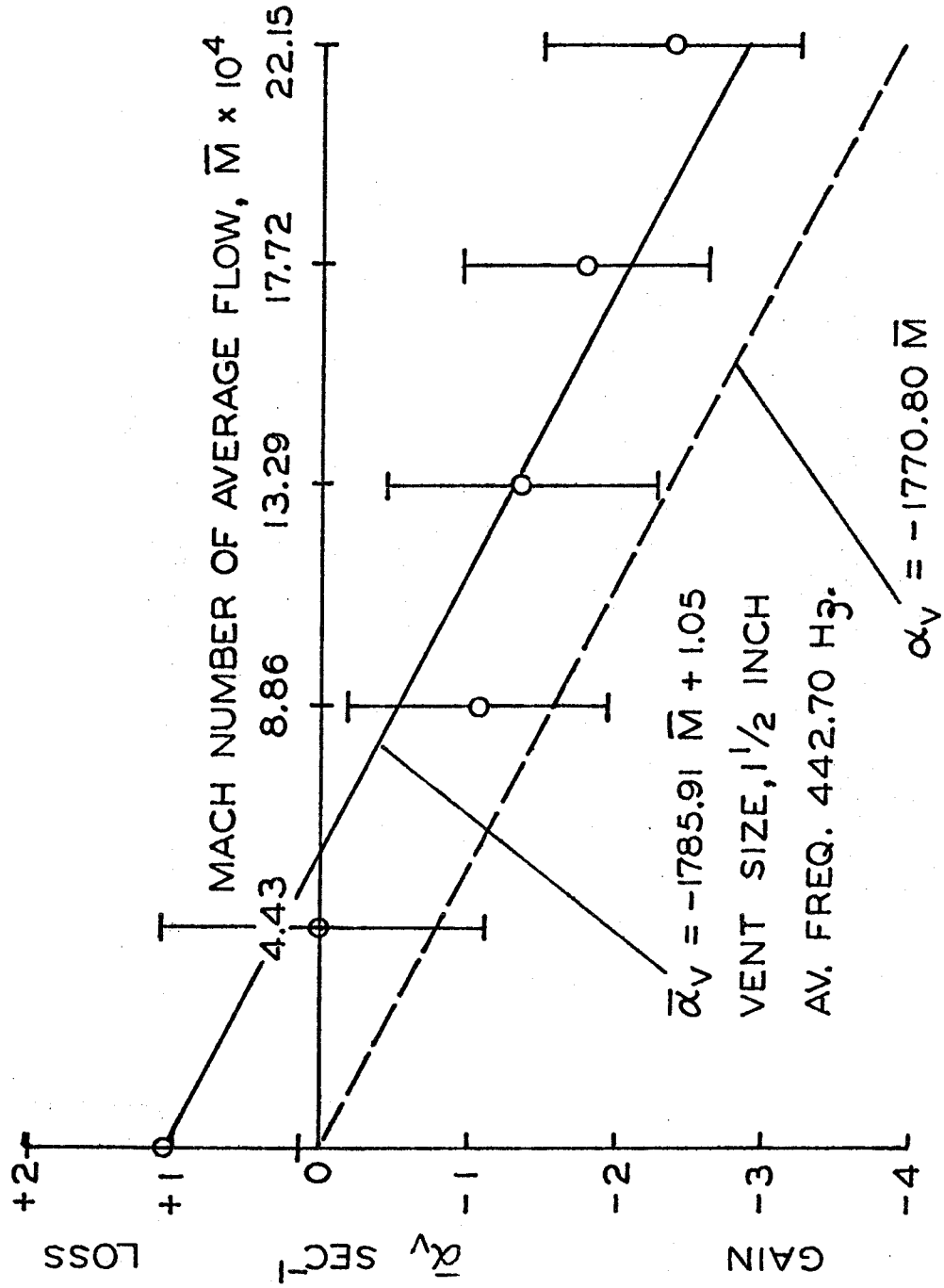

Figure 7.3 Attenuation Constant for 1 1/2" Circular Vent, Frequency 442.70 Hz

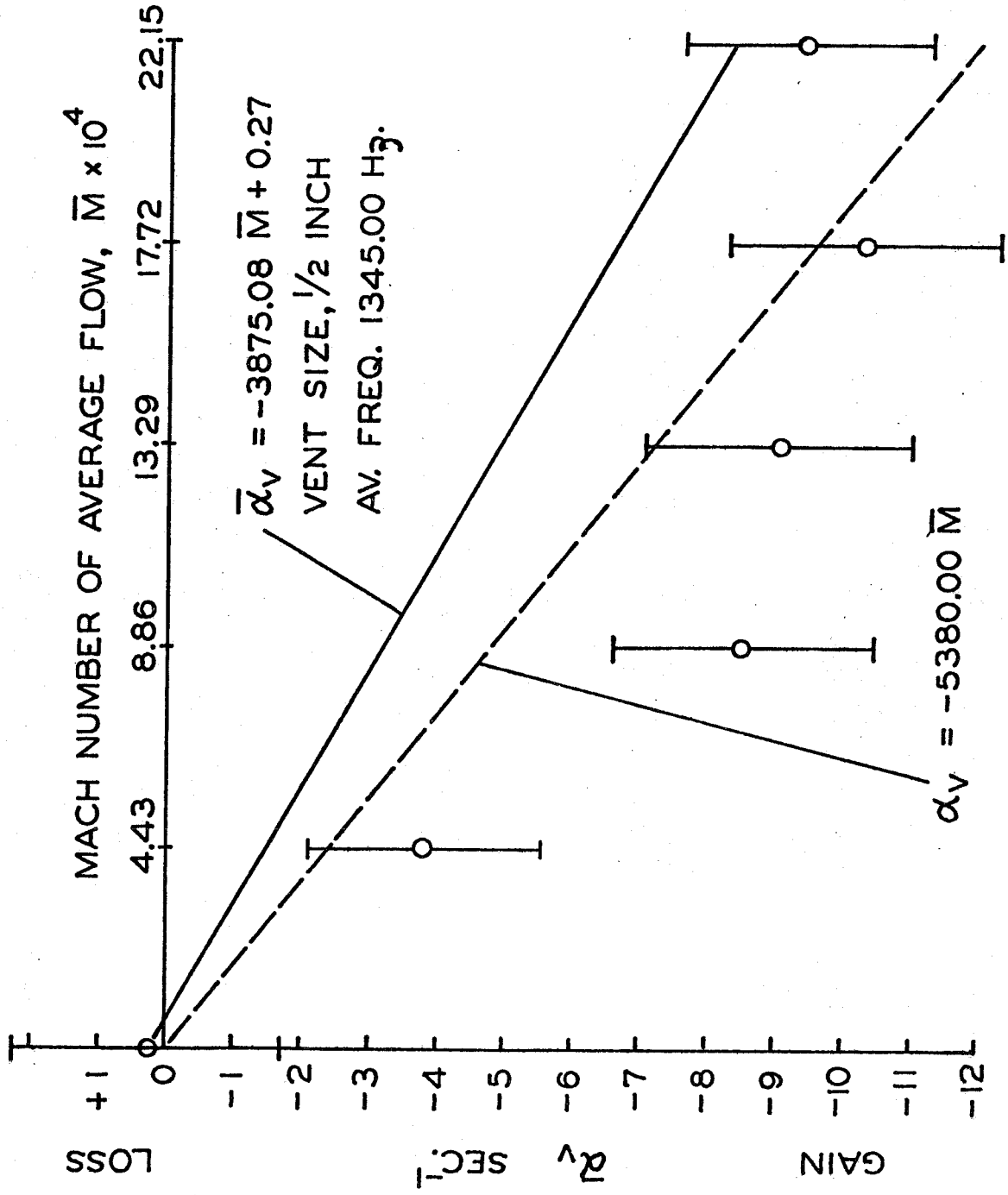

Figure 7.4 Attenuation Constant for 1/2" Circular Vent, Frequency 1345 Hz

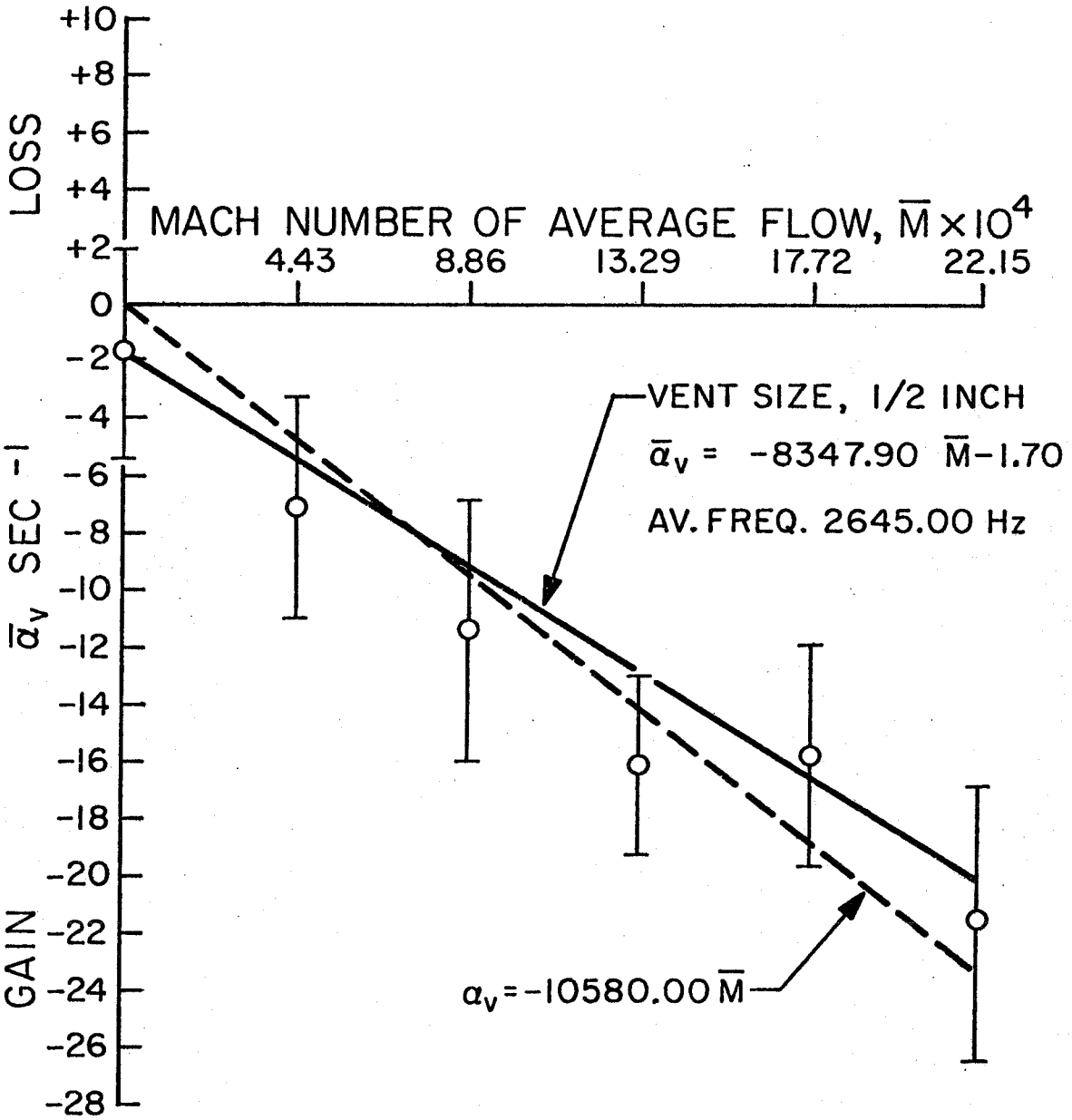

Figure 7.5 Attenuation Constant for 1/2" Circular Vent, Frequency 2645.00 Hz

Assume α_d is independent of $\bar{M}$. Standard deviations on the slope are calculated according to the technique discussed in reference 15. For

$$\frac{d\bar{A}_b^{(r)}}{d\bar{M}} \quad \text{and} \quad \Delta\left(\frac{dA_b^{(r)}}{d\bar{M}}\right),$$

averages of the values for the two porous plates are taken. Frequency $\bar{f}$, once again is taken as the frequency at which the data were taken with the impedance tube. $\bar{\alpha}_{rad}$ here corresponds to radiation losses through the vent for the case of no flow as measured experimentally. See §7.1 for further details. Table 7.5 lists the slope and variation on the slope for $\bar{\alpha}_v$ with respect to the Mach number for all five different vents tested at the frequency of 442.70 Hz. Table 7.6 gives similar results for the 1/2" circular vent tested at the frequencies of 1345 Hz and 2645 Hz.

TABLE 7.5

SLOPES AND STANDARD DEVIATION OF THE ATTENUATION CONSTANT FOR FIVE DIFFERENT EXHAUST VENTS, FREQUENCY 442.70 Hz

	$\frac{d\bar{\alpha}_v}{d\bar{M}}$ (sec^{-1})	$\Delta\left(\frac{d\alpha_v}{d\bar{M}}\right)$ (sec^{-1})
Circular Vent Diameter (inches)		
1/2	-1474.56	333.02
1	-1369.31	252.03
1 1/2	-1785.91	196.57
Slot Vent Width (inches)		
0.167	-1272.57	184.97
0.375	-1619.67	171.95

TABLE 7.6

SLOPES AND STANDARD DEVIATION OF THE ATTENUATION CONSTANTS FOR TWO CIRCULAR EXHAUST VENTS SIZE 1/2"

$\bar{f}$ (Hz)	$\frac{d\bar{\alpha}_v}{d\bar{M}}$ (sec^{-1})	$\Delta\left(\frac{d\alpha_v}{d\bar{M}}\right)$ (sec^{-1})
1345	-3875.08	1309.10
2645	-8347.90	2057.76

VIII. THEORETICAL CALCULATIONS AND THEIR COMPARISON WITH EXPERIMENTAL RESULTS

8.1 Calculated Values Using the One-Dimensional Approximations

Rewriting equation (3.8) for our cold flow resonance tube with the sign convention adopted in chapter 6,

$$\alpha_v = -4 f \overline{M} + \alpha_{rad} \tag{8.1}$$

As discussed earlier in section 7.3, theoretical value of α_{rad} was assumed to be zero for our case and equation (8.1) hence can be written as

$$\alpha_v = -4 f \overline{M} \tag{8.2}$$

also,

$$\frac{d\alpha_v}{d\overline{M}} = -4 f \tag{8.3}$$

Further (α_v/f) can be regarded as a reduced attenuation coefficient for the vent, and its relation with the average Mach number of the flow can be given by

$$(\alpha_v/f) = -4 \overline{M} \tag{8.4}$$

These are the simple results we wish to check. The three major features of the above equations are:

(i) The vent produces a gain α_v, proportional to the average Mach number of the flow in the main chamber.

(ii) The gain is proportional to the frequency of the funda-

mental longitudinal mode.

(iii) The gain is independent of the size and shape of the vent.

Theoretical calculations can be carried out using the equations (8.2), (8.3) and (8.4). Table 8.1 gives typical numbers for the absolute values of α_v as a function of both fundamental frequency f and flow Mach number $\overline{M}$. Table 8.2 gives typical values of the slope representing the variation of α_v with flow Mach number $\overline{M}$. Table 8.3 gives results for the reduced attenuation coefficient for the exhaust vent as a function of the average Mach number of the flow.

8.2 Comparison of Theoretical Calculations with Experimental Results

Chapter 7 describes the experimental results obtained for the influence of the exhaust vent for various different operating parameters including the resonance frequency of the tube; flow Mach number, and different sizes and shapes of the circular vents.

Let us look more closely at the results given in tables 7.1 - 7.6 and tables 8.1 and 8.2. Comparing the results at the frequency near 445 Hz reveals the fact that for the case of no flow, one-dimensional calculations fail to estimate the radiation of acoustic energy from the exhaust vents. Experiments show that (see table 7.1) for circular vents, this radiation loss represented by α_{rad}, increases with the diameter of the vent, which is obvious. There is no suitable theoretical calculation to determine the radiation loss. The large uncertainty observed in obtaining these numbers

TABLE 8.1

VARIATION OF ABSOLUTE VALUES OF α_v AS A FUNCTION OF BOTH FREQUENCY f AND FLOW MACH NUMBER $\overline{M}$

Frequency (Hz)	Flow Mach Number $\overline{M} \times 10^4$	α_v (sec^{-1})
445	0	0
	4.43	- 0.79
	8.86	- 1.58
	13.29	- 2.37
	17.72	- 3.15
	22.15	- 3.94
1345	0	0
	4.43	- 2.38
	8.86	- 4.77
	13.29	- 7.15
	17.72	- 9.53
	22.15	-11.92
2645	0	0
	4.43	- 4.69
	8.86	- 9.37
	13.29	-14.06
	17.72	-18.75
	22.15	-23.43

TABLE 8.2

VALUES OF THE SLOPE REPRESENTING VARIATION OF α_v WITH $\overline{M}$

Frequency	$\frac{d\alpha_v}{d\overline{M}}$ (sec^{-1})
442.70	- 1770.80
1345	- 5380.00
2645	-10580.00

TABLE 8.3

VALUES OF (α_v/f) AS A FUNCTION OF THE AVERAGE MACH NUMBER OF THE FLOW USING EQUATION (8.4)

$\overline{M} \times 10^4$	$(\alpha_v/f) \times 10^4$
0	0
4.43	-17.72
8.86	-35.44
13.29	-53.16
17.72	-70.88
22.15	-88.60

experimentally was due to the fact that the alignment of the whole resonance tube system was affected by the weight of the vent plug used to plug the vent itself. This leads to some changes in the end conditions at the quad seals at the end of the tube (see figure 5.4 for detail) producing changes both in the resonance frequency and in the values of α_{net}. In spite of this unavoidable difficulty, the trend of the results is reasonable. These results could not be obtained for the slot vents because of the practical difficulty in plugging the slot vents. For the resonance frequency of 1345 Hz, α_{rad} is more, as expected. For the resonance frequency of 2645 Hz, α_{rad} was measured to be a gain. This experimental error is extremely difficult to avoid just because $-\Delta f/\Delta L$ is around 1000 for this case. Also, any vibrational disturbances and plugging of the vent cause a substantial change in both the resonance frequency and in the end conditions at the pistons, making measurement of α_{rad} very difficult.

Table 7.2 gives values of $(\overline{\alpha}_d)_{\substack{other \\ losses}}$. These are indicative of the inherent errors due to losses associated with the piston fitting in the teflon insert at the end of the resonance tube. All the results reported here were obtained after minimizing these losses. These losses increase approximately linearly with the resonance frequency. Assuming that these losses are not affected by the flow through the pistons, their influence does not seem to affect the overall conclusions discussed below.

Comparison of the absolute values of α_v at various resonance

frequencies shows that (see tables 7.3, 7.4 and 8.1) the one-dimensional formula predicts these numbers fairly well. The actual process involved in the flow turning at the exhaust vent is three-dimensional and the one-dimensional results can be accepted as a reasonably good first approximation. Table 7.3 shows that the values of a_v are approximately independent of the size of the circular vent at a given resonance frequency, which is also a characteristic of the one-dimensional results.

Another interesting number to be compared with the one-dimensional prediction is the slope, $\frac{da_v}{d\bar{M}}$ representing the variation of a_v with flow Mach number. The experimental data in tables 7.5, 7.6 and 8.2 show that for a given frequency and size of vent, values of $\frac{da_v}{d\bar{M}}$ found from experiments are within 30% of the value predicted by the one-dimensional analysis. The slope is also found to be independent of size and shape of the vent at a given frequency as implied by the one-dimensional formula. This slope also scales with increase in resonance frequency within 30% of the prediction.

From the results described in tables 7.3 and 7.4, reduced attenuation coefficient for the vent can be computed. Table 8.4 gives these computed values of the reduced attenuation coefficients for different circular vents and frequencies as a function of the average Mach number of the flow. A graph is then plotted for the reduced attenuation constant ($\bar{a}_v/f$) vs. average Mach number of the flow for all of the circular vents. Figure 8.1 shows such a plot. The solid line represents the results obtained from the one-dimensional

TABLE 8.4

VALUES OF $(\overline{a}_v/\overline{f})$ AS A FUNCTION OF THE AVERAGE MACH NUMBER OF THE FLOW AS OBTAINED FROM THE EXPERIMENTS WITH CIRCULAR VENTS

Frequency Hz	$\overline{M} \times 10^4$	$(\overline{a}_v/\overline{f}) \times 10^4$		
		Dia. 1/2"	Dia. 1"	Dia. 1-1/2"
	0	+ 1.36	+12.88	+23.72
	4.43	-13.33	- 0.23	- 0.90
	8.86	-20.33	-20.78	-23.94
442.7	13.29	-25.98	-25.07	-30.49
	17.72	-53.99	-44.50	-39.98
	22.15	-71.15	-44.05	-53.31
	0	+ 2.01		
	4.43	-28.98		
	8.86	-63.35		
1345	13.29	-67.43		
	17.72	-76.43		
	22.15	-69.89		
	0	- 6.43		
	4.43	-26.99		
	8.86	-42.95		
2645	13.29	-60.64		
	17.72	-59.40		
	22.15	-81.36		

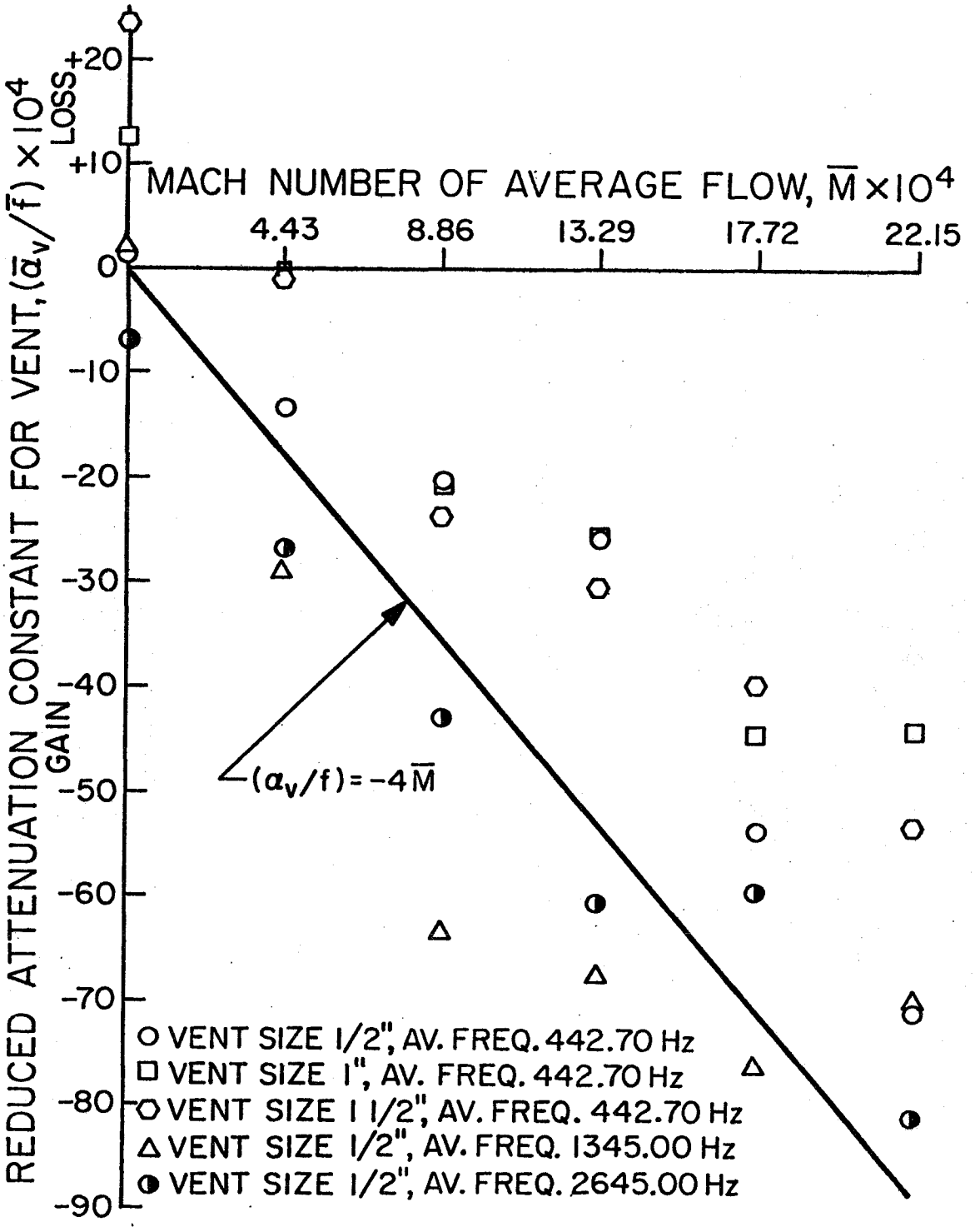

Figure 8.1 Reduced Attenuation Constant for Vent as a Function of Average Mach Number of the Flow

formula as described by equation (8.4). The approximate agreement of experimental data with the one-dimensional calculation given by equation (8.4) is obvious from this plot. Much better agreement can be obtained if the correction corresponding to the reduced attenuation constant due to α_{rad} is applied to that due to α_{v}. But, because of the uncertainties mentioned earlier in the measurements of α_{rad}, and the uncertainty of the approximation used in equation (3.3), this was not attempted here.

IX. CONCLUSIONS

The most significant conclusion of this work is the experimental demonstration that a subsonic exhaust vent in the lateral boundary of a cold flow resonance tube provides a gain of acoustic energy for the fundamental mode within the resonance tube. For all the cases tested, the gain of acoustic energy increases approximately linearly with the Mach number, as predicted by the one-dimensional analysis. The one-dimensional results give the values for the slope representing the variation of the attenuation coefficient of the exhaust vent with respect to the average Mach number of the flow within roughly 30% of those measured. Three main features of the theoretical behavior have been verified: the subsonic vent produces a gain proportional to the average Mach number; proportional to the frequency; and independent of the shape. The major uncertainties on the experimental results for α_v are mainly due to the limitations of the present apparatus. Much better results and accuracies can be obtained with the following modifications:

(i) complete vibration isolation of the anechoic chamber from its surroundings

(ii) improved alignment techniques and

(iii) stiffer electro-mechanical shakers.

The fundamental purpose of these experiments with acoustics at ambient temperature is to establish the validity of theoretical results which are purely acoustical. Then when tests involving combustions are carried out on the T-burners, the acoustical aspect of the prob-

lem is known well. Truly unknown contributions associated with the combustion processes can then be concentrated upon. In particular, the influence of the exhaust vent has been a serious source of uncertainty in the interpretation of data taken with T-burners. It appears now that that part of the problem has been clarified, and that data taken with T-burners should be treated accordingly.

The values for α_v found here (say near the frequency of 445 Hz) are quite small, less than 5 sec^{-1}, because we have used rather small total mass flow. For the T-burners commonly used in practice, the total mass flux may be 5 - 10 times larger than the values used here. Consequently, according to equation (8.1), the values of α_v may be 5 - 10 times larger, around 25 - 50 sec^{-1}. But the net values of the growth constant observed in T-burner testing are commonly in this range. The contribution of the vent is therefore obviously an important consideration and hence cannot be neglected.

LIST OF SYMBOLS

a_o	speed of sound
A	defined by equation (C. 4)
A_b	admittance function of burning propellant or porous plate
B	defined by equation (C. 4)
C_v	specific heat of gases
D	diameter of the resonance or impedance tube
D_{nn}	damping constant defined by equation (B. 16)
e_o	stagnation internal energy of gases
e_{os}	value of e_o at the edge of the combustion zone
$\mathcal{E}$	acoustic energy density
E_n^2	$E_n^2 = \int \psi_n^2 dV$
E_{nn}	constant appearing in equation (B. 16)
f	resonance frequency, also right hand side of equations (A. 12) and (B. 2), also coefficient of friction as described in equation (3. 2)
F_n	forcing function defined by equation (B. 7)
G	function defined by equation (B. 22)
h	right hand side of equations (A. 10) and (B. 1)
h_o	stagnation enthalpy of the gases in the chamber
h_{os}	value of h_o at the edge of the combustion zone
i	complex number defined by $\sqrt{-1}$
k	complex wave number defined by equation (2. 2), also see equation (C. 2)
k_ℓ	wave number for the ℓth normal mode given by $\ell\pi/L$
L	length of the resonance tube

L_o	displacement of a cylindrical grain, see figure A.3
L_b	length of grain along the lateral boundary, see figure A.3
m_b	mass flux of gases inward at the burning surface
m_v	mass flux through vent
$\overline{M}$	average Mach number of the flow in resonance tube
$\overline{M}_b$	Mach number of the gases at the edges of the combustion zone, $\overline{M}_b = u_b/a_o$
$\vec{n}$	unit normal vector outward at a boundary
$\hat{p}_\ell$	spatial mode shape of pressure for the ℓth longitudinal mode
$\hat{p}_N$	spatial mode shape of pressure for the Nth three-dimensional mode
p_o	stagnation pressure
p	static pressure, see equation (3.2)
P_1	function defined by equation (A.9)
Pr	Prandtl number for the gases in the chamber
q	perimeter of the chamber cross section
Q	heat released in homogeneous reaction
$\vec{r}$	space vector
R	radius of the resonance or impedance tube
R_b	response function of the propellant
R_o	mass averaged gas constant
$\mathcal{R}$	ratio defined by equation (C.18)
s	entropy of the gases in the chamber
S_b	area of the burning surface in one half of a T-burner or resonance tube
S_{bs}	area of burning surface on the lateral boundary in one half of a T-burner, see figure A.3

S_c	cross section area of the resonance tube
t	time
T	temperature of gases in the chamber
T_s	temperature of gases at the burning surface
ΔT	$T - T_s$
u	axial speed of gases
u_a	acoustic velocity
u_b	speed of gases entering at the burning surface
u_s	axial speed of gases at the burning surface
u_p	velocity of piston
V	volume of the chamber, also velocity of gas described in equation (3.2)
w	mass rate of flow of gas stream as described in equation (3.2)
w_g	injected gas as described in equation (3.2)
y_g	V_g'/V as described in equation (3.2)
z	coordinate parallel to the axis of a T-burner (or resonance tube), z = 0 at the left hand side
α	attenuation constant
α_b	attenuation constant associated with porous plate
α_{be}	attenuation constant associated with end burning propellant
α_{bs}	attenuation constant associated with the burning surface on the lateral boundaries of the combustion chamber
α_d	attenuation constant for radiation and viscous losses
α_{ft}	attenuation constant associated with the flow turning losses
α_{net}	net measured attenuation constant as defined by equation (4.1)

α_o	defined by equation (C.8)
α_{rad}	attenuation constant associated with radiation losses through the exhaust vent with $\overline{m}_v = 0$ as defined by equation (3.3)
α_v	attenuation constant for the exhaust vent, see Chapter 6 for sign convention, also see equation (3.3)
β_o	defined by equation (C.8)
γ	ratio of specific heats of gas
λ	wave length of oscillation
λ_c	coefficient of heat transfer of gas
η_n	amplitude of nth mode of oscillation
κ	defined by equation (C.5)
σ	standard deviation
ψ	mode shape, also see equation (C.8)
μ	coefficient of viscosity
ω	angular frequency of longitudinal mode
$\tilde{\omega}$	defined by equation (A.16), also see equation (B.20) for modal description
ν	kinematic viscosity
ρ	density of gas
ρ_o	stagnation density of gas

Subscripts and Superscripts

$\bar{(\ )}$	time average for theoretical work, also statistical average for the purpose of data reduction
$\dot{(\ )}$	time derivative
$\vec{(\ )}$	vector quantity
$\hat{(\ )}$	amplitude $\phi' = \hat{\phi}\, e^{i\omega t}$
$(\ )'$	fluctuation

$( )^r$	real part
$( )^i$	imaginary part
$( )^*$	complex conjugate
$( )_i$	value for the i th longitudinal mode
$( )_\ell$	value for the ℓ th longitudinal mode
$( )_n$	value for the n th longitudinal mode
$( )_N$	value for the N th three-dimensional mode
$\Delta( )$	standard deviation of
$\nabla( )$	gradient of
$\lvert\ \rvert$	absolute value
$d( )$	element of

REFERENCES

1. Culick, F.E.C., "Research on Combustion Instability and Application to Solid Propellant Rocket Motors", AIAA Paper No. 71-753, AIAA/SAE 7th Propulsion Joint Specialist Conference (June 1971).

2. Culick, F.E.C., "Research on Combustion Instability and Application to Solid Propellant Rocket Motors", AIAA Paper No. 72-1049, AIAA/SAE 8th Joint Propulsion Specialist Conference (December 1972).

3. Perry, E.H., "Investigations of the T-burner and its Role in Combustion Instability Studies", Ph.D. Thesis, California Institute of Technology, Pasadena, California (May 1970).

4. Derr, R.L., "Evaluation of a Variable Area T-burner for Metallized Propellants", AFRPL-TR-72-97, Lockheed Propulsion Company, Redlands, California (February 1973).

5. Culick, F.E.C. (Ed.), "T-burner Testing of Metallized Solid Propellants, Final Report", AFRPL-TR-74-28, California Institute of Technology, Pasadena, California (October 1974).

6. Culick, F.E.C., "The Stability of One-Dimensional Motions in a Rocket Motor", Combustion Science and Technology, Vol. 7, (1973), pp. 165 - 175.

7. Culick, F.E.C., "Stability of Three-Dimensional Motions in a Combustion Chamber", Combustion Science and Technology, Vol 10, (1975), pp. 109 - 124.

8. Shapiro, A.H., The Dynamics and Thermodynamics of Compressible Fluid Flow, Vol. 1, Ronald Press Company, New York, (1953),

REFERENCES (CONT'D)

pp. 225 ff.

9. Culick, F.E.C., "Remarks on Calculating the Energy Losses Associated with an Acoustic Boundary Layer Having a Normal Mean Flow", (unpublished).

10. Culick, F.E.C., "Remarks on Entropy Production in One-Dimensional Approximation to Unsteady Flow in Combustion Chambers", Combustion Science and Technology, Vol. 15, (1977), pp. 93 - 97.

11. Culick, F.E.C. and Dehority, G.L., "An Analysis of Axial Acoustic Waves in a Cold Flow Rocket", NWC TP 4544, Naval Weapons Center, China Lake, California (May 1968).

12. Auerbach, J.M., "Experimental Studies of the Noise Produced in a Supersonic Nozzle by Upstream Acoustics and Thermal Disturbances", Ph.D. Thesis, California Institute of Technology, Pasadena, California (March 1975).

13. Henderson, M.C. and Donnelly, G.J., "Acoustic Resonance Tube for High Pressure and Low f/b", Journal of Acoustical Society of America, Vol. 34, No. 6, (June 1962), pp. 779 - 784.

14. Quinn, T.J., Cololough, A.R. and Chandler, T.R.D., "A New Determination of the Gas Constant by an Acoustic Method", Philosophical Transactions, Vo. 283, No. 11, (November 1976), pp. 367 - 420.

15. Young, H.D., Statistical Treatment of Experimental Data, McGraw-Hill Book Company Inc., New York, (1962), pp. 122 ff.

16. Culick, F.E.C., "Non Linear Behavior of Acoustic Waves in

REFERENCES (CONT'D)

Combustion Chambers - I", Acta Astronautica, Vol. 3, (1976), pp. 715 - 734.

17. Culick, F.E.C., "Non Linear Behavior of Acoustic Waves in Combustion Chambers - II", Acta Astronautica, Vol. 3, (1976), pp. 735 - 757.

18. Morse, P.M., Vibration and Sound (2nd Edition), McGraw-Hill Book Company, New York, (1948), pp. 242 ff.

APPENDIX A. LINEAR STABILITY ANALYSIS

Chapter 2 is a brief summary of linear analytical techniques for combustion instability problems related to solid propellant rocket motors, including T-burners. Here we treat in greater detail both one-dimensional and three-dimensional approaches to the problem. The primary sources for this discussion are references 5, 6 and 7.

A. 1 One-Dimensional Stability Analysis

Figures (A. 1), (A. 2) and (A. 3) show typical combustion chambers. Though the simplest geometry is selected here, analytical procedures discussed below may be applied to any practical geometry.

The basic assumptions used are:

(1) The gases are treated as a single component "average gas" having constant specific heat and obeying the law of perfect gas.

(2) Viscous forces and heat transfer within the gas are ignored.

(3) Particulate matter is treated in an average way as a fluid.

(4) The average Mach number of the flow is assumed to be small and the acoustic Mach number is assumed to be smaller yet. The limit $M'/\overline{M}_b \to 0$ defines the problem of linear stability.

With these assumptions, the central idea of linear analysis

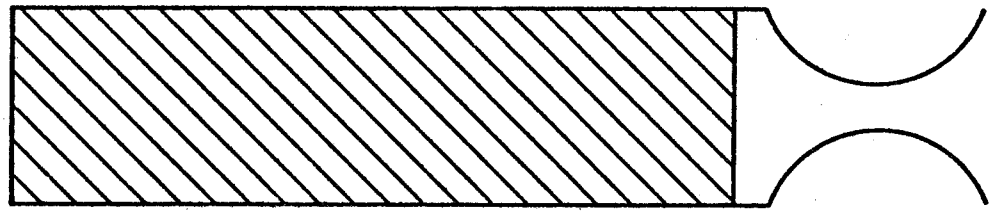

(a) End Burning Propellant Grain

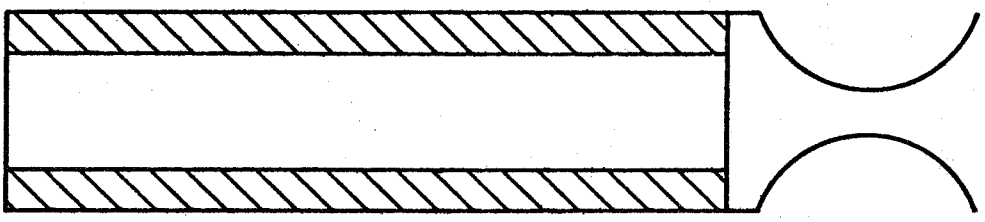

(b) Tubular Burning Propellant Grain

Figure A. 1 Sketches of Typical Solid Propellant Rocket Motors

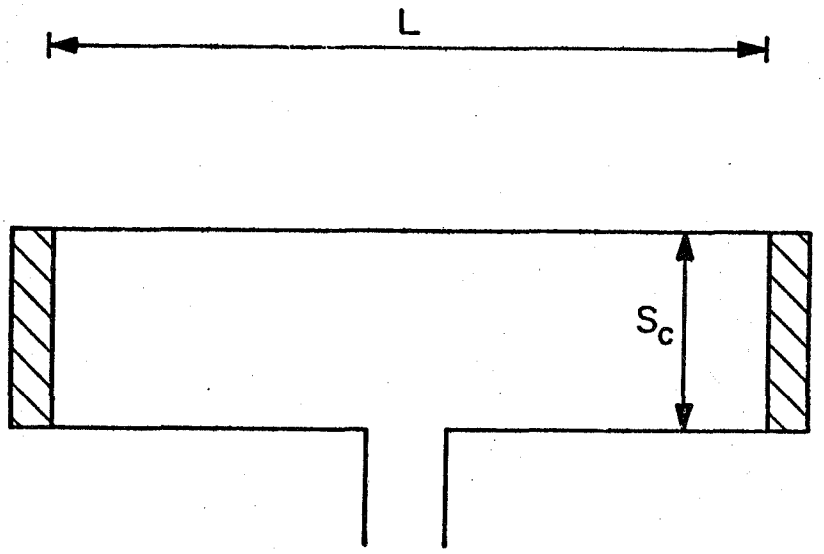

Figure A.2 Sketch of Typical T-Burner with Disc Type of End Burning Propellant Grain

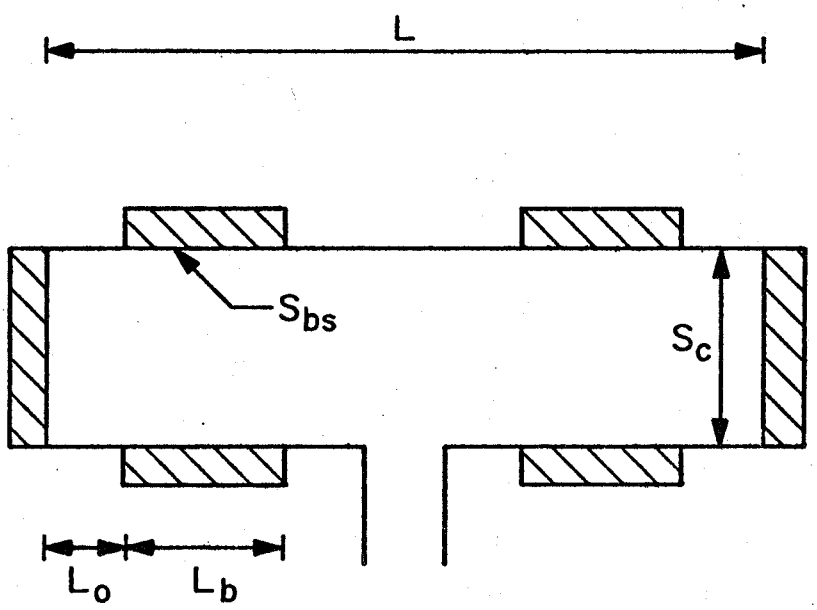

Figure A.3 Sketch of Typical T-Burner with Cylindrical and Disc Type of Propellant Grains

boils down to treating the influence of combustion and flow as perturbations of an acoustic problem in a closed chamber. The simplest unperturbed problem is of pure longitudinal acoustic waves in a uniform tube. Then the perturbations to this problem include the mean flow; the combustion at the burning surface of the propellant; residual combustion within the volume of the chamber; the influence of condensed material in the gas; and the exhaust nozzle. Here we will treat the most simple problem leading to flow turning losses in general and influence of the exhaust vent in particular. We will restrict ourselves to a constant area duct of cross section S_c and much simpler propellant grains without particulate matter.

With these assumptions, governing conservation equations are (see reference 6):

Conservation of mass

$$S_c \frac{\partial}{\partial t}(\rho) + S_c \frac{\partial}{\partial z}(\rho u) = \int m_b \, dq \qquad (A.1)$$

where z is an axial coordinate and velocity u is in z direction. m_b is the normal mass flux of the gases inward at the burning surface and q is the perifery.

Conservation of momentum

$$S_c \frac{\partial}{\partial t}(\rho u) + S_c \frac{\partial}{\partial z}(\rho u^2) + S_c \frac{\partial p}{\partial z} = 0 \qquad (A.2)$$

Because the flow is normal to the surface, its axial momentum is zero.

Conservation of energy

$$S_c \frac{\partial}{\partial t}(\rho e_o) + S_c \frac{\partial}{\partial z}\left[(\rho u e_o)\right] + S_c \frac{\partial}{\partial t}(pu)$$

$$= \int h_{os}\, m_b\, dq + Q\, S_c \qquad (A.3)$$

where Q is the heat released in homogenous reaction in gas phase (energy/vol. sec).

Using equation (A. 1), equation (A. 2) can be rewritten as:

$$\rho \frac{\partial u}{\partial t} + \rho u \frac{\partial u}{\partial z} + \frac{\partial p}{\partial z} = -\frac{u}{S_c} \int m_b\, dq \qquad (A.4)$$

An equation for the pressure is formed by combining the continuity, momentum and energy equations, with appropriate use of the equation of state for a perfect gas. First, by subtracting u times (A. 4) from equation (A. 3), the energy equation for temperature can be written with $de = C_v dT$ as:

$$C_v\left[\frac{\partial}{\partial t}(\rho T) + \frac{\partial}{\partial z}(\rho u T)\right] + p \frac{\partial u}{\partial z}$$

$$= \frac{C_v T}{S_c} \int m_b\, dq + \frac{1}{S_c} \int m_b\, (h_{os} - e_o)\, dq$$

$$+ \frac{u^2}{S_c} \int m_b\, dq + Q \qquad (A.5)$$

Now adding $C_v T$ times continuity equation (A. 1) to equation (A. 5) we get:

$$\frac{\partial p}{\partial t} + u\frac{\partial p}{\partial z} + \gamma p \frac{\partial u}{\partial z} = \frac{R_o}{C_v}\frac{1}{S_c}\int \left[h_{os} - e_o + C_v T \right] m_b \, dq$$

$$+ \frac{R_o}{C_v}\frac{1}{S_c} u^2 \int m_b \, dq + Q \qquad \text{(A. 6)}$$

The expansion procedure is now applied to both equations (A. 4) and (A. 6). To first order in both amplitude of unsteady motions and Mach number of the mean flow, we have (see reference 6):

$$\rho_o \frac{\partial u'}{\partial t} + \frac{\partial p'}{\partial z} = -\rho_o \frac{\partial}{\partial z}(\bar{u}\, u') - \frac{u'}{S_c}\int \overline{m_b} \, dq \qquad \text{(A. 7)}$$

$$\frac{\partial p'}{\partial t} + \gamma p_o \frac{\partial u'}{\partial z} = -\bar{u}\frac{\partial p'}{\partial z} - \gamma p' \frac{\partial}{\partial z}(\bar{u}) + P_1' \qquad \text{(A. 8)}$$

Where P_1' is the fluctuation of:

$$P_1 = \int \left[a^2 + \gamma R_o \Delta T + \frac{R_o}{2C_v}(u_b^2 - u^2) \right] m_b \, dq$$

$$+ \frac{R_o}{C_v}\frac{u^2}{S_c}\int m_b \, dq + \frac{R_o}{C_v} Q \qquad \text{(A. 9)}$$

The temperature of the gas leaving the surface should in general be allowed to be different from that in the gas. This possibility is accounted for by writing $T_s = T + \Delta T$. The fluctuation $\hat{T}_s$ has been replaced by $\hat{T} + \Delta\hat{T}$ and $\hat{T}$ is given by the relation for isentropic acoustical motions, $\hat{T}/T_o = (\gamma - 1)\hat{p}/\gamma p_o$. Hence $\Delta\hat{T}$ represents the non-isentropic part of the temperature fluctuation.

Equations (A. 7) and (A. 8) are used to form the wave equation,

$$\frac{\partial^2 p'}{\partial z^2} - \frac{1}{a_o^2} \frac{\partial^2 p'}{\partial t^2} = h \qquad \text{(A. 10)}$$

with

$$h = - \rho_o \frac{\partial^2}{\partial z^2} (\bar{u} u') - \frac{1}{S_c} \frac{\partial}{\partial z} \left[u' \int \bar{m}_b \, dq \right]$$

$$+ \frac{\bar{u}}{a_o^2} \frac{\partial^2 p'}{\partial t \, \partial z} + \frac{\gamma}{a_o^2} \frac{\partial p'}{\partial t} \frac{\partial \bar{u}}{\partial z} - \frac{1}{a_o^2} \frac{\partial P_1'}{\partial t} \qquad \text{(A. 11)}$$

The boundary condition on p', to be applied at the ends can be obtained using equation (A. 7) as:

$$\frac{\partial p'}{\partial z} = - f \qquad \text{at} \quad z = 0, \; L \qquad \text{(A. 12)}$$

with

$$f = \rho_o \frac{\partial}{\partial z} (\bar{u} u') + \rho_o \frac{\partial u'}{\partial t} + \frac{u'}{S_c} \int \bar{m}_b \, dq \qquad \text{(A. 13)}$$

With this formulation we will proceed to get the solution for complex wave number k defined by:

$$k = (\omega - i\alpha)/a_o \qquad \text{(A. 14)}$$

where α is growth or decay constant. For harmonic motions, all fluctuations can be written as:

$$p' = \hat{p} \exp (i\tilde{\omega} t) \qquad \text{(A. 15)}$$

where

$$\tilde{\omega} \equiv a_o k \qquad \text{(A. 16)}$$

Then equation (A. 10) becomes:

$$\frac{d^2 \hat{p}}{dz^2} + k^2 \hat{p} = \hat{h} \qquad \text{(A. 17)}$$

and boundary condition (A. 12) can be written as:

$$\frac{d\hat{p}}{dz} = -\hat{f} \qquad \text{at} \quad z = 0,\ L \tag{A.18}$$

The solution for k^2 is readily found by using the solution of the problem defined by the classical unperturbed case, for which the governing equations are:

$$\frac{d^2\hat{p}_\ell}{dz^2} + k_\ell^2 \hat{p}_\ell = 0 \tag{A.19}$$

$$\frac{d\hat{p}_\ell}{dz} = 0 \qquad \text{at} \quad z = 0,\ L \tag{A.20}$$

Multiply equation (A. 17) by $\hat{p}_\ell$ and subtract from it $\hat{p}$ times equation (A. 19). Integrating the results over the volume of the chamber gives:

$$k^2 = k_\ell^2 + \frac{1}{E_\ell^2}\left\{ \int_0^L \hat{h}\hat{p}_\ell S_c\, dz + \left[\hat{f}\,\hat{p}_\ell S_c\right]_0^L \right\} \tag{A.21}$$

where

$$E_\ell^2 = \int_0^L \hat{p}\,\hat{p}_\ell S_c\, dz \approx \int_0^L \hat{p}_\ell^2 S_c\, dz \tag{A.22}$$

Now the task remains to integrate the right hand side of the equation (A. 21) since $\hat{h}$ and $\hat{f}$ are known. This gives:

$$(k^2 - k_\ell^2) E_\ell^2$$

$$= i\rho_o a_o k_\ell \left[\left(\hat{u} + \frac{\bar{u}\hat{p}_\ell}{\rho_o a_o^2} \right) \hat{p}_\ell S_c \right]_0^L$$

$$+ i(\gamma - 1) \frac{k_\ell S_c}{a_o} \int_0^L \hat{p}_\ell^2 \frac{d\bar{u}}{dz} dz$$

$$+ \frac{i}{\rho_o a_o k_\ell} \int_0^L \left(\frac{d\hat{p}_\ell}{dz} \right)^2 \int \bar{m}_b \, dq \, dz$$

$$- \frac{ik_\ell S_c}{a_o} \int_0^L \hat{P}_1 \hat{p}_\ell dz \qquad \text{(A.23)}$$

After some calculations, the integral over $\hat{P}_1$ can be calculated as:

$$- \frac{ik_\ell S_c}{a_o} \int_0^L \hat{P}_1 \hat{p}_\ell dz = i\rho_o a_o k_\ell \int_0^L$$

$$x \int \left[\frac{\hat{m}_b}{\rho_o} + \frac{\Delta \hat{T}}{\rho_o T_o} \bar{m}_b \right] dq \, dz$$

$$- i(\gamma - 1) \frac{k_\ell}{\rho_o a_o} \int_0^L \hat{p}_\ell^2 \bar{m}_b \, dq \, dz$$

$$- i \frac{k_\ell}{a_o} \frac{R_o}{C_v} \int_0^L \hat{p}_\ell \hat{Q} S_c dz \qquad \text{(A.24)}$$

Combining equations (A.23) and (A.24) and using the continuity equation for steady state we finally get (see reference 6):

$$(k^2 - k_\ell^2)\, E_\ell^2 = i\rho_o a_o k_\ell \left\{ \left[\hat{p}_\ell \left(\hat{u} + \frac{\overline{u}\hat{p}_\ell}{\rho_o a_o^2} \right) S_c \right]_0^L \right.$$

$$\left. - \int_0^L \hat{p}_\ell \int \left[\frac{\hat{m}_b}{\rho_o} + \frac{\overline{m}_b}{\rho_o} \frac{\Delta \hat{T}}{T_o} \right] dq\, dz \right\}$$

combustion and exhaust nozzle

$$+ \frac{i k_\ell}{a_o} \left\{ \frac{1}{\rho_o} \int_0^L \frac{1}{k_\ell^2} \left(\frac{d\hat{p}_\ell}{dz} \right)^2 \int \overline{m}_b\, dq\, dz \right\}$$

mean flow/acoustics surface interactions

$$- \frac{i k_\ell}{a_o} \frac{R_o}{C_v} \int_0^L \hat{p}_\ell \hat{Q} S_c\, dz$$

residual combustion (A.25)

Using equation (A.14), growth constant α can now be calculated from the imaginary part of equation (A.25). For $\alpha \ll \omega \equiv a_o k_\ell$, and with residual combustion ignored, we have:

$$\alpha = - \frac{\rho_o a_o^2}{E_\ell^2} \left\{ \left[\hat{p}_\ell \left(\hat{u}^{(r)} + \frac{\overline{u}\hat{p}_\ell}{\rho_o a_o^2} \right) S_c \right]_0^L \right.$$

end surfaces

$$\left. - \int_0^L \hat{p}_\ell \int \overline{u}_b \left[\frac{\hat{m}_b}{\overline{m}_b} + \frac{\Delta \hat{T}}{T_o} \right]^{(r)} dq\, dz \right\}$$

lateral surfaces

combustion and exhaust nozzle

$$- \frac{1}{2E_\ell^2 \rho_o} \int_0^L \frac{1}{k_\ell^2} \left(\frac{d\hat{p}_\ell}{dz} \right)^2 \int \overline{m}_b \, dq \, dz$$

mean flow/acoustics (flow turning) interactions (A.26)

Viscous and heat transfer at the boundary may be incorporated directly now with:

$$\alpha_d = -\oint \left[\left(\mu \frac{\partial \hat{u}^{(i)}}{\partial y} \right)_{y=0} \frac{d\hat{p}_\ell}{dz} + \frac{\omega}{a_o^2} \frac{R_o}{C_v} \left(\lambda_c \frac{\partial \hat{T}^{(r)}}{\partial y} \right)_{y=0} \hat{p}_\ell \right] \frac{a_o^2 \, dS}{2\omega E_\ell^2} \tag{A.27}$$

Further details relating to equation (A.27) are given in references 5 and 9.

Equations (A.26) and (A.27), when applied to the T-burners shown in figures (A.2) and (A.3), produce a simple relation which is the base for interpreting all the data obtained from the hot firings of T-burners. There are two functions commonly used to describe the effect of small amplitude harmonic pressure fluctuations on the burning of a propellant; the response function R_b and the admittance function A_b:

$$R_b = \frac{\hat{m}_b / \overline{m}_b}{\hat{p}/p_o} \tag{A.28}$$

$$A_b = \frac{\hat{u}_b / a_o}{\hat{p}/\gamma p_o} \tag{A.29}$$

Also,

$$\overline{m}_b = \rho_o \overline{u}_b \tag{A.30}$$

with these, one may easily show that:

$$\hat{u}_b + \frac{\overline{u}_b \hat{p}_\ell}{\rho_o a_o^2} = \frac{\hat{m}_b}{\rho_o} + \overline{u}_b \frac{\Delta \hat{T}}{T_o} \tag{A.31}$$

Combining equations (A.28) through (A.31) we get:

$$\frac{\gamma p_o}{a_o \hat{p}} \left(\hat{u}_b + \frac{\overline{u}_b \hat{p}}{\rho_o a_o^2} \right) = A_b + \overline{M}_b$$

$$= \frac{1}{\rho_o} \frac{\gamma p_o}{a_o \hat{p}} \left(\hat{m}_b + \overline{m}_b \frac{\Delta \hat{T}}{T_o} \right)$$

$$= \gamma \overline{M}_b \left(R_b + \frac{\Delta \hat{T}/T_o}{\hat{p}/p_o} \right) \tag{A.32}$$

Because of the potential dependence of the response function on the position of the surface, and because it is the real part which appears in equation (A.26), it is convenient to use the notation:

$$B_e = A_b^{(r)} + \overline{M}_b \qquad \text{end surface} \tag{A.33}$$

$$B_s = A_b^{(r)} + \overline{M}_b \qquad \text{side (lateral) surface} \tag{A.34}$$

With the assumption that $\hat{p} \sim \hat{p}_\ell \approx \cos k_\ell z$, the first two terms of the right hand side of the equation (A.26) can now be simplified with simple integration to:

$$\alpha_{be} = 4 f B_e \qquad \text{contribution from end surfaces} \tag{A.35}$$

and

$$\alpha_{bs} = 4 f B_s \frac{S_{bs}}{S_c} \left\{ \frac{1}{L_b} \int_0^{L/2} \hat{p}_\ell^2 \, dz \right\}$$

$$\text{contribution from lateral surfaces} \tag{A.36}$$

where $f = a_o/2L$ is the frequency of the fundamental mode of longitudinal oscillations in the tube and $S_{bs} = q L_b$ is the total area for lateral inflow (see figure A.3 for details).

The third term on the right hand side of equation (A.26), (i.e., mean flow/acoustic interactions) also provides two contributions. First, over the lateral burning surface only, given by α_{ft}; and a second, arises formally from the center vent, given by α_v^*.

Thus, the result for the general T-burner configuration shown in figure A.3 is the formula for the growth constant:

$$\alpha = \alpha_{be} + \alpha_{bs} + \alpha_{ft} + \alpha_v + \alpha_d \qquad (A.37)$$

For the T-burner configuration shown in figure A.2, used in this work, equation (A.37) reduces to:

$$\alpha = \alpha_{be} + \alpha_v + \alpha_d \qquad (A.38)$$

Note that the geometry of the T-burner shown in figure 3.2 resembles figure (A.2) and our cold flow simulated resonance tube shown in figure 4.2. Chapter 2 describes in further detail the use and the limitations of equation (A.38) to calculate B_e using data obtained from T-burner firings. It is an implicit assumption that the dynamical behavior of burning propellants can best be characterized by a response function R_b, which is essentially a property of the propellant. With a simple assumption of $\Delta\hat{T} = 0$, and using equation (A.32), one can obtain R_b in principle. But with the validity of this assumption in serious doubt, the only other alternative is to measure R_b directly. Experimental techniques are not presently available for realizing this alternative.

---

* In particular, see the first term in equation (3.3).

Further, the production of entropy associated with the interactions between the incoming flow at the lateral burning surface and the oscillatory flow in the main chamber can also be given by (see references 9 and 10 for further details):

$$\rho_o T_o \frac{d}{dt} \int_0^L \overline{s}' S_c \, dz =$$

$$\frac{1}{2\rho_o a_o^2} \int_0^L \frac{1}{k_\ell^2} \left(\frac{d\hat{p}_\ell}{dz} \right)^2 \int \frac{\overline{m}_b}{\rho_o} \, dq \, dz - \frac{1}{4} \int_0^L (\hat{u} \hat{u}_s^* + \hat{u}^* \hat{u}_s)$$

$$\int \overline{m}_b \, dq \, dz \qquad \text{(A.39)}$$

The second term is a correction term if the flow entering at the boundary has a fluctuation of velocity in the direction of axial fluctuation in the main chamber.

The result described above is essentially the counterpart for unsteady flow, of processes which have long been recognized in steady flow in a constant area duct with mass addition at the boundary (see reference 8, p. 225). The flow turning in unsteady flow is indeed a dissipative process (mainly due to viscous interactions) accompanied by an increase in the entropy of gas within the main chamber.

A.2 Three-Dimensional Stability Analysis

The stability of three-dimensional motions can be analyzed in two different ways: by constructing the integral balance for energy in a combustion chamber; and computation of the complex wave

numbers of the normal modes, by using the differential equations of motion. References 5 and 7 discuss both these approaches in detail. The calculation of the balance of acoustic energy eventually gives the formula for α which can be put in the form:

$$\alpha = -\frac{\rho_o a_o^2}{2E_N^2} \oiint \left[\hat{p}\,\hat{\vec{u}}^{(r)} + \vec{\bar{u}}\,\frac{\hat{p}^2}{\rho_o a_o^2} + \rho_o (\vec{\bar{u}}.\hat{\vec{u}})\,\hat{\vec{u}} \right] . \hat{n}\, dS \qquad (A.40)$$

On a closer look, it can be found that the first two terms are precisely those encountered in the formula for α as obtained using complex wave number approach. Equation (A.40) can hence be written as:

$$\alpha = -\frac{a_o}{2E_N^2} \oiint \hat{p}^2 (A_b^{(r)} + \overline{M}_b)\, dS - \frac{(\rho_o a_o)^2}{2E_N^2} \oiint (\vec{\bar{u}}.\hat{\vec{u}})\,\hat{\vec{u}}.\hat{n}\, dS \qquad (A.41)$$

where the first contribution is from all burning surfaces and exhaust vents and nozzles.

It is interesting to note that both the formulas produced for the growth constant α are identical in most respects, but neither analysis contains contributions from "flow turning" effects which are found in one-dimensional analysis as discussed earlier. The reason for this is that the "flow turning" is a process which in real flow occurs in a boundary region and necessarily involves viscous forces; a mechanism for attenuating acoustic energy. The one-dimensional analysis provides an approximate means of computing these losses. Only if viscous effects are taken into account will a three-dimensional analysis contain this contribution from the flow turning process. No solutions for three-dimensional viscous flows are available for

the problem of our interest here. For an alternative approach, both the flow turning effects and loss due to heat transfer and viscous stresses acting in the acoustic boundary layer on the wall of the tube may be added to the formula for α as obtained from a classical three-dimensional inviscid analysis. Then equation (A. 40) [and hence equation (A. 41)] can be written as:

$$\alpha = - \frac{\rho_o a_o^2}{2E_N^2} \oiint \left[\hat{p} \hat{\vec{u}}(r) + \frac{\vec{\bar{u}} \hat{p}^2}{\rho_o a_o^2} + \rho_o (\vec{\bar{u}} . \hat{\vec{u}}) \hat{\vec{u}} \right] . \hat{n} \, dS$$

$$+ \alpha_{ft} + \alpha_v + \alpha_d \qquad \text{(A. 42)}$$

As described earlier in chapter 2, for most of the work with T-burners, the one-dimensional analysis has been used and seems to work well.

APPENDIX B. ANALYSIS OF APPARATUS FOR ACOUSTIC TESTS

The apparatus used for acoustic tests consists of a tube driven by the oscillating pistons at both ends generating the fundamental acoustic mode of oscillation within the tube. When the frequency of the driver is swept through the resonance frequency of the tube, the amplitude of the acoustic pressure oscillation varies very much like that of the resonance curve for a simple spring/mass/dashpot system. The analysis described here helps one to draw a comparative picture. In particular, it throws light on our need to relate the 3 db down band width of the resonance curve to the net losses in the system. Though analysis is directed specifically to the configuration modelling the T-burner, it can be modified for any geometry with little effort. References 16 and 17 describe the necessary background for this analysis.

From the conservation equations, after suitable combination and expansion, a linear inhomogenous wave equation can be constructed for the pressure oscillations:

$$\nabla^2 p' - \frac{1}{a_o^2} \frac{\partial^2 p'}{\partial t^2} = h \qquad \text{(B. 1)}$$

with the boundary condition:

$$\hat{n} . \nabla p' = -f \qquad \text{(B. 2)}$$

The explicit forms of h and f are not important at this stage; a complete discussion can be found in references 16 and 17. To describe this continuous system (the gas in the chamber) as a

"lumped" system one can write the pressure field as a synthesis of normal modes with time varying amplitudes,

$$p' = p_o \sum \eta_n(t) \psi_n(\vec{r}) \tag{B.3}$$

where the mode shapes $\psi_n(\vec{r})$ satisfy the homogeneous scalar wave equation and the boundary condition that the normal component of gradient vanishes:

$$\nabla^2 \psi_n + k_n^2 \psi_n = 0 \tag{B.4}$$

$$\hat{n} \cdot \nabla \psi_n = 0 \tag{B.5}$$

The procedure for computing the amplitudes $\eta_n(t)$ is given in references 16 and 17. First multiply (B.1) by ψ_n and subtract (B.4) multiplied by p' and integrate over the volume of the chamber. Then introduce the expansion (B.3) and the boundary conditions (B.2) and (B.5). A little mathematics finally leads to the equation for η_n:

$$\frac{d^2\eta_n}{dt^2} + \omega_n^2 \eta_n = F_n \tag{B.6}$$

with the 'force' F_n:

$$F_n = -\frac{a_o^2}{p_o \int \psi_n^2 dV} \left\{ \int \psi_n h dV + \oiint \psi_n f dS \right\} \tag{B.7}$$

These equations are basic to all analysis of combustion instability problems and may be used to describe the behavior of the problems of interest here.

The important difference between the analysis of combustion instability - a phenomenon occurring in a self-excited system - and the situation of our interest, i.e., the cold flow resonance tube, is

that the 'force' F_n now contains a part representing the influence of an external agent, the 'driver'. In the test apparatus used here there is a net flow of mass, momentum and energy through the piston boundary exciting the standing waves in the tube. Over and above this, the primary driving of the waves is the force exerted on the acoustic field within a tube by motion of a portion of the boundary. This is represented in the function F_n as a part of the term arising in the boundary condition:

$$\hat{n} \cdot \nabla p' = - \rho_o \frac{\vec{\partial} u'}{\partial t} \cdot \hat{n} + \ldots \qquad (B.8)$$

To understand this contribution let us first discuss figure B. 1.

In the cold flow resonance tube apparatus, movable pistons are fitted at the ends of the tube. These have porous surfaces through which the average flow is introduced. The entire piston is oscillated using the electromagnetic shaker with velocity $\vec{u}'_p$. In addition to this, the velocity of the gas passing through the porous surface fluctuates in response to the acoustic field. Hence, the approximation will be assumed true that the unsteady velocity of the gases just downstream of the piston may be written as:

$$u' = \vec{u}'_p + \vec{u}'_a \qquad (B.9)$$

where $\vec{u}'_a$ is the acoustic velocity for the harmonic motions.

$$\hat{\vec{u}}_a \cdot \hat{n} = A_b \left(\frac{a_o}{\gamma p_o} \right) \hat{p} \qquad (B.10)$$

where A_b is the admittance function to be measured with the impedance tube apparatus. Now because the admittance function is a complex number:

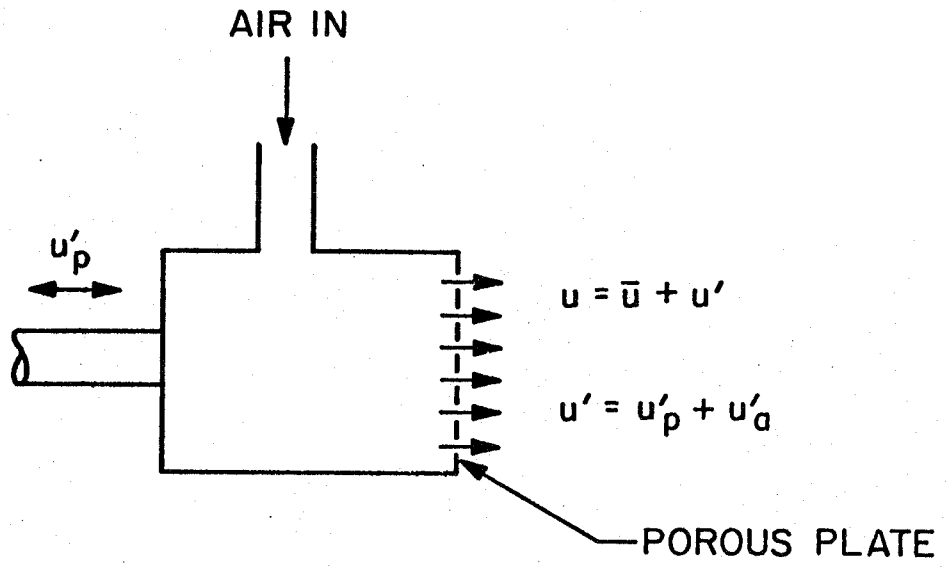

Figure B.1 Sketch of a Movable Piston with Average Flow Inward

$$A_b = A_b^{(r)} + i\, A_b^{(i)} \tag{B.11}$$

and for motions which are not precisely harmonic, equation (B.10) can be written as:

$$\vec{u}'_a \cdot \hat{n} \approx \frac{a_o}{\gamma p_o} \left(A_b^{(r)} + i\, A_b^{(i)} \right) p'$$

$$\approx \frac{a_o}{\gamma p_o} \left(A_b^{(r)} + \frac{1}{\omega_n} A_b^{(i)} \frac{\partial}{\partial t} \right) p' \tag{B.12}$$

with equations (B.9) and (B.12), equation (B.8) can be rewritten as:

$$\hat{n} \cdot \nabla p' = -\rho_o \frac{\partial \vec{u}'_p}{\partial t} \cdot \hat{n} - \frac{1}{a_o} \left(A_b^{(r)} \frac{\partial p'}{\partial t} + \frac{1}{\omega_n} A_b^{(i)} \frac{\partial^2 p'}{\partial t^2} \right) \cdots \tag{B.13}$$

According to equations (B.2) and (B.7), this leads to a part of F_n:

$$F_n^{(p)} = -\frac{a_o^2}{\int \psi_n^2 dV} \oiint \psi_n \left[\rho_o \frac{\partial \vec{u}'_p}{\partial t} \cdot \hat{n} + \frac{1}{a_o} \left(A_b^{(r)} \frac{\partial p'}{\partial t} + \frac{1}{\omega_n} A_b^{(i)} \frac{\partial^2 p'}{\partial t^2} \right) \right] dS \tag{B.14}$$

Now substituting equation (B.3) in the last terms of equation (B.14) and because the perturbed mode is not very different from the normal mode, use the approximation $\ddot{\eta}_i = -\omega_i^2 \eta_i$ to find:

$$F_n^{(p)} \approx -\frac{\gamma}{\int \psi_n^2 dV} \oiint \psi_n \frac{\partial \vec{u}'_p}{\partial t} \cdot \hat{n}\, dS - \frac{a_o}{\int \psi_n^2 dV} \left(A_b^{(r)} \dot{\eta}_n - \omega_n A_b^{(i)} \eta_n \right)$$

$$\oiint \psi_n^2 dS - \frac{a_o}{\int \psi_n^2 dV} \sum^{i \neq n} \oiint \psi_n \psi_i \left[A_b^{(r)} \dot{\eta}_i - \frac{\omega_i^2}{\omega_n} A_b^{(i)} \eta_i \right] dS \tag{B.15}$$

For linear behavior, the remaining part of F_n given by equation (B.7) can all be expressed as a sum of contributions proportional to $\dot{\eta}_i$ and those proportional to η_i. Consequently, F_n can be written

as:

$$F_n = -\frac{\gamma}{\int \psi_n^2 dV} \iint \psi_n \frac{\partial \vec{u}'_p}{\partial t} \cdot \hat{n} \, dS - \frac{a_o}{\int \psi_n^2 dV} \left(A_b^{(r)} \dot{\eta}_n - \omega_n A_b^{(i)} \eta_n \right) \iint \psi_n^2 dS - \frac{a_o}{\int \psi_n^2 dV} \sum_{i \neq n}^{} \iint \psi_n \psi_i \left[A_b^{(r)} \dot{\eta}_i - \frac{\omega_i^2}{\omega_n} A_b^{(i)} \eta_i \right] dS$$

$$- D_{nn} \dot{\eta}_n - E_{nn} \eta_n - \sum_{i \neq n}^{} \left[D_{ni} \dot{\eta}_i + E_{ni} \eta_i \right] \qquad \text{(B. 16)}$$

Equation (B. 6) can now be written more explicitly as:

$$\frac{d^2 \eta_n}{dt^2} + \left[D_{nn} + \frac{2 a_o A_b^{(r)}}{\int \psi_n^2 dV} S_c \right] \frac{d\eta_n}{dt} +$$

$$\left[\omega_n^2 - \frac{2 a_o \omega_n A_b^{(i)}}{\int \psi_n^2 dV} S_c \right] \eta_n = -\frac{\gamma}{\int \psi_n^2 dV} \iint \psi_n \frac{\partial \vec{u}'_p}{\partial t} \cdot \hat{n} \, dS \qquad \text{(B. 17)}$$

In the above equation, linear coupling terms are dropped out (i. e., the terms for $i \neq n$), the main reason being the absence of the physical process (combustion in particular) giving significant linear coupling. See references 16 and 17 for further details. Moreover, these terms should not arise in the usual linear stability analysis of interest here because of the restriction enforced from the beginning (see chapter 2) that it is sufficient to study linear stability of the normal mode of the chamber and hence the motion consists only of a wave having a single frequency. Moreover, it is also important to point out that the right hand side is dominated by the term representing the pistons driven by electromagnetic force. This force is at the same frequency as the fundamental frequency of the device.

Equation (B. 17) is the formal justification for treating a continuous system as a driven oscillator whose displacement amplitude is η_n. For a harmonically forced piston:

$$\vec{u}'_p = \hat{\vec{u}}_p e^{i\omega t} \tag{B. 18}$$

and with $\eta_n = \hat{\eta}_n \exp(i\omega t)$, equation (B. 17) leads to the frequency response given by:

$$\hat{\eta}_n = \frac{-i\omega \hat{G}}{(\tilde{\omega}_n^2 - \omega^2) + i(2a\omega)} \tag{B. 19}$$

where

$$\tilde{\omega}_n^2 \equiv \omega_n^2 + E_{nn} - \frac{2a_o \omega_n A_b^{(i)} S_c}{\int \psi_n^2 dV} \tag{B. 20}$$

$$2a \equiv D_{nn} + \frac{2a_o A_b^{(r)} S_c}{\int \psi_n^2 dV} \tag{B. 21}$$

$$\hat{G} \equiv \frac{\gamma}{\int \psi_n^2 dV} \oiint \psi_n \hat{\vec{u}}_p \cdot \hat{n} \, dS \tag{B. 22}$$

The frequency $\tilde{\omega}_n$ is measured in experiments and it differs by only a small amount. The frequency response, equation (B. 19) is shown in figure B. 2. For $a/\omega \ll 1$, it has half power width of $2a$. This is the basis for the experimental technique used: the frequencies $\tilde{\omega}_n$, ω_+ and ω_- are measured and $\Delta\omega \equiv \omega_+ - \omega_- = 2a$ is calculated from that.

Owing to the assumption on which the linear split of perturbation velocity is made according to equation (B. 9), one finds eventually

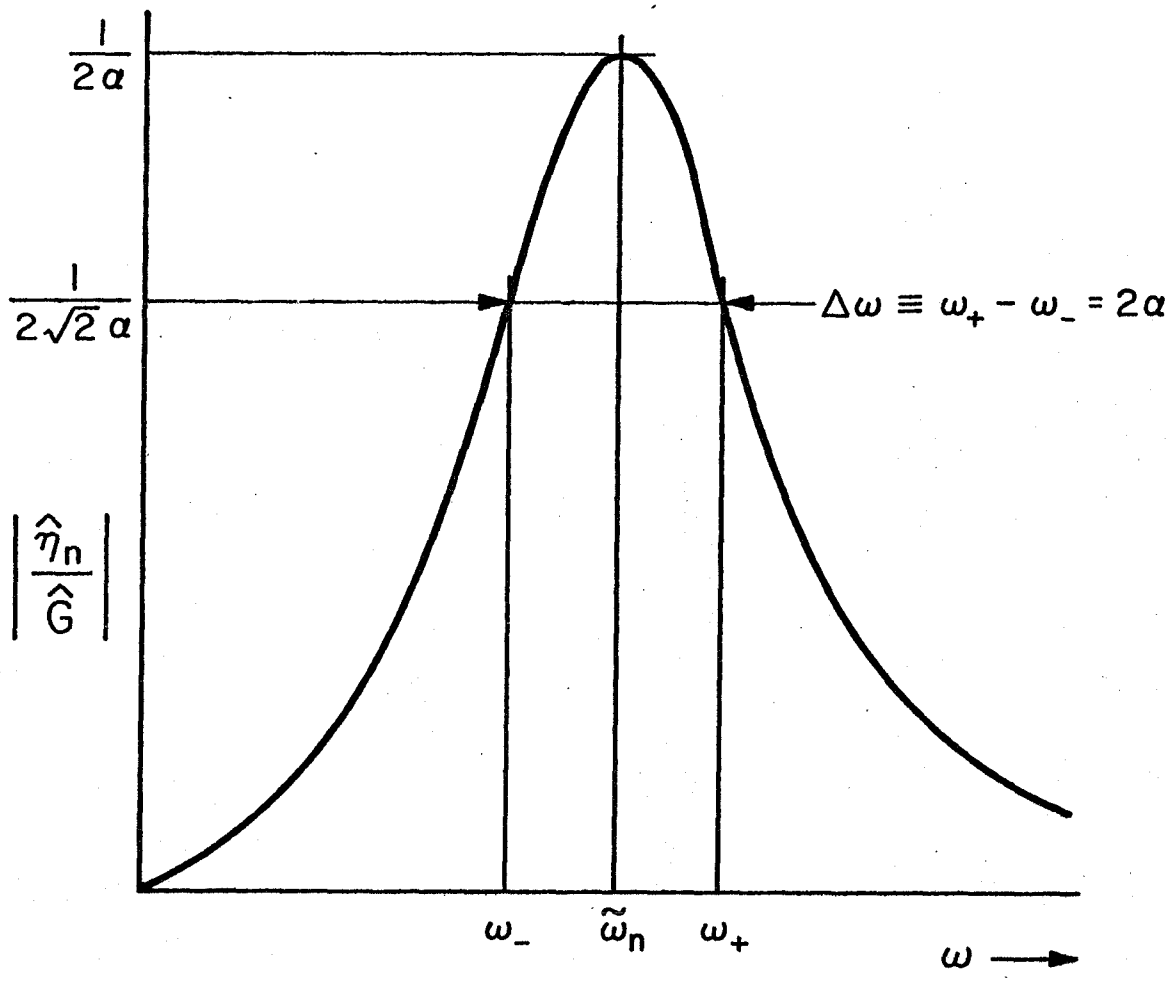

Figure B.2 Frequency Response According to Equation (B.19)

that for the use of equation (B. 19), the admittance function for the stationary piston must be measured. It is A_b defined by equation (B. 10), for the fluctuation of gas relative to the face of the piston which appears in $\tilde{\omega}_n$ and especially in α. For this very reason, a rigid piston mounting of the piston at the end of the impedance tube was used in the impedance tube experiments.

APPENDIX C. ANALYSIS OF THE IMPEDANCE TUBE

The impedance tube, or standing wave apparatus as it is widely called, is commonly used for easy and quick determination of impedance and hence admittance function of acoustic materials. The standing wave tube method of measuring acoustic admittance of sample of interest is illustrated in figure C. 1. A sample of the surface to be tested is placed at one end of the circular tube and a suitable driver is placed at the other end. Both incident and reflecting acoustic waves from the sample front form a standing wave system within the tube. This standing wave system is sustained within the tube because the power input by the sound source precisely compensates the energy losses in the tube.

Many discussions of the standing wave apparatus are readily available; for example, reference 18 is the most typical. The brief summary described here closely follows this reference. Some of the nomenclature is defined in figure C. 1.

For very low Mach numbers encountered in our tests ($\overline{M} < 3 \times 10^{-4}$), Doppler effect is neglected and it is sufficient to assume that the pressure fluctuations satisfy the one-dimensional wave equation:

$$\frac{\partial^2 p'}{\partial z^2} - \frac{1}{a_o^2} \frac{\partial^2 p'}{\partial t^2} = 0 \qquad \text{(C. 1)}$$

For harmonic waves with real frequency ω, set $p' = \hat{p}(z)\exp(-i\omega t)$. With this equation (C. 1) now becomes

$$\frac{d^2 \hat{p}}{dz^2} + k^2 \hat{p} = 0 \qquad \text{(C. 2)}$$

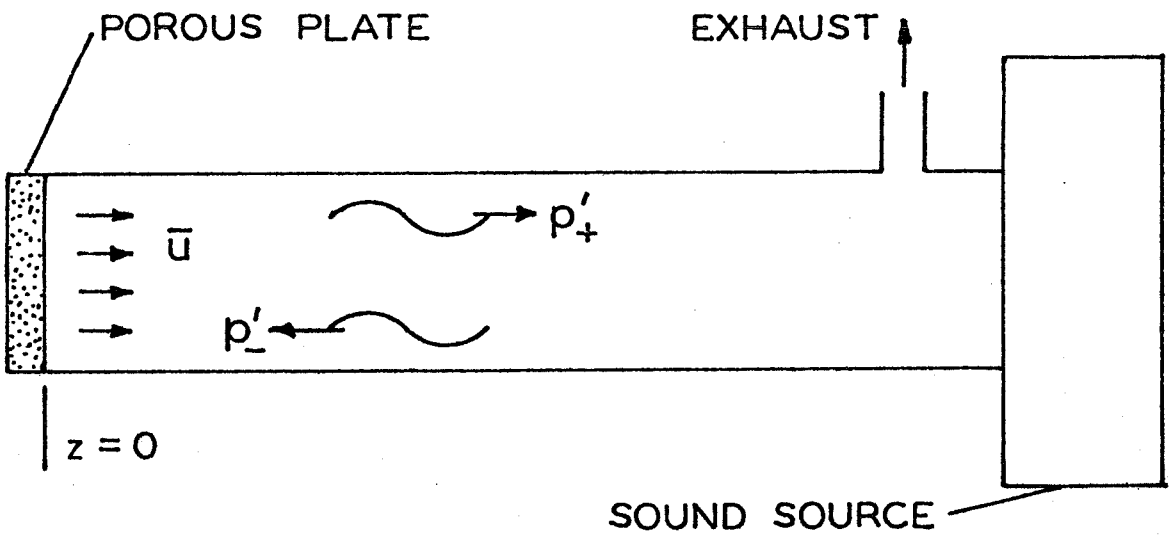

Figure C.1 Sketch of the Impedance Tube

where $k = \omega / a_o$ is the real wave number. Solution to equation (C.2) may be written in the form

$$\hat{p} = \hat{p}_+ + \hat{p}_- \quad , \quad \hat{u} = \hat{u}_+ + \hat{u}_- \tag{C.3}$$

with

$$\left.\begin{aligned} \hat{p}_+ &= B e^{-\kappa z + ikz} \quad , \quad \hat{u}_+ = \frac{B}{\rho_o a_o} e^{-\kappa z + ikz} \\ \hat{p}_- &= A e^{+\kappa z - ikz} \quad , \quad \hat{u}_- = -\frac{A}{\rho_o a_o} e^{+\kappa z - ikz} \end{aligned}\right\} \tag{C.4}$$

The attenuation coefficient κ is introduced to represent distributed losses along the tube wall. These are entirely due to viscous losses and heat transfer within the acoustic boundary layer at the tube wall. For this case κ is given by the classical formula

$$\kappa = 2(\pi\nu)^{\frac{1}{2}} \left[1 + \frac{\gamma - 1}{\sqrt{P_r}} \right] \frac{f^{\frac{1}{2}}}{D a_o} \quad (m^{-1}) \tag{C.5}$$

After numerical values have been substituted for the material properties

$$\kappa = 2.94 \times 10^{-5} \frac{f^{\frac{1}{2}}}{R} \tag{C.6}$$

at 21.11° C and 1.033×10^4 kg_f/m^2 pressure, where R is the radius of the tube in meters.

It is a matter of convenience to write the relation between B and A, defining the complex quantity ψ,

$$B = -Ae^{2\psi} \tag{C.7}$$

Also define α_o, β_o :

$$\psi = \pi\alpha_o + i\pi\beta_o \tag{C.8}$$

The pressure and velocity fluctuations, equations (C.3) and (C.4) hence can be written as

$$\hat{p} = A\left[e^{\kappa z - ikz} - e^{-\kappa z + ikz + 2\psi}\right] \qquad (C.9)$$

$$\hat{u} = \frac{-A}{\rho_o a_o}\left[e^{\kappa z - ikz} + e^{-\kappa z + ikz + 2\psi}\right] \qquad (C.10)$$

Alternatively, using the definitions of the hyperbolic functions, equations (C.9) and (C.10) can be rewritten as

$$\hat{p} = -2Ae^{\psi}\sinh(\psi - \kappa z + ikz) \qquad (C.11)$$

$$\hat{u} = \frac{-2A}{\rho_o a_o} e^{\psi}\cosh(\psi - \kappa z + ikz) \qquad (C.12)$$

Now define α, β :

$$\left.\begin{aligned} \alpha &= \alpha_o - \kappa z \\ \beta &= \beta_o + \frac{2z}{\lambda} \end{aligned}\right\} \qquad (C.13)$$

So, equation (C.11) can be rewritten as

$$\hat{p} = -2Ae^{(\pi\alpha_o + i\pi\beta_o)}\sinh\pi(\alpha + i\beta) \qquad (C.14)$$

The absolute value of acoustic pressure hence is

$$|\hat{p}| = 2Ae^{\pi\alpha_o}\left[\cosh^2\pi\left(\alpha_o - \frac{\kappa z}{\pi}\right) - \cos^2\pi\left(\beta_o + \frac{2z}{\lambda}\right)\right]^{\frac{1}{2}} \qquad (C.15)$$

Because the hyperbolic cosine is monotonic, but the cosine oscillates, $|\hat{p}|$ exhibits maxima and minima as $\beta = \beta_o + 2z/\lambda$ changes with z. The values of β and the corresponding values of the $|\hat{p}|$ are given by

$$\beta = \pm 1/2, \pm 3/2 \ldots\ldots \quad |\hat{p}|_{max} = 2Ae^{\pi\alpha_o}\left|\cosh\pi\left(\alpha_o - \frac{\kappa z}{\pi}\right)\right| \qquad (C.16)$$

$$\beta = \pm 1, \pm 2 \ldots\ldots \quad |\hat{p}|_{min} = 2Ae^{\pi\alpha_o} \left| \sinh\pi(\alpha_o - \frac{Kz}{\pi}) \right| \qquad (C.17)$$

For small values of Kz/π, the usual case in practice, the values of acoustic pressure maxima are almost constant and for the values of $|\hat{p}|_{min}$ increase linearly with the position away from the sample.

Let $z_{1\,max}$ and $z_{1\,min}$ denote the first maximum and first minimum, measured from the face of the sample being tested. Then the most convenient experimentally measured ratio is given by

$$\mathcal{R} = \frac{|\hat{p}|_{1\,max}}{|\hat{p}|_{1\,min}} = \frac{\cosh(\pi\alpha_o - Kz_{1\,max})}{\sinh(\pi\alpha_o - Kz_{1\,min})} \qquad (C.18)$$

From equation (C.18), the constant α_o is

$$\alpha_o = \frac{1}{\pi}\tanh^{-1}\left\{\frac{\cosh(Kz_{1\,max}) - \mathcal{R}\sinh(Kz_{1\,min})}{\mathcal{R}\cosh(Kz_{1\,min}) + \sinh(Kz_{1\,max})}\right\} \qquad (C.19)$$

A second constant β_o, is given as

$$\beta_o = 1 - 2\frac{z_{1\,min}}{\lambda} \qquad (C.20)$$

Finally, the admittance function of the surface may be related to α_o and β_o as follows:

$$A_b = -\frac{\hat{u}/a_n}{\hat{p}/\gamma p_o}\bigg|_{z=0} = -\coth\pi(\alpha_o + i\beta_o) \qquad (C.21)$$

From this formula, the real and imaginary parts of the admittance function can be calculated. As defined here, the real part of A_b is negative for absorption of acoustic energy.

The real part of equation (C.21) is

$$-A_b^{(r)} = \frac{\coth(\pi\alpha_o)\left[1 + \cot^2(\pi\beta_o)\right]}{\coth^2(\pi\alpha_o) + \cot^2(\pi\beta_o)} \qquad (C.22)$$

It is this number which is calculated using a small computer program as described in Appendix E. Also it is interesting to note that for very small values of α_o i.e., for rigid surfaces, the first minimum occurs in the tube very close to $z = \lambda/4$ for which equation (C.20) gives $\beta_o = 1/2$. The distributed losses are relatively small and if $\kappa z_{1\,min}$ is dropped from equation (C.19) and using equations (C.18) and (C.22)

$$-A_b^{(r)} \approx \frac{|\hat{p}|_{1\,min}}{|\hat{p}|_{1\,max}} \qquad (C.23)$$

which is used as a quick measure of admittance function of the acoustically hard materials.

APPENDIX D. CALIBRATION PROCEDURES AND ESTIMATES OF ERRORS

The quantities to be determined, the real part of admittance function of porous plate and decay constants, are relatively small and their variation with respect to flow Mach numbers is also relatively slow. Moreover, the decay or growth constant associated with the exhaust vent is to be determined by subtraction of relatively large decay constants. Thus the indirect method of measurement adopted here and described in chapter 4, requires considerable care and good instrumentation to obtain the highest possible accuracy. Considerable effort has been devoted to achieve the necessary level of accuracy.

D. 1 Calibration of the Air Supply System

As a part of this calibration, Brooks full view rotometer type of flow meter (0 - 3.22 SCFM, linear scale) had been separately calibrated using Precision wet test meter (0 - 100 SCFH air flow). The flow circuit for calibration of the flow meter is shown in figure D. 1. For better accuracies, a vapor correction was applied to the data obtained. The flow circuit for the calibration of porous plate is schematically shown in figure D. 2. The same circuit is used to provide the axial flow in the resonance tube tests. The supply pressure and flow rate are controlled and maintained constant by a series of coarse and fine regulators and a fine metering needle valve. The supply pressure is monitored with Statham differential pressure gauge (0 - 50 psid). The pressure drop across the porous plate is measured with similar pressure gauge (0 - 10 psid). The calibration of the wet test meter was provided by Precision Scientific Company,

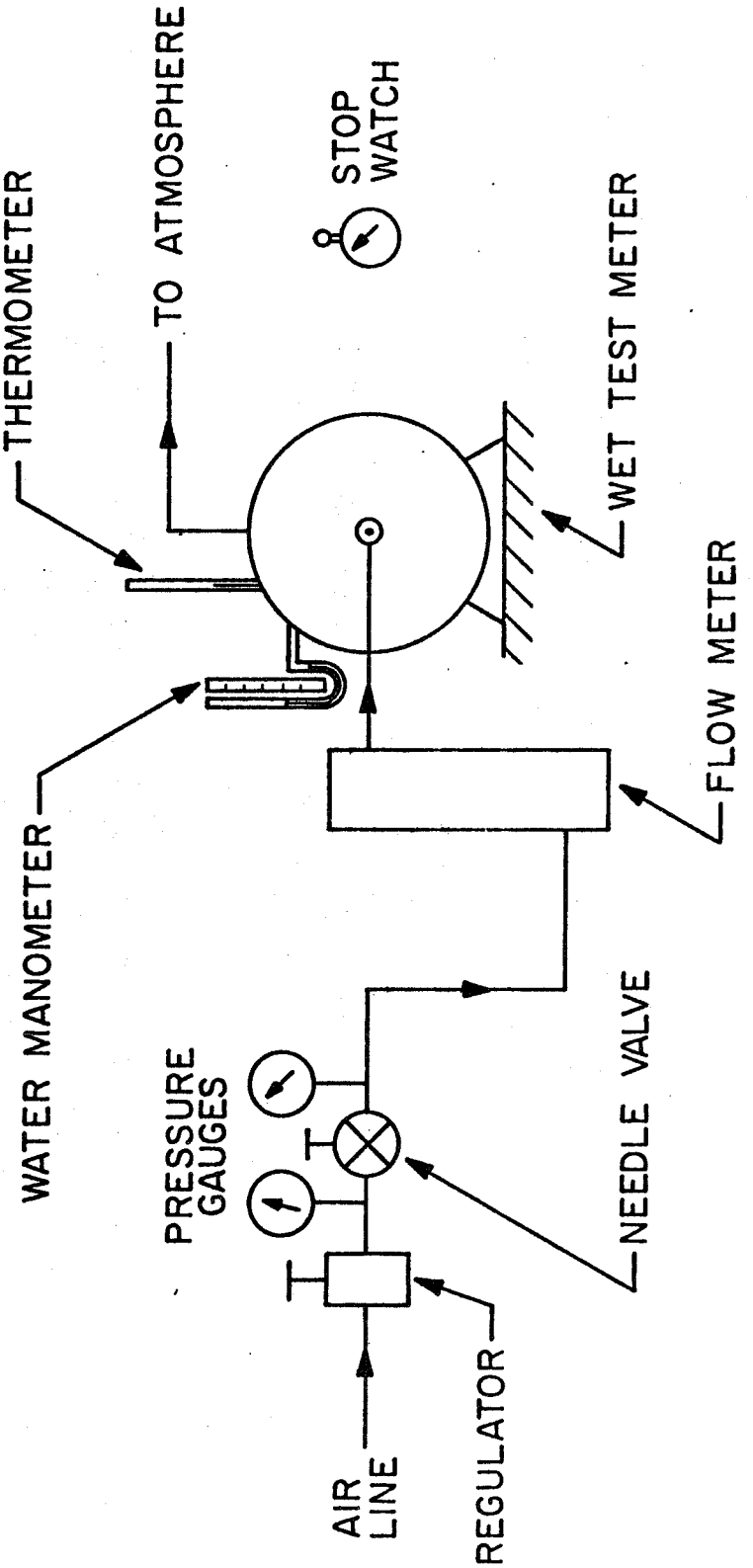

Figure D.1 Flow Circuit for Calibration of Flow-Meter

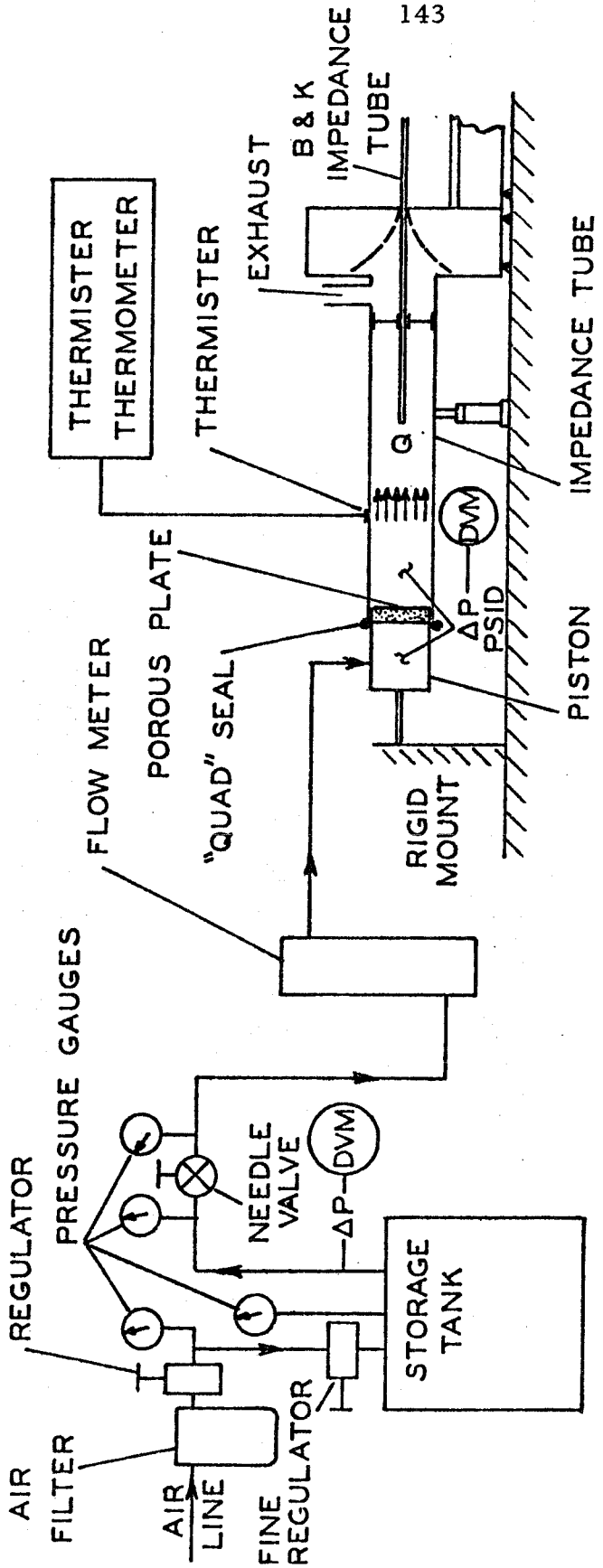

Figure D.2 Flow-Circuit for Calibration of Porous Plates.

while the pressure gauges have been calibrated at the Standards and Calibration Laboratory of the Jet Propulsion Laboratory.

The results for flow rates vs. pressure drop across the two porous plates are given in figure D.3. These porous plates were chosen to provide very high acoustic impedance, which implies a relatively large pressure drop for a given flow rate. The data obtained are within the tolerances (± 30%) quoted by the manufacturer. All of the calibrations were checked periodically.

D.2 Calibration of the Accelerometers and Charge Amplifiers

To drive the fundamental mode of acoustic oscillation of the cold flow resonance tube, the driver pistons at both ends of the resonance tube should oscillate with the same amplitude of oscillation and 180 degree phase difference between them (this is obvious from the pressure distribution for the fundamental mode of the tube here). The amplitude part of our requirements is assured by calibrating both the charge amplifiers (Unholtz-Dickie, Model D-11 Series) and the accelerometers (Endevco, Model 2275 isobase type with low noise microdot cables) at the Environmental and Testing Laboratory of the Jet Propulsion Laboratory. Figure D.4 is a schematic diagram of the apparatus used for calibration. Calibration charts (essentially a frequency response curve at 0 to 0.25 g (peak) level of excitation and frequency range of 25 - 4000 Hz) were prepared for both the sets of charge amplifiers and accelerometers. Figure D.5 represents typical frequency response curve for the charge amplifiers and accelerometers used in the experiments. Settings of charge amplifiers were then adjusted to obtain the necessary voltage output of

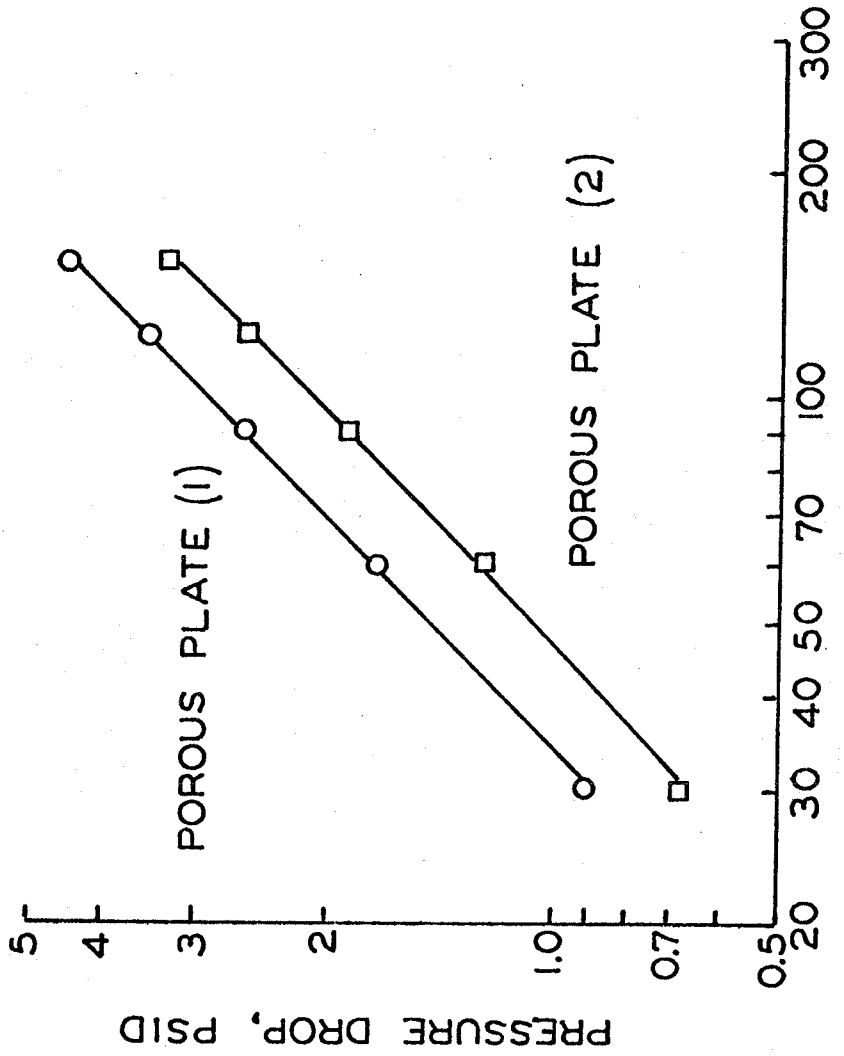

Figure D.3 Data for Flow Rates Through Porous Plates

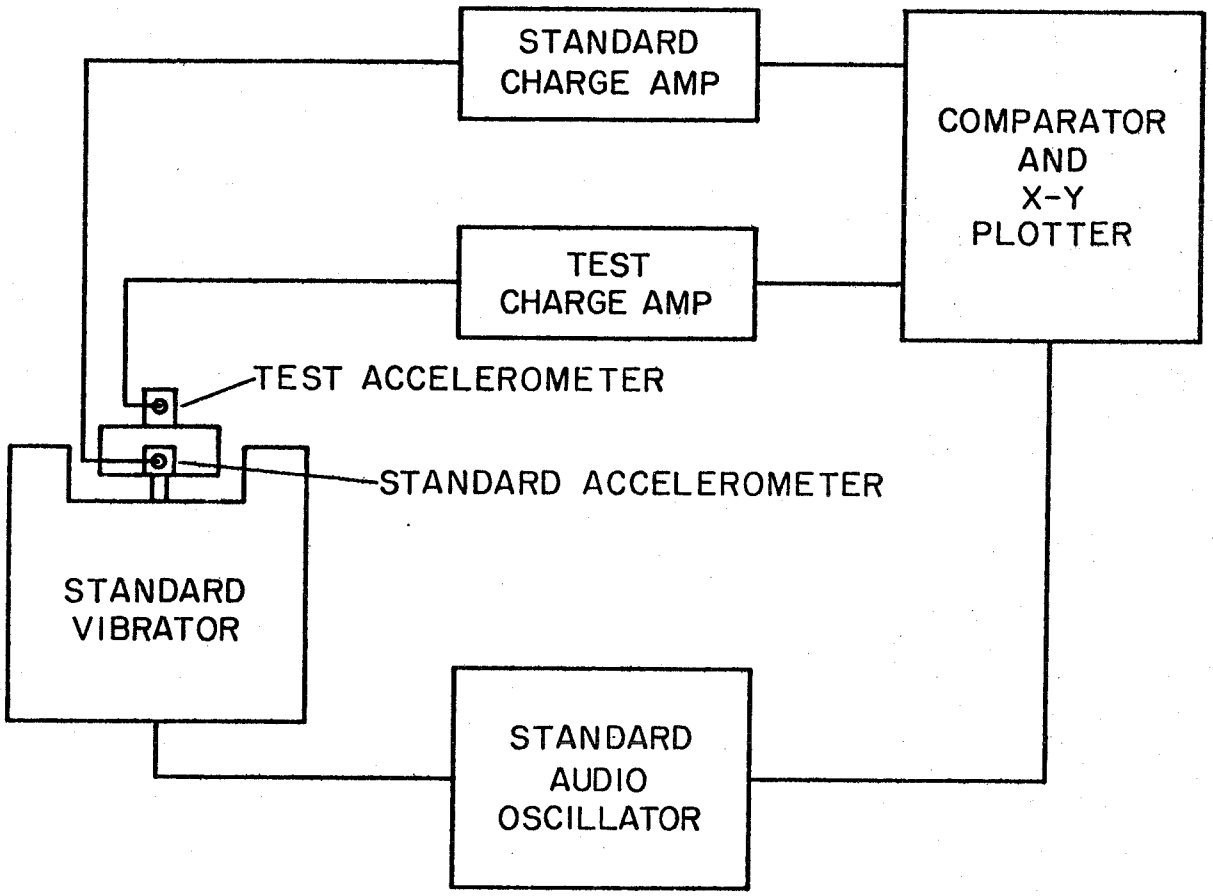

Figure D.4 Schematic Diagram of Apparatus for Calibrating Accelerometers and Charge Amplifiers

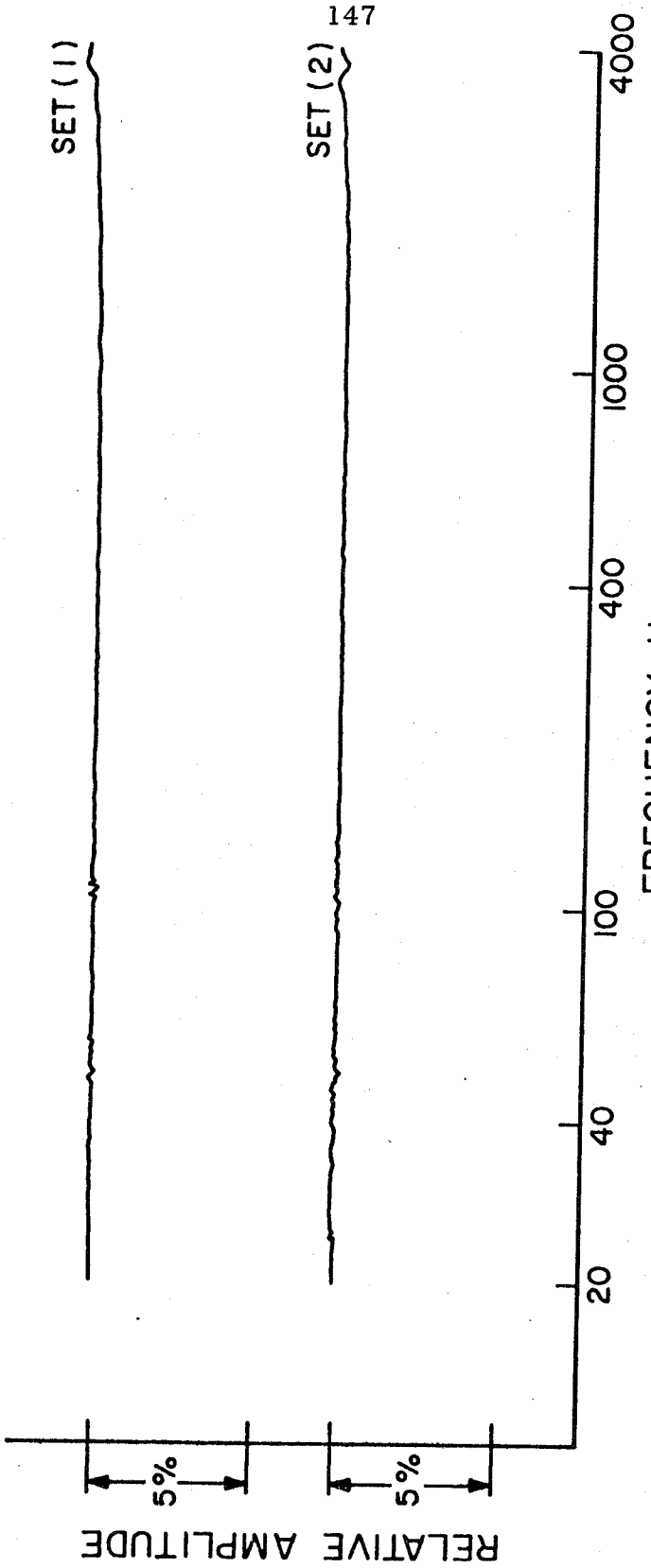

Figure D.5 Frequency Response Curve for Accelerometers and Charge Amplifiers

2.5 V rms for the crossover frequency of 100 Hz at the excitation level of 0 to 0.25 g (peak). With the help of the frequency response curve, then the necessary output of the charge amplifier and accelerometer system can easily be calculated at any frequency of interest.

D.3 Calibration of Microphones

The values of the sensitivities and the frequency response curves are provided by the manufacturer. Periodic verifications have been made on the sensitivity check using B & K pistonphone microphone calibrator, Model 4220,used together with B & K measuring amplifier, Model 2607.

D.4 Calibration of Related Instruments

Princeton Applied Research lock-in amplifier Model 124A, Wavetek synthesizer Model 171, Wavetek phase meter Model 740 and the Data Precision digital voltmeter Model 3500 were sent periodically to the calibration laboratory of the respective manufacturers for calibration. The Spectral Dynamics tracking filter Model SD-122 and carrier generator Model SD-120 were calibrated only once at the calibration laboratory of the manufacturer. The Tektronix dual beam oscilloscope type 551, with type D and type 53/54 C plug in units, were calibrated periodically at the calibration facilities available at the electronics shop in the Department of Aeronautics at Caltech.

D.5 Sources and Estimates of Errors

Estimates of errors were carried out with the best available information and some laboratory experiments. The complexities involved with the determination of estimation of errors associated

with the primary sources of calibration, limited us to estimates of errors determined with respect to the secondary sources of calibration and to occasionally accept the estimates provided by manufacturers for some of the instruments where such secondary sources of calibration were not available. Also it is worthwhile to mention here that the error estimates provided by the manufacturers were often found to be conservative. Figure D.6 describes the usual hierarchical structure involved in the calibration procedures. Because of the large number of variables involved, it was thought wise to describe the estimates of errors in two sections.

D.5.1 Resonance Tube Experiments

(i) acceleration of the pistons: ± 0.08% of the secondary calibration done at the Environmental and Testing Laboratory at the Jet Propulsion Laboratory. ± 1% of the primary calibration done at the National Bureau of Standards

(ii) relative phase of pistons: ± 0.60°. This error estimate was provided by the manufacturer (Wavetek)

(iii) frequency: ± 0.002% of the setting: as measured by the primary source of calibration provided by the Jet Propulsion Laboratory. ± 0.005% of the setting; as provided by the manufacturer (Wavetek)

(iv) flow rates: ± 0.05% of the overall secondary calibration done at Spalding Laboratory at Caltech, Standards and Calibration Laboratory at the Jet

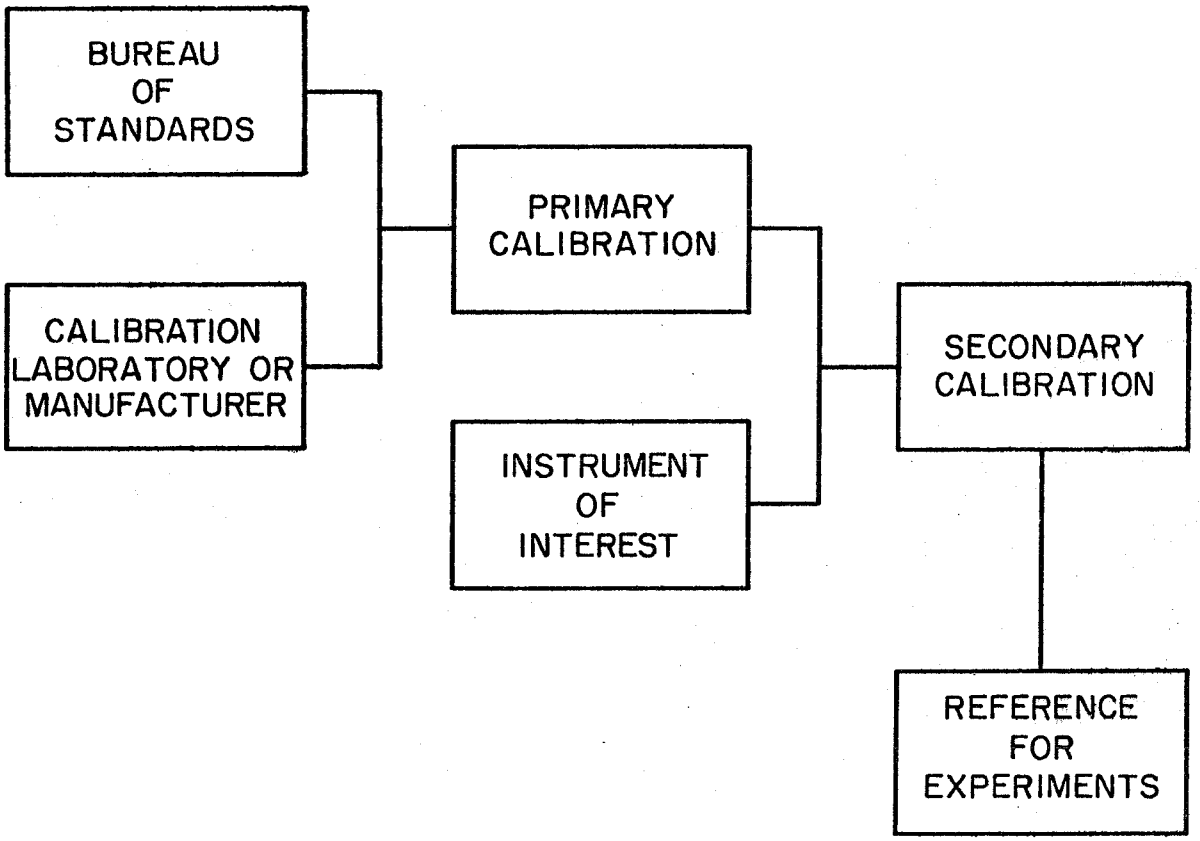

Figure D.6 Hierarchical Structure in Calibration Procedures

Propulsion Laboratory and Daniel and Florence Guggenheim Jet Propulsion Center at Caltech. $\pm \frac{1}{2}\%$ of the setting, error estimate provided by the manufacturer of the wet test meter (Precision Scientific Company). There is, however, a small uncertainty in $\overline{M}$ arising from the overall calibration effort as discussed above; indeed, this has a small effect on the final results for $\overline{\alpha}_v$. For example, suppose $\Delta M \pm 1\%$ (a value much larger than actually occurs). Several check calculations have been carried out to estimate the extent to which this error affects the uncertainty in the attenuation constant for the vent. Over the range of conditions covered by these data, the uncertainties in α_v is increased by a factor of 1.01 to 1.07. Thus, the error bars shown in the final results are only slightly increased and the qualitative conclusions in respect to the influence of the vent are unaffected. It should be noted that the average Mach number will be treated as the precisely known independent variable with these uncertainties in mind.

(v) acoustic pressure signal: $\pm$ 0.10% of the reading. The absolute values shift the resonance curve vertically if that error is independent of frequency and amplitude for the range covered. For further

remarks, see item (iv) for the error estimates in the impedance tube experiments.

(vi) The greatest uncertainties and sources of errors are associated with the end conditions at the pistons. These are mainly due to the flow through the pistons and building vibrations, both of which may produce abrupt fluctuations in the relative phase and occasional shifts in the average position of the piston. The latter can also be affected by the pressure difference between the inside structure of the shakers and resonance tube, which is a function of flow rates through pistons and this amounts to be of the order of a couple of mm's of mercury. Fluctuations in supply air pressure may contribute to the same. A very small change in the alignment -- the axis of the piston may not be precisely aligned with the axis of the tube -- can also be troublesome because the leakage spaces created provide sources for acoustic energy losses which are difficult to account for. Lubrication with silicon oil, the external "quad-seal", pressure equalization and fine regulation of the supply air pressure (± 0.15% per hour of the setting) helped alleviate this problem. It is interesting to note that without these improvements, we encountered serious difficulties with large test to test varia-

tions of the resonance frequency accompanied also by changes in the pressure amplitude for the same piston motion. The initial setting was done to obtain the maximum acoustic pressure amplitude, suggesting the lowest value of the losses described above. These also account partly for the mismatch described in chapter 7.

D.5.2 Impedance Tube Experiments

(i) acceleration of the piston mounting: ± 0.0010 g (0 to peak). For correct results, the piston and its mounting should be absolutely rigid and hence stationary. Best results were obtained after a sturdy clamp was installed to anchor the piston to the end of the impedance tube. Excitation of the loud speaker was kept as low as possible to facilitate this.

(ii) Determination of the acoustic pressure minima is affected by the flexibility and mounting of the long probe. Spurious room noise also has some influence. Neither of these errors is known. Ultimately, the major limitation is set by signal/noise ratio, primarily due to flow noise generated by flow through porous plate. Phase quadrature technique of measurement with lock in amplifier together with the fact described in Appendix C that there is a $\lambda/4$ and hence 90° phase difference between maxima and minima of

acoustic pressure signals when acoustically hard material is tested in the impedance tube. Also the use of B & K measuring amplifier with absorption coefficient scale helps one to determine the approximate pressure minima quickly and fairly accurately.

(iii) special resolution of pressure minima: ± 0.50 mm

(iv) Unlike the acoustic pressure measurements taken with the resonance tube, it is necessary for the experiments with the impedance tube to know the absolute values of the acoustic pressure amplitude. The amplitude linearity of the lock in amplifier enters in determining the absolute values of the signals. Here, the internal calibrator of the instrument was used to estimate this error. A practical difficulty arises because we need to measure signals ranging from 1% to 80% of the full scale sensitivity on a single sensitivity of the lock in amplifier. When the signal was only 1% of the full scale sensitivity setting, the error in amplitude was determined to be ± 0.10% (due to the amplitude nonlinearity of the scale) and for signals greater than 30% of the full scale it was almost impossible to detect the very small error. Measurements of pressure minima in the impedance tube are necessarily made at the lower end of the full scale

while the measurements of pressure maxima and all data for the resonance tube are taken at the higher end of the scale. We estimate that the error due to amplitude nonlinearity of the lock in amplifier scale produces an additional error amounting to roughly 5% of the existing error bars shown in the final results for $\overline{\alpha}_v$.

Finally, it may be noted that day to day changes in temperatures are ignored. The eventual effect on the attenuation constant is roughly $\pm$ 0.5%, arising from the influence on K and speed of sound. Also, lateral oscillations of the resonance tube on its mounts seem to affect K. Our estimate shows that K increases by approximately 1.50 % or so. Both of these eventually lead to minor corrections on $\overline{\alpha}_v$ which were not carried out because of the uncertainties in their determination and the nature of the experiments performed to determine them.

APPENDIX E. COMPUTER PROGRAMS

Three computer programs were developed as a part of this work. The first of the programs calculates the negative real part of the admittance function of a porous plate using data obtained from the impedance tube experiments. The second program takes the results of the three trials of the impedance tube experiments and does simple statistics with it, calculating the mean and standard deviation of these three sets of numbers. It also does the least squares fitting to a straight line of these mean numbers and gives us the equation of the straight line, showing variation of the negative real part of the admittance function with average Mach number of the flow. The third program treats the data obtained from the experiments with the resonance tube. It takes the results of the three trials of the resonance tube experiments. After statistical treatment of the data, it gives us the equation of the straight line showing variation of the mean value of the net loss coefficient in the resonance tube with average Mach number of the flow, using the least squares fitting technique. Reference 15 has been used as the basis for the statistical treatment of our data.

Program to Calculate the Negative Real Part of the Admittance Function of a Porous Plate

```
C     TO DETERMINE THE ADMITTANCE FUNCTION OF PORCUS PLATE
C     USING B&K IMPEDANCE TUBE MODIFIED WITH 1/2 INCH
C     MICROPHONE
C     PSS GRADE G WITH THICKNESS 1/8 INCH IS USED
C     PUS POROUS PLATE(1) IS TREATED FIRST
C     FROM EXPERIMENT FIRST MAXIMA & MINIMA OF ACOUSTIC
C     PRESSURE ARE TAKEN
C     ALL PRESSURES ARE IN MV RMS
C     MKS SYSTEM IS USED THROUGHT
C     FREQUENCY HAS A UNIT OF HERTZS
C     VELOCITY OF SOUND IS CALCULATED AT 1 ATA PRESSURE &
C     21.11 DEGREE CENTIGRADE TEMPERATURE
C     RADIATION OF ACOUSTIC ENERGY THROUGH TUBE WALL IS NOT
C     ACCOUNTED FOR
C     BECAUSE THE MACH NOS ARE TOO SMALL THEIR INCLUSION IN
C     IMPEDANCE TUBE THEORY IS AVOIDED
C     FOR DATA SEE FINAL DATA FILE NO. 2 DATE 11/28/77 WORK
C     TRIAL 1
      COMPLEX Y1,Y2,ADMN
      DIMENSION VELO(6),PMAX(6),PMIN(6),XMAX(6),XMIN(6)
      DIMENSION XMAXA(6),XMINA(6)
      READ(5,1)(VELO(I),I=1,6)
      READ(5,1)(PMAX(J),J=1,6)
      READ(5,1)(PMIN(K),K=1,6)
      READ(5,1)(XMAX(L),L=1,6)
      READ(5,1)(XMIN(M),M=1,6)
1     FORMAT(6F12.5)
      RAD=(1.500*2.54-0.50)/100.0
      FREQ=2645.00
      VSOUND=343.9745
      ALAMDA=VSOUND/FREQ
      AKLOSS=(2.94*0.00001*SQRT(FREQ))/RAD
      XZERO=0.00175
      DO 125 N=1,6
      FLVELO=VELO(N)*0.3048
      AMACH=FLVELO/VSOUND
      XMAXA(N)=XMAX(N)+XZERO
      XMINA(N)=XMIN(N)+XZERO
      R=PMAX(N)/PMIN(N)
      A=AKLOSS*XMAXA(N)
      B=AKLOSS*XMINA(N)
      C=COSH(A)
      D=SINH(A)
      E=COSH(B)
      F=SINH(B)
      PA=(C-(R*F))/((R*E)+D)
      IF (PA.GE.1.0) GO TO 100
      Z1=0.50*(ALOG(1.0+PA))
      Z2=0.50*(ALOG(1.0-PA))
      Z=Z1-Z2
      PI=22.0/7.0
```

```
      ALPHAO=Z/PI
      BETAO=1.0-(2.0*XMINA(N)/ALAMDA)
      Y1=CMPLX(PI*ALPHAO,PI*BETAO)
      Y2=-Y1
C     ADMITTANCE FUNCTION IS NEGATIVE BY DEFINATION
      ADMN=(CEXP(Y1)+CEXP(Y2))/(CEXP(Y1)-CEXP(Y2))
      RADMN=REAL(ADMN)
      AIADMN=AIMAG(ADMN)
C     ALPHA DUE TO PISTON IS NEGETIVE BY DEFINATION
C     NOTE THAT THIS ALPHA IS THE RESPONSE OF THE WHOLE
C     FLOW SYSTEM INCLUDING THE POROUS PLATE ITSELF
C     SYSTEM INCLUDING THE POROUS PLATE ITSELF
      ALPHAP=4.0*FREQ*(RADMN+AMACH)
      WRITE(6,10)
10    FORMAT(1X,'FREQ HZ   MACH NO   -VE REAL PART OF
     ?ADMITTANCE')
      WRITE(6,15)FREQ,AMACH,RADMN
15    FORMAT(3F12.6)
      WRITE(6,20)
20    FORMAT(1X,'-VE IMAGINARY PART OF ADMITTANCE')
      WRITE(6,25)AIADMN
25    FORMAT(F10.6)
      WRITE(6,30)
30    FORMAT(1X,'ALAPHAZERO  BETAZERO')
      WRITE(6,35)ALPHAO,BETAO
35    FORMAT(2F10.6)
      WRITE(6,40)
40    FORMAT(1X,'THEORETICAL VALUE OF KAPPA')
      WRITE(6,45)AKLOSS
45    FORMAT(F10.6)
      WRITE(6,50)
50    FORMAT(1X,'ALPHA DUE TO POROUS PLATE(1) *UNITS 1/SEC
     ?*')
      WRITE(6,55)ALPHAP
55    FORMAT(F11.6)
      GO TO 115
100   WRITE(6,105)
105   FORMAT(1X,'ERROR   VALUE OF TANH(PI*ALPHAO) IS')
      WRITE(6,110)PA
110   FORMAT(F10.6)
115   CONTINUE
      WRITE(6,120)
120   FORMAT(/'*************************************************
     ?*******'/)
125   CONTINUE
      STOP
      END
//DATA   DD     *
C     FOR DATA SEE FINAL DATA FILE NO.2 DATE 11/28/77 WORK
C     TRIAL 1
//
```

Program to Statistically Treat and to Fit the Data for the Negative Real Part of the Admittance Function of a Porous Plate Using the Least Squares Fitting Technique

```
C     TO DETERMINE THE VARIATION OF -VE REAL PART OF THE
C     ADMITTANCE FUNCTION OF NON OSCILLATING POROUS PLATE
C     WITH FLOW MACH NO
C     POROUS PLATE (1) IS TREATED FIRST
C     NUMBER SETS OF EXPERIMENTS DONE ARE THREE
C     FOR DATA SEE FINAL DATA FILE NO 2 DATE 11/28/77 WORK
C     DATA IS TAKEN WITH EXCITATION FREQUENCY OF 2645.00 HZ
      DIMENSION DATA(3,9),X(9),Y(9),A(2),ABR(3)
      DOUBLE PRECISION STOR(2,7)
      A(1)=0.
      A(2)=0.
      N=6
      READ(5,95)((DATA(I,J),J=1,N)
95    FORMAT(6(F10.6))
      DO 12 K=1,N
      READ(5,14) ABR
14    FORMAT(3(F10.6))
      DATA(2,K)=(ABR(1)+ABR(2)+ABR(3))/3.
      DATA(3,K)=SQRT(((ABR(1)-DATA(2,K))**2+(ABR(2)-DATA(2,
     ?K))**2+(ABR(3)-DATA(2,K)**2)/3.)
      X(K)=DATA(1,K)
      Y(K)=DATA(2,K)
12    CONTINUE
      CALL LSQUAR(DATA,N,2,A,CHISQ,STOR)
      WRITE(6,80)
80    FORMAT(1X,'IMPEDANCE TUBE RESULTS FOR POROUS PLATE
     ?(1) AT FREQUENCY OF 2645.00 HZ',//)
      WRITE(6,98)(X(I),Y(I),DATA(3,I),I=1,N)
98    FORMAT(1X,'MACH NUMBER',4X,'-VE REAL PART OF ADMITTA
     ?NCE FUNCTION',4X,'STANDARD DEVATION',/,6(/,2X,F8.6,
     ?20X,F8.6,23X,F8.6))
      SUMXSQ=0.
      SUMX=0.
      SUM=0.
      DO 5 I=1,N
      SUM=SUM+(A(2)*X(I)+A(1)-Y(I))**2
      SUMXSQ=SUMXSQ+X(I)**2
      SUMX=SUMX+X(I)
5     CONTINUE
      SIGSQ=SUM/N
      DELTA= N*SUMXSQ-SUMX**2
      SIGA2=SQRT(N*SIGSQ/DELTA)
      SIGA1=SQRT(SIGSQ*SUMXSQ/DELTA)
      WRITE(6,999) A(2),SIGA2,A(1),SIGA1
999   FORMAT(/,1X,'NABR = ',E13.6,' +- ',E13.6, ' TIMES
     ?MACH NUMBER',1X,'PLUS ',F10.6,' +- ',E13.6)
      STOP
      END
//DATA   DD    *
C     FOR DATA SEE FINAL DATA FILE NO 2 DATE 11/28/77 WORK
//
```

Program to Statistically Treat and to Fit the Data for Total Losses in the Resonance Tube Using the Least Squares Fitting Technique

```
C     THIS IS A PROGRAM TO FIT LINEARLY WITH LEAST SQUARES
C     RELATION BETWEEN MACH NUMBER AND ALPHA NET FROM
C     RESONANCE TUBE EXPERIMENTS
C     VENT SIZE IS 1/2 INCH AND IT IS LOCATED AT THE CENTER
C     OF THE RESONANCE TUBE
C     RESONANCE FREQUENCY IS NEAR 2645.00 HZ
C     NUMBER SETS OF EXPERIMENTS DONE ARE THREE
      DIMENSION DATA(3,9),X(9),Y(9),A(2),ABR(3)
     ?,FREQ(3,6),AVGFRE(6),SDFREQ(6)
      DOUBLE PRECISION STOR(2,7)
      A(1)=0.
      A(2)=0.
      N=6
      READ(5,95)((DATA(I,J),J=1,N)
95    FORMAT(6(F10.6))
      DO 12 K=1,N
      READ(5,14) ABR
14    FORMAT(3(F10.2))
      DATA(2,K)=(ABR(1)+ABR(2)+ABR(3))/3.
      DATA(3,K)=SQRT(((ABR(1)-DATA(2,K))**2+(ABR(2)-DATA(2,
     ?K))**2+(ABR(3)-DATA(2,K))**2)/3.)
      X(K)=DATA(1,K)
      Y(K)=DATA(2,K)
12    CONTINUE
      READ(5,16)((FREQ(I,J),I=1,3),J=1,6)
16    FORMAT(3F10.2)
      SUMFRE=0.0
      DO 24 K=1,N
      AVGFRE(K)=(FREQ(1,K)+FREQ(2,K)+FREQ(3,K))/3.
      SDFREQ(K)=SQRT(((FREQ(1,K)-AVGFRE(K))**2+(FREQ(2,K)-
     ?AVGFRE(K))**2+(FREQ(3,K)-AVGFRE(K))**2)/3.)
      SUMFRE=AVGFRE(K)+SUMFRE
24    CONTINUE
      OVERFR=SUMFRE/N
      SQF=0.0
      DO 25 J=1,6
      DO 26 I=1,3
26    SQF=SQF+(FREQ(I,J)-OVERFR)**2
25    CONTINUE
      OVERSD=SQRT(SQF/18.)
      CALL LSQUAR(DATA,N,2,A,CHISQ,STOR)
      WRITE(6,80)
30    FORMAT(1X,'RESULTS FOR RESONANCE TUBE WITH 1/2 INCH
     ?VENT',//)
      WRITE(6,98)(X(I),Y(I),DATA(3,I),AVGFRE(I),SDFREQ(I),
     ?I=1,N)
98    FORMAT(1X,'MACH NUMBER      ALPHA NET   STANDARD DEV.
     ?FREQUENCY NET     STANDARD DEV. OF FREQ. ',6(/,2X,
     ?F6.2,11X,F4.2, 10X,F7.2,15X,F4.2))
      WRITE(6,99)OVERFR,OVERSD
99    FORMAT(/,1X,'OVERALL AVG FREQ = ',F7.2, ' +- ',F4.2)
```

```
      SUMXSQ=0.
      SUMX=0.
      SUM=0.
      DO 5 I=1,N
      SUM=SUM+(A(2)*X(I)+A(1)-Y(I))**2
      SUMXSQ=SUMXSQ+X(I)**2
      SUMX=SUMX+X(I)
5     CONTINUE
      SIGSQ=SUM/N
      DELTA= N*SUMXSQ-SUMX**2
      SIGA2=SQRT(N*SIGSQ/DELTA)
      SIGA1=SQRT(SIGSQ*SUMXSQ/DELTA)
      WRITE(6,999) A(2),SIGA2,A(1),SIGA1
999   FORMAT(/,1X,'NALPA= ',E13.6,' +- ',E13.6, ' TIMES
     ?MACH NUMBER ',1X,' PLUS ',F10.6,' +- ',E13.6)
      STOP
      END
//DATA   DD     *
C     SEE THE DATA FOR RESONANCE FREQUENCY NEAR 2645.00 HZ
C     IN FINAL DATA FILE NO.2
//
```

APPENDIX F. DETERMINATION OF THE INFLUENCE OF THE EXHAUST VENT NEAR THE SECOND MODE

As an additional check for the validity of the one-dimensional calculations, tests have been carried out with the resonance tube operated near its second longitudinal mode. Let us first examine the case of a centrally located circular vent. Equation (3.4) for the second longitudinal mode is given by:

$$\alpha_{ft} = -\frac{1}{2E_{2\ell}^2}\frac{1}{\rho_o k_{2\ell}^2}\oiint(\nabla\hat{p}_{2\ell})^2\,\overline{m}_b\,dS \qquad (F.1)$$

For the second longitudinal mode, the waves within the resonance tube are,

$$\hat{p}_{2\ell} \sim \cos(2k_\ell z) \qquad \text{with} \qquad k_\ell = \pi/L\ .$$

Then

$$(\nabla\hat{p}_{2\ell})^2 = \{2k_\ell \sin(2k_\ell z)\}^2 = 0 \text{ at } z = L/2\ .$$

Thus, equation (F.1) when applied to the process of flow turning at the centrally located exhaust vent gives,

$$\left(\alpha_{ft}\right)_{\overline{m}_b \to -\overline{m}_v} = 0 \qquad (F.2)$$

Thus, from equation (3.3), α_v for the second longitudinal mode is given by:

$$\alpha_v = \alpha_{rad} \qquad (F.3)$$

To measure this loss, a resonance tube was constructed with a centrally located circular vent of 1/2" diameter and whose

fundamental longitudinal frequency was 670 Hz. This resonance tube was then made to run at its second mode, i.e., at the frequency of 1340 Hz. The resonance curve is obtained as usual by varying the input frequency to the drivers; the relative phase is maintained at 0^{o}, while the amplitude of the drivers is held constant. Table F.1 contains data taken for three series of tests performed at each Mach number for this case. The average value and standard deviations of both net attenuation constants (recall, $2\alpha_{net}$ equals the width of the resonance curve $\Delta\omega$ at the half power points) and resonance frequencies are also given. As discussed earlier (see § 6.2), two series of tests have been carried out with no flow: one with the vent closed and the other with the vent open. The difference between these two cases should represent the loss due to radiation of acoustic energy through the vent. Figure F-1 shows the variation of the average values of the net attenuation coefficient as a function of the Mach number of the average flow at the resonance frequency near 1340 Hz. The solid line in the figure represents the least squares fit, assuming that α_{net} varies linearly with the average Mach number of the flow. Details of the computer programs for this purpose are given in Appendix E.

For this case, the basic governing equation (7.1) takes the form:

$$\alpha_{net} = 2 \times 1345 \times (A_b^{(r)} + \overline{M}) + \alpha_v + \alpha_d \qquad (F.4)$$

Further statistical treatment of the experimental data can be carried out in exactly the same way as discussed in chapter 7. The

necessary data for the real part of the admittance function for two porous plates were taken from the previous results at the frequency of 1345 Hz. See tables 6.3 and 6.4 for details. Further, it was assumed that the real part of the admittance function at the frequency of 1349.84 Hz (average resonance frequency of the first 18 experiments done with the vent open, see table F.1) is the same as that at the frequency of 1345 Hz. Table F.2 gives the attenuation constant due to radiation of acoustic energy from the vent, while table F.3 gives the results corresponding to the verification of the data for the circular vent with no flow and vent closed. Table F.4 gives the values of the average attenuation coefficient and standard deviation for the circular vent for our case and table F.5 gives the values of the slope and standard deviation of the attenuation constant. The final results for the attenuation constant due to the exhaust vent are plotted in figure F.2. The dotted straight lines in the figure represent the theoretical variation of α_v at the frequencies of 670 Hz and 1340 Hz, given by equation (8.2), while the solid straight line represents equation (7.12). The slope $\frac{d\bar{\alpha}_v}{d\bar{M}}$ can be calculated using equation (7.13). Also, note that the same sign convention is adopted here for the purpose of data reduction. For further details see chapter 7.

From the results given in tables F.4 and F.5, it is obvious that there is a non-zero influence of the exhaust vent at the second mode of operation of the resonance tube. In the absence of suitable theoretical calculations for acoustic energy loss associated with

radiation through the vent for the second longitudinal mode, the gain obtained here raises some doubt about the assumption made previously that α_d is independent of $\overline{M}$. Results represented previously in chapter 7 may have contained in them this influence which is difficult to separate just because of the unabailability of the corresponding data pertaining to this work. The interactions between the boundary layer due to the mean flow and the acoustic boundary layer due to the externally driven acoustic mode in the resonance tube, may give rise to this observed reduction of the acoustic energy loss at the boundary. This reduction seems to increase approximately linearly with the Mach number of the mean flow. Until separate experiments are designed to prove this, it can only be regarded as a tentative conclusion.

TABLE F.1

DATA TAKEN WITH RESONANCE TUBE, $\frac{1}{2}$" CIRCULAR VENT, SECOND MODE FREQUENCY 1349.84 Hz

$\overline{M} \times 10^4$	α_{net} (sec^{-1})	f (Hz)	$\overline{\alpha}_{net}$ (sec^{-1})	σ_{α} (sec^{-1})	$\overline{f}$ (Hz)	σ_f (Hz)
0	70.92	1350.60	70.98	0.04	1350.70	0.14
	71.01	1350.60				
	71.01	1350.90				
4.43	72.21	1349.20	72.05	0.12	1349.37	0.12
	71.94	1349.50				
	72.00	1349.40				
8.86	71.54	1349.80	71.57	0.05	1349.97	0.12
	71.65	1350.10				
	71.53	1350.00				
13.29	71.24	1349.00	71.34	0.12	1349.00	0.00
	71.28	1349.00				
	71.51	1349.00				
17.72	71.23	1349.50	71.25	0.04	1349.70	0.22
	71.21	1349.50				
	71.30	1350.00				
22.15	71.81	1350.00	71.93	0.15	1350.33	0.24
	71.84	1350.50				
	72.14	1350.50				
0 (Vent Closed)	71.41	1338.90	71.46	0.04	1339.10	0.22
	71.51	1339.00				
	71.47	1339.40				

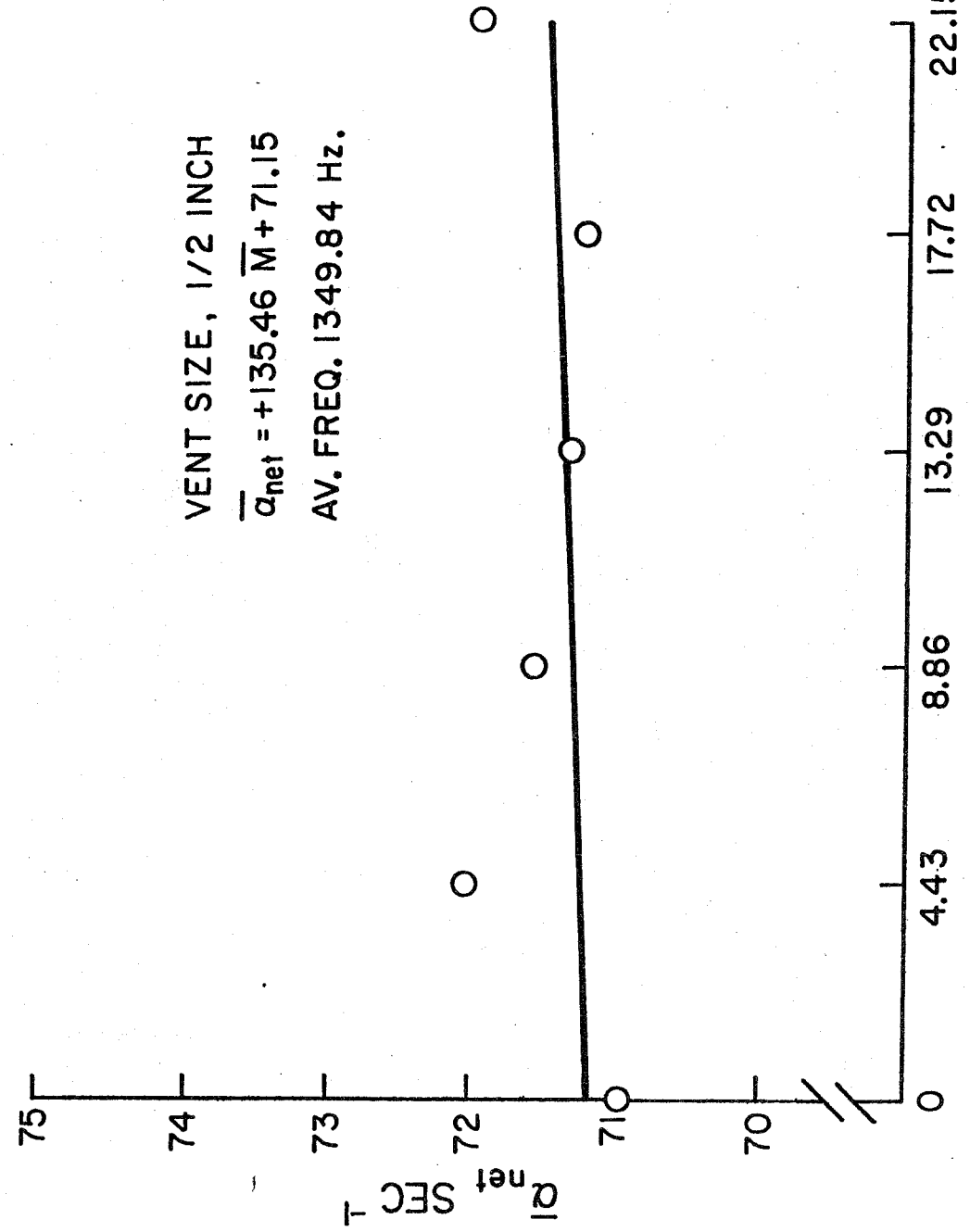

Figure F.1 Net Values of Attenuation Constant, $\frac{1}{2}$" Circular Vent, Second Mode Frequency 1349.84 Hz

TABLE F.2

ATTENUATION CONSTANT DUE TO RADIATION OF ACOUSTIC ENERGY FROM $\frac{1}{2}$" CIRCULAR EXHAUST VENT AT THE SECOND MODE

$2\overline{f}$ (Hz)	$-(\Delta\overline{f}/\Delta L)$ (Hz/Inch)	$\overline{\alpha}_{rad}$ (sec^{-1})	σ_{rad} (sec^{-1})
1345	132.59	-0.48	0.01

TABLE F.3

VERIFICATION OF THE DATA FOR $\frac{1}{2}$" CIRCULAR EXHAUST VENT AT THE SECOND MODE, WITH NO FLOW AND VENT CLOSED

Description	$2\overline{f} \approx 1345$ (Hz)
$\overline{\alpha}_{net}(sec^{-1})$	71.46
$\Delta\alpha_{net}(sec^{-1})$	0.04
$\overline{A}_b^{(r)} \times 10^2$	1.5639
$\Delta A_b^{(r)} \times 10^6$	146
$K\ a_o\ (sec^{-1})$	19.47
$(\overline{\alpha}_d)_{\substack{other\\losses}}\ (sec^{-1})$	9.92
$(\Delta\alpha_d)_{\substack{other\\losses}}\ (sec^{-1})$	0.43

TABLE F.4

VALUES OF THE AVERAGE ATTENUATION COEFFICIENT AND STANDARD DEVIATION FOR $\frac{1}{2}$" CIRCULAR EXHAUST VENT AT THE SECOND MODE

$\overline{M} \times 10^4$	$\bar{\alpha}_v$ (sec^{-1})	$\Delta\alpha_v$ (sec^{-1})
0	-0.48	0.86
4.43	-1.38	0.80
8.86	-4.16	0.81
13.29	-4.66	0.96
17.72	-5.51	0.83
22.15	-5.27	0.86

TABLE F.5

SLOPE AND STANDARD DEVIATION OF THE ATTENUATION CONSTANT FOR $\frac{1}{2}$" CIRCULAR EXHAUST VENT AT THE SECOND MODE

$\frac{d\bar{\alpha}_v}{d\bar{M}}$ (sec^{-1})	$\Delta\left(\frac{d\alpha_v}{d\bar{M}}\right)$ (sec^{-1})
-1979.34	711.90

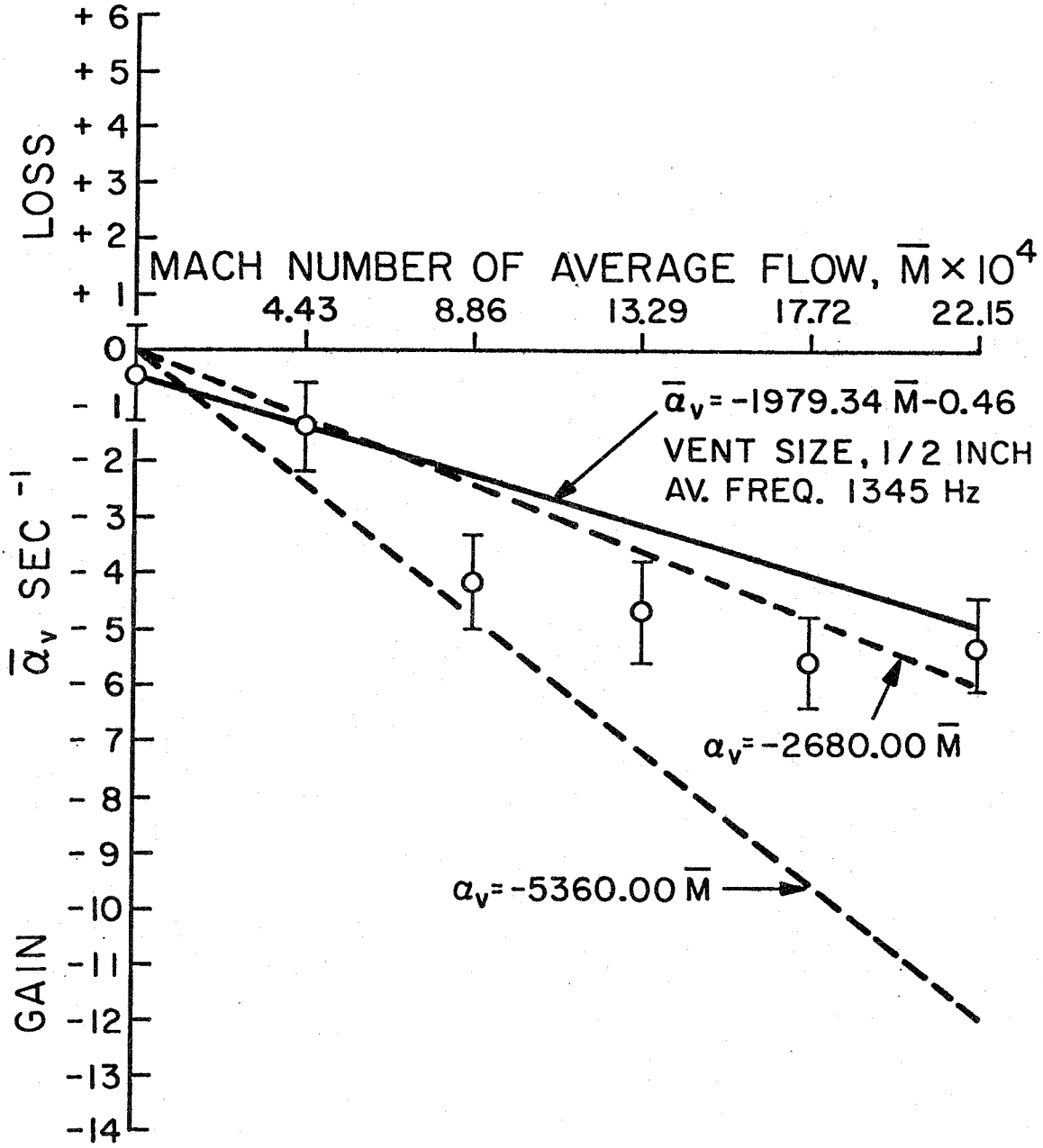

Figure F.2 Attenuation Constant for $\frac{1}{2}$" Circular Vent, Second Mode Frequency 1345.00 Hz